

INVESTIGATING THE EFFECTS OF PARTICLE RADIATION EXPOSURE ON LUNG
CARCINOGENESIS

APPROVED BY SUPERVISORY COMMITTEE

Jerry W. Shay, Ph.D.
Professor of Cell Biology

Benjamin Chen, Ph.D.
Associate Professor, Internal Medicine

Asaithamby Aroumougame, Ph.D.
Assistant Professor of Radiation Oncology

Esra Akbay, Ph.D.
Assistant Professor of Pathology

In dedication to

Ama, daddy, wife, brother and Hawa Taal for their love and support.

INVESTIGATING THE EFFECTS OF PARTICLE RADIATION EXPOSURE ON LUNG
CARCINOGENESIS

By

KRISHNA LUITEL

DISSERTATION/THESIS

Presented to the Faculty of the Graduate School of Biomedical Sciences

The University of Texas Southwestern Medical Center at Dallas

In Partial Fulfillment of the Requirements

For the Degree of

DOCTOR OF PHILOSOPHY

The University of Texas Southwestern Medical Center at Dallas

Dallas, Texas

May 2019

© Copyright

by

Krishna Luitel, 2019

All Rights Reserved

ACKNOWLEDGMENTS

I would like to express my gratitude to several people who supported and encouraged me during my graduate work here at UTSW. Firstly, I would like to express my sincerer gratitude to my mentors Drs. Jerry W. Shay and Dr. Woodring Wright for accepting me into their laboratory and then providing continuous support, mentorship and guidance for the last five years. I am very thankful for my thesis committee members Dr. Benjamin Chen, Dr. Asaithamby Aroumougame, and Dr. Esra Akbay for their valuable advice, invaluable contributions, suggestions, and ideas throughout the duration of my graduate work. I would also like to thank my previous committee member Dr. David Boothman and Dr. Pier Scaglioni for their insightful comments and encouragement. I could not have imagined for a better mentor than Dr. Shay whose door was always open whenever I had questions about my research or writing or presentations.

Besides my mentors, I would like to thank all past and present members of the Shay/Wright lab who have assisted me throughout my research with advice and inputs. I am grateful to lab members for making my time both enjoyable as well as having inspiring discussions about science. I am thankful to Dr. Aadil Kaisani who trained me during the rotations in the Shay/Wright lab and laying the groundwork for my thesis project, Dr. Sang Bum Kim, Dr. Mariam El-Ashmawy, Dr. Ronald Bozeman, and Dr. Ilgen Mender for training me and helping me troubleshoot the experiments after I joined the lab. I would like to give special thanks to Summer Barron for providing animal support for my graduate work.

I am also grateful to the entire support team Dr. Peter Guida, Dr. Adam Rusek, Dr. Michael Sivertz, Paula Bennett and Debbie Synder at the NASA Space Radiation

Laboratories (NSRL) located in Brookhaven National Laboratory (Upton, New York), for helping us to organize experiments at their facilities. I would also like to thank Dr. James Richardson at UTSW for training and helping me understand lung cancer pathology.

The completion of my dissertation and graduate work would not have been possible without the continuous love and support from my wife, Hemanta Ghimire. I would also like to acknowledge support from my friends “Hawa Taal” for their encouragement and motivations.

Finally, I cannot begin to express my thanks for my parents Rajendra and Rajani Luitel and brother Shree Hari Luitel for their sacrifices and unwavering love and support throughout my years of study in the United States.

INVESTIGATING THE EFFECTS OF PARTICLE RADIATION EXPOSURE ON LUNG CARCINOGENESIS

Krishna Luitel, PhD

The University of Texas Southwestern Medical Center at Dallas, 2019.

JERRY W. SHAY, PhD

Lung cancer accounts for more cancer-related deaths than any other cancer type among both men and women. The overall increase in radiation risk for human cancer types has been substantiated by the epidemiological data obtained from atomic bomb survivors and uranium mine workers. The lung has a large surface area which makes it a prominent target for radiation exposure making it susceptible to radiation-induced cancer. Recently particle radiation therapy such as the use of protons and carbon has increased in the treatment of cancer. The long-term biological effects of proton radiation remain less well characterized in terms of radiotherapy and well as for astronauts during deep space explorations.

We compared the long-term side effects of proton radiation to equivalent doses of X-rays in the initiation and progression of premalignant lesions in a transgenic mouse lung cancer model (K-ras^{LA1}). We show proton irradiation causes more complex DNA damage that is not completely repaired resulting in increased oxidative stress in the lungs both acutely and persistently. Proton irradiated mice had lower median survival and increased carcinoma incidence as compared to un-irradiated controls or X-ray exposed mice.

Additionally, the space radiation environment consists of a wide variety of ion species with a various range of energies. To understand the effects of mixed ion beam radiation, we exposed K-ras^{LA-1} mice with three ion beams: Proton (H), Helium (He), and Silicon (Si) at a low dose rate of 0.5cGy/min. Using the three ion beams, we performed whole body irradiation in two different orders: 3B-1 (H-He-Si) and 3B-2 (Si-He-H) and used only H as a reference. We found that whole-body irradiation with 3B-1 increases the incidence of cancer initiation and systemic oxidative stress in mice 100 days post-irradiation compared to 3B-2 and H irradiation. Additionally, we saw an increase in adenomas with atypia and adenocarcinomas in 3B-1 irradiated mice but not in 3B-2 and H irradiated mice. We also found that a non-toxic anti-inflammatory, anti-oxidative radioprotector (CDDO-EA) reduced 3B-1 induced oxidative stress and cancer initiation almost back to baseline. Thus, exposure to 3B-1 elicits significant changes in lung cancer initiation that can be mitigated using CDDO-EA.

TABLE OF CONTENTS

TITLE PAGE	i
DEDICATION	ii
TITLE PAGE	iii
COPYRIGHT	iv
ACKNOWLEDGEMENT	v
ABSTRACT	viii
TABLE OF CONTENTS	x

CHAPTER ONE: INTRODUCTION

1.1 The Lung Biology	1
1.2 Cancer and Lung Cancer Statistics	9
1.3 Pathology of Lung Cancer	15
1.4 Molecular Aberrations in Lung Cancer	17
1.5 Risk Factors for Lung Cancer	21
1.6 Introduction to Radiation	23
1.7 Space Radiation and Risk of Lung Cancer	27
1.8 Lung Cancer Mouse Model	33

CHAPTER TWO: PROTON RADIATION-INDUCED CANCER PROGRESSION	37
2.1 Introduction	37
2.2 Material and Methods	
2.2.1 Mice and Irradiation	40
2.2.2 Premalignant Lesions, Invasive Carcinoma Assessment, and Mouse Survival	41
2.2.3 Western Blot Analysis	42
2.2.4 Oxyblot	43
2.2.5 Immunofluorescence	44
2.2.6 Quantitative Real-time PCR	45
2.2.7 Immunohistochemistry	45
2.2.8 Malondialdehyde Assay on Serum	47
2.2.9 Statistical Analysis	47
2.3 Results	
2.3.1 Proton exposure causes complex and extensive DNA damage in the lung	48
2.3.2 Proton irradiation causes both acute and chronic oxidative stress	52
2.3.3 Increases in number and sizes of premalignant lesions in K-ras ^{LA1} mouse model	59
2.3.4 Inflammatory cells infiltration in the premalignant lesions	61
2.3.5 Proton exposure reduces lifespan and increases invasive carcinoma	66

2.4 Discussion	72
2.5 Future Directions	76
CHAPTER THREE: TRITERPENOIDS (CDDO-EA): A POTENT RADIO-PROTECTOR AGAINST HEAVY ION RADIATION IN A LUNG CANCER MOUSE MODEL	77
3.1 Introduction	77
3.2 Material and Methods	
3.2.1 Mice and Irradiation	83
3.2.2 Lung Tumor Histopathology	83
3.2.3 Experimental Design of CDDO-EA as a Countermeasure Experiment	84
3.2.4 Western Blot Analysis	86
3.2.5 Statistical Analysis	87
3.3 Results	
3.3.1 CDDO-EA diet reduces the progression of tumors in the K-rasLA1 mouse model	88
3.3.2 CDDO-EA as countermeasure sSPE radiation	91
3.3.3 CDDO-EA as countermeasure HZE particles radiation	95
3.3.4 CDDO-EA mitigator to radiation effect	98
3.4 Discussion	100
3.5 Future Directions	103

CHAPTER FOUR: LUNG CANCER PROGRESSION USING FAST	104
SWITCHING MULTIPLE ION BEAM EXPOSURES AND COUNTERMEASURE	
PREVENTION	
4.1 Introduction	104
4.2 Material and Methods	107
4.2.1 Animals and Irradiation	107
4.2.2 Synthetic Triterpenoid Treatment	108
4.2.3 Lung Tumor Evaluation and Histology	108
4.2.4 Malondialdehyde Assay on Serum	109
4.2.5 Statistical Analysis	110
4.3 Results	117
4.3.1 Total Body Irradiation Using Multiple Ion Beam	111
4.3.2 Order of Particles in Multiple Ion Beam Radiation Matter	113
4.3.3 Skipping a Day for Silicon in 3B-1 Irradiation Protocol	117
Attenuates Its Effect	
4.3.4. CDDO as Countermeasure Against 3B-1 Irradiation	119
4.3.5. Titration of Silicon total dose to better simulate the	121
space environment	
4.4 Discussion	125
 CHAPTER FIVE: DISCUSSION AND FUTURE DIRECTIONS	 129
 BIBLIOGRAPHY	 133

PRIOR PUBLICATIONS

- 2019** **Luitel K.**, Bozeman R., Kaisani A., Kim S.B., Barron S., Richardson J.A., Shay JW. Understanding lung cancer progression using multiple ion beam exposure (in preparation).
- 2018** **Luitel K.**, Bozeman R, Kaisani A, Kim SB, Barron S, Richardson JA, Shay JW. Proton radiation-induced cancer progression. *Life Sci Space Res (Amst)* 2018; 19, 31-42.
- 2018** Mender I, LaRanger R, **Luitel K**, Peyton M, Girard L, Lai TP, Batten K, Cornelius C, Dalvi MP, Ramirez M, Du W, Wu LF, Altschuler SJ, Brekken R, Martinez ED, Minna JD, Wright WE, and Shay JW. Telomerase-mediated Strategy for Overcoming Non-Small Cell Lung Cancer Targeted Therapy and Chemotherapy Resistance. *Neoplasia*, 2018 Aug;20(8):826-837.
- 2018** Zhang L., Kim S.B, **Luitel K.**, Shay JW. Cholesterol Depletion by TASIN-1 Induces Apoptotic Cell Death through the ER Stress/ROS/JNK Signaling in Colon Cancer Cells. *Molecular Cancer Therapeutics*, 2018 May;17(5):943-95.1
- 2016** El-Ashmawy M., Coquelin M., **Luitel K.**, Batten K., Shay JW. Organotypic Culture in Three Dimensions Prevents Radiation-Induced Transformation in Human Lung Epithelial Cells. *Scientific Rep.* 2016 Aug 19; 6:31669.
- 2014** Tran HD., **Luitel K.**, Kim M., Zhang K., Longmore GD., Tran DD. Transient SNAIL1 Expression Is Necessary for Metastatic Competence in Breast Cancer. *Cancer Res.* 2014 Nov 1;74(21):6330-40. (Equal Contribution)

LIST OF FIGURES

Figure 1.1. Gross human lung anatomy.	2
Figure 1.2. Structures of the respiratory zone with central and peripheral airways of the lung.	4
Figure 1.3. Graphic illustrations of cell types in peripheral airways and central airways.	7
Figure 1.4. Trends in cancer death by sex.	12
Figure 1.5. Direct and indirect action of ionizing radiation.	24
Figure 1.6. Illustration of the generally accepted biological effects after absorption of ionizing radiation.	26
Figure 1.7. Space environment with a combination of galactic cosmic radiation (GCR) and (largely) proton radiation due to solar particle events (SPEs).	29
Figure 1.8. Comparison of particle tracks and delta (δ) rays from the primary track.	32
Figure 1.9. Tumor progression in Kras ^{LA1} mouse model.	35
Figure 2.1. Proton-induced DNA damage responses in WT mouse lungs.	49
Figure 2.2. Proton-induced DNA damage responses in WT mouse lungs.	51
Figure 2.3. Proton exposure causes higher and extensive oxidative stress in WT mouse lungs.	54
Figure 2.4. Radiation exposure altered expression of genes associated with oxidative stress.	55

Figure 2.5. Proton exposure leads to chronic oxidative stress and DNA damage in WT mice.	56
Figure 2.6. Proton irradiation increased the tumor burden in K-ras ^{LA1} mice.	60
Figure 2.7. Representative images (H and E) of lung tissues irradiated with either X-rays or proton or unirradiated control showing the pockets of inflammatory cells near to the premalignant lesions.	63
Figure 2.8. Immune cells infiltrations into premalignant lesions.	65
Figure 2.9. Tumorigenic effect of proton irradiation in the K-ras ^{LA1} mouse model.	68
Figure 2.10. Tumorigenic effect of an acute proton (50 MeV/n) and proton (150 MeV/n) in K-ras ^{LA1} mouse model.	70
Figure 3.1. Chemical Structures of different types of triterpenoids.	79
Figure 3.2. CDDO-EA as a radioprotector.	82
Figure 3.3. Experimental design - CDDO-EA as a radioprotector.	85
Figure 3.4. CDDO-EA diet reduces the progression of tumors in the K-ras ^{LA1} mouse model.	90
Figure 3.5. The decrease in number and sizes of premalignant lesions K-ras ^{LA1} mouse model.	92
Figure 3.6. CDDO-EA decreases the incidence of invasive carcinoma in K-ras ^{LA1} mice irradiated with a simulated solar particle event (50-150 MeV/n).	93
Figure 3.7. CDDO-EA decreases the incidence of invasive carcinoma in K-ras ^{LA1} mice irradiated with ⁵⁶ Fe (600MeV/n) 1.0 Gy.	96
Figure 3.8. CDDO-EA modulates Inflammation-related signaling.	97

Figure 3.9. CDDO-EA as a mitigator.	98
Figure 3.10. CDDO-EA decreases wild type mouse survival after an acute lethal dose of 7.5-Gy total body X-ray irradiation.	99
Figure 4.1. Experimental design for the three-beam radiation.	112
Figure 4.2. Tumorigenic effect of multiple ion radiation in K-ras ^{LA1} mouse model.	115
Figure 4.3. Skipping a day for silicon ion in 3B-1 total body irradiation rescues the biological damage in the mice.	118
Figure 4.4. CDDO as a countermeasure against multiple beam ion radiation.	120
Figure 4.5. Titration of Silicon ion dose in 3B-1 irradiation shows a dose response.	123

LIST OF TABLES

Table 1.1. Estimated new cancer cases and deaths in the United States in 2019	10
Table 1.2. Five-year Relative Survival Rates by Stage of Diagnosis US (2008-2014)	14
Table 1.3. Driver mutations identified in lung adenocarcinoma of tumor specimens from 1,00 patients.	18
Table 2.1. Effect of radiation exposure to K-ras ^{LA1} mice.	71

LIST OF ABBREVIATIONS

4-HNE - 4-hydroxynonenal

8-oxo-dG - 8-oxo-2'-deoxyguanosine

⁵⁶Fe - Iron 56

ACS - American Cancer Society

ADC - Adenocarcinoma

ALK - Anaplastic Lymphoma Kinase

AMs - Alveolar Macrophages

ANOVA - Analysis Of Variance

BCMs - Biological Countermeasures

BNL - Brookhaven National Laboratory

CAT - Catalase

CDDO-EA - 2-cyano-3,12-dioxoleana-1,9(11)-dien-28-oate-ethyl amide

CDDO-Me - C-28 methyl ester of 2-cyano-3,12-dioxolean-1,9-dien-28-oic acid oleana-1,9(11)-dien-28-oic acid

CO₂ - Carbon dioxide

DAPI - 4',6-diamidino-2-phenylindole

DMF - Dose Modifying Factor

DNA - Deoxyribonucleic Acid

DSB - Double-Strand Break

EDTA - Ethylenediaminetetraacetic Acid

EGFR - Epidermal Growth Factor Receptor

EM - Electromagnetic
FDA - Food and Drug Administration
FHIT - Fragile Histidine Triad Protein
Foxp3 – Forkhead box protein P3
GCR - Galactic Cosmic Radiation
GPX1 - Glutathione peroxidase 1
GPX2 - Glutathione peroxidase 2
GPX8 - Glutathione peroxidase 8
Gy - Gray
 ^+H - Proton
He- Helium
H&E - Hematoxylin and Eosin
HO-1 - Heme Oxygenase
HZE - High Atomic Number and Energy
IACUC - Institution of Animal Care and Use Committee
IF - Immunofluorescence
IR - Ionizing Radiation
K-Ras - v-Ki-ras2 Kirsten rat sarcoma viral oncogene homolog
Keap1 - Kelch-like ECH-associated protein 1
LCC - Large Cell Carcinoma
LEO - Low Earth Orbit
LET - Linear Energy Transfer
LSS - Life Span Study
MAPK - Mitogenic-Activated Protein Kinase

MDA - Malondialdehyde

MeV/n - Mega Electronvolt per Nucleon

mTOR - Mammalian Target Of Rapamycin

MYC - v-myc Avian Myelocytomatosis viral oncogene homolog

NADPH - Nicotinamide Adenine Dinucleotide Phosphate Dehydrogenase

NASA - National Aeronautics and Space Association

NBF - Neutral Buffered Formalin

NF- κ B - Nuclear Factor Kappa-Light-Chain-Enhancer of Activated B Cells

NOS - Nitric Oxide Species

NQO1 - NADPH Dehydrogenase Quinone

Nrf2 - Nuclear Factor Erythroid-derived 2 -like 2

NSAID - Nonsteroidal Anti-Inflammatory Drug

NSCLCs - Non-Small Cell Lung Cancer

NSRL - NASA Space Radiation Laboratory

O₂ - Oxygen

PBS - Phosphate Buffered Saline

PFA - Paraformaldehyde

PI3K - Phosphatidylinositol-4,5-Bisphosphate 3-Kinase

PNEC - Pulmonary Neuroendocrine Cells

PRX1 - Peroxiredoxin 1

PTEN - Phosphatase and Tensin Homolog

qRT-PCR - Quantitative Reverse Transcription Polymerase Chain Reaction

RNA - Ribonucleic Acid

ROS - Reactive Oxygen Species

RT-PCR - Reverse Transcription Polymerase Chain Reaction

SCC - Squamous Cell Carcinoma

SCLC - Small Cell Lung Cancer

SDS - Sodium Dodecyl Sulfate

Si - Silicon

SOD1 - Superoxide Dismutase 1

SPE - Solar Particle Events

SSBs - Single-Strand Breaks

STAT3 - Signal Transducer and Activator of Transcription 3

TBI - Total Body Irradiation

TK – Tyrosine Kinases

TP53 - Tumor Suppressor p53

US - United States

UTSW – University of Texas Southwestern Medical Center

CHAPTER ONE

Introduction to Lung Biology, Lung Cancer, and Radiation

1.1 The Lung Biology

The respiratory system consists of the lungs, trachea and associated muscles that mediate the movement of air into and out of the body. Lungs are situated in a thoracic cavity where the left and right lungs are separated by the mediastinum. The base of the lungs is boarded with dome-shaped muscle diaphragm. The contraction and relaxation of the diaphragm and intercostals muscles cause changes in pleural pressure resulting in inhalation and exhalation (**Figure 1.1**) (Mentzer, Tsuda, & Loring, 2018). Human lungs are bilateral but asymmetrical, the right lung is different compared to the left lung. The right lung consists of three lobes (superior, middle and inferior) while the left lung consists of two lobes (superior and inferior), and lobes are separated by fissures. The lung is a complex cone-shaped organ protected in

the ribcage and is responsible for exchanges of gases between the circulatory system and atmosphere (Saint-Criq & Gray, 2017). The left lung has an indentation called the cardiac notch which allows space for the heart. The lung consists of highly branched tree-like tubular system ending in thousands of terminal tubules ultimately giving rise to mature airways and alveoli (**Figure 1.1**). In these structures, gases are exchanged by simple diffusion allowing oxygen (O_2) to be carried to the blood and carbon dioxide (CO_2) released into the air (Herriges & Morrissey, 2014).

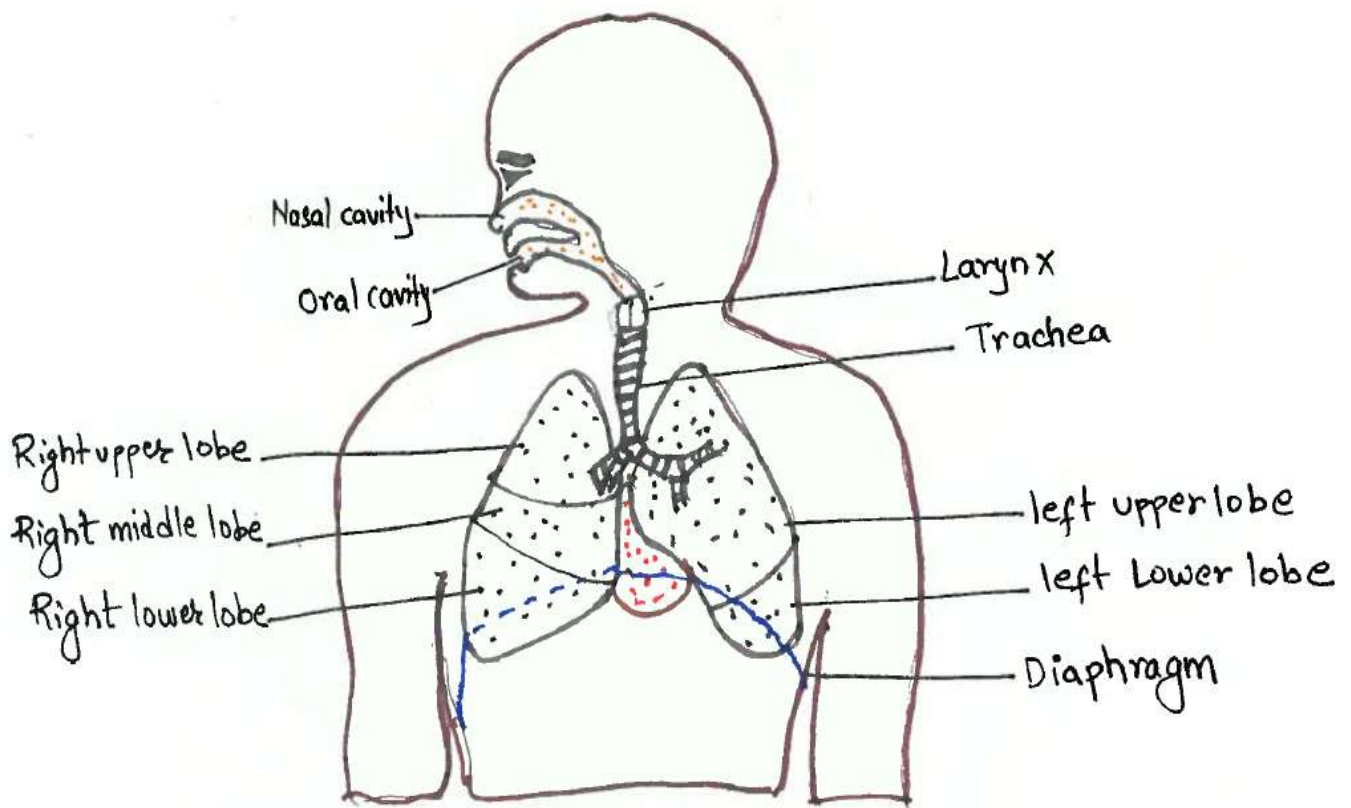


Figure 1.1 Gross human lung anatomy

The respiratory system can be divided into two functional zones, conducting airways (central) and respiratory airways (peripheral), with distinct structural elements that reflect their unique functions (**Figure 1.2**).

The conducting airways begin from the nose (nasal cavity), pharynx, larynx, trachea, ending in bronchi and bronchioles which are not directly involved in the gas exchanges. The structural components in the conducting zone help in the conduction of air, removal of debris and pathogens from the air, warming and humidifying incoming air. The air enters through the single tracheal tube that divides repeatedly to form airways of ever decreasing diameter giving rise to primary bronchi, secondary bronchi and tertiary bronchi (Young, O'Dowd, & Woodford, 2014). The trachea extends from the larynx towards the lungs which is surrounded and supported by 15-20 U-Shaped rings of hyaline cartilage, pieces which are connected by dense connective tissue (**Figure 1.2**). These rings of cartilage provide the rigidity to the airway preventing it from collapsing during inhalation and exhalation.

The inner layers of the trachea wall consist of a variety of epithelial cell types; pseudostratified columnar epithelial cells with cilia, goblet cells, and basal cells. These epithelial cells are supported by a connective tissue layer also called the lamina propria which contains numerous glands. Under the lamina propria there is submucosa containing mucous glands. In the proximal trachea goblet and basal cells are more common whereas ciliated columnar cells are more common on the

distal trachea where tracheal narrows nears its bifurcation (Suttie, Leininger, & Bradley, 2018). Goblet cells are glandular cells producing mucin which helps to moisten and protect the airways from potentially harmful foreign airborne particles. The basal cells lie on the basal lamina beneath the other cells and it has been suggested that basal cells function as stem cells for repair of epithelial cells damage (Evans, Cox, Shami, Wilson, & Plopper, 1989; Treuting, Dintzis, Frevert, Liggitt, & Montine, 2012). The ciliated epithelium moves in a coordinated fashion to drive inhaled foreign particles toward the upper respiratory tract (**Figure 1.3**). The trachea divides into right and left primary bronchi, and the primary bronchi enter the lung at the hilum. The primary bronchi keep branching giving rise to secondary bronchi then to tertiary bronchi forming a bronchial tree. The tertiary bronchi branches into smaller airways called bronchioles which are about 1mm in diameter (**Figure 1.3**) (Fails, Magee, & Frandson, 2018). Most cells in the terminal bronchus are the Clara cells. The bronchioles further branches until they become the tiny terminal bronchioles which mark the end of conducting airways and do not take part in gas exchange. There are more than 1000 terminal bronchial in each lung. The muscular walls of the bronchioles do not contain cartilage like those of bronchi, but the muscular wall can change the size of the tubing to increase or decrease airflow the tube. The terminal bronchioles lead to respiratory bronchioles then to alveolar ducts, and finally terminating into a dilated spaced called alveolar sacs which open into the alveoli (**Figure 1.2 and 1.3**) (Wheater & Burkitt, 1987). Respiratory cells are comprised of ciliated, cuboidal cells and a small number of non-ciliate cell Clara cells, but devoid of goblet cells. The epithelium cells in the airways undergo a further transition from

that of terminal bronchioles making Clara cells the predominant cell types in the peripheral respiratory system (Treuting et al., 2012; Wheater & Burkitt, 1987). Respiratory airways facilitate gas exchanges within respiratory bronchioles, alveolar ducts, alveolar sacs and alveoli (**Figure 1.3**) (Hislop, 2002; Rawlins, 2011). An alveolus is a grape-like sac consisting of a pocket which is lined with flattened epithelial cells, and each alveolus is surrounded by a rich network of pulmonary capillaries. The alveolar walls consist of surface epithelium, connective tissue, and blood vessels.

Epithelial cells form a continuous lining of the alveolar wall, consisting of two cells types Type I and Type II pneumocytes. Type I pneumocytes are the squamous epithelial cells which are flat cells covering approximately ninety-five of the alveolar surface areas, and these cells are directly involved in gas exchanges between the numerous alveoli and the blood (Wallig, Haschek, Rousseaux, Bolon, & Mahler, 2018) (**Figure 1.3**). Type II pneumocytes are cuboidal cells, and these cells occupy a much smaller proportion (approximately five percent) of the alveolar surface area. Type II cells are involved in secretion of a surface-active material called surfactant which reduces the surface tension of the alveoli. Alveolar macrophages (AMs) are phagocytic cells found in the interstitial compartment of alveoli but not in the alveolar wall. Alveolar macrophages engulf particles and infectious agents and function as an antigen presenting cell that regulates host defense and lung homeostasis (Laskin, Sunil, Gardner, & Laskin, 2011).

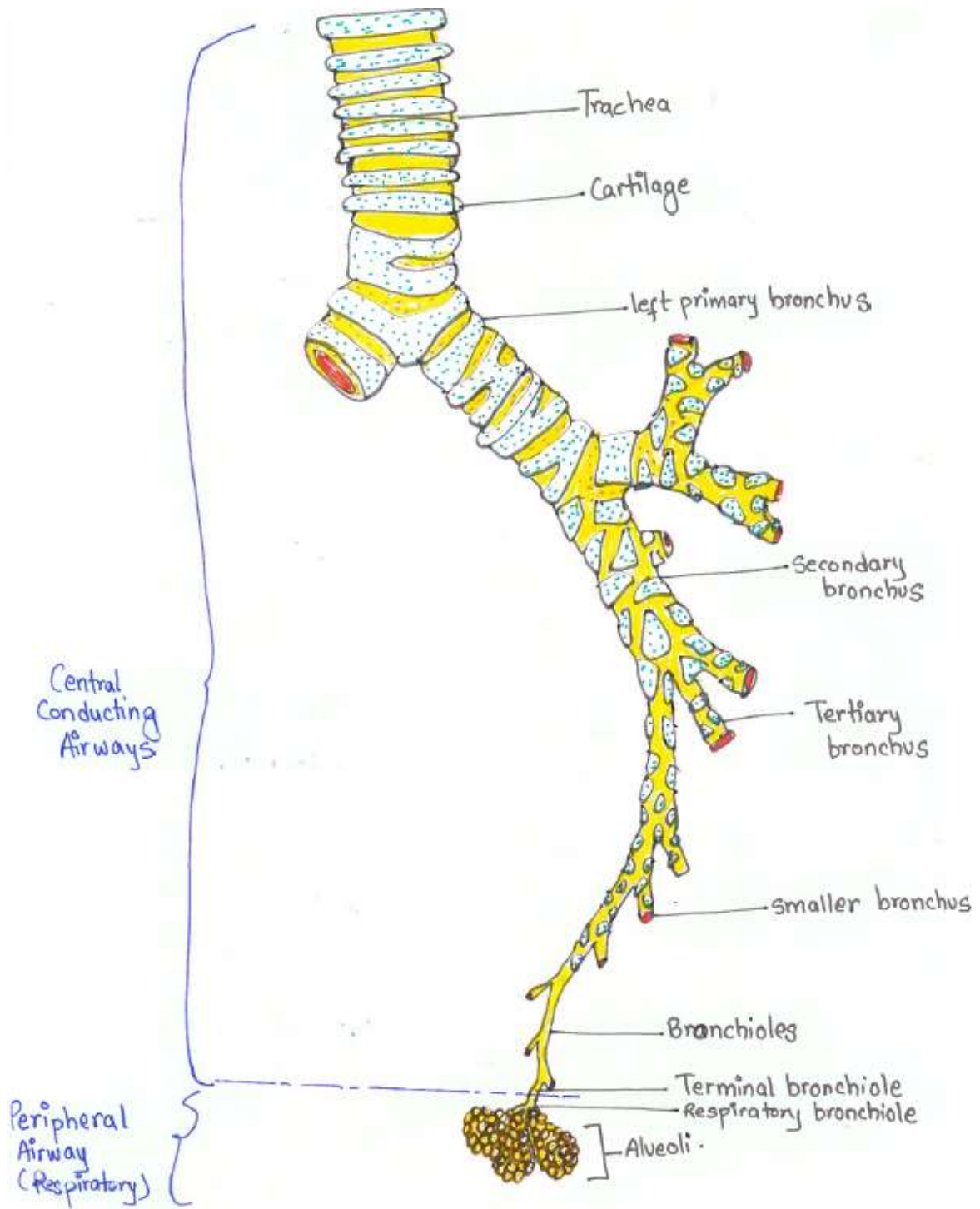


Figure 1.2. Structures of the respiratory zone with central and peripheral airways of the lung.

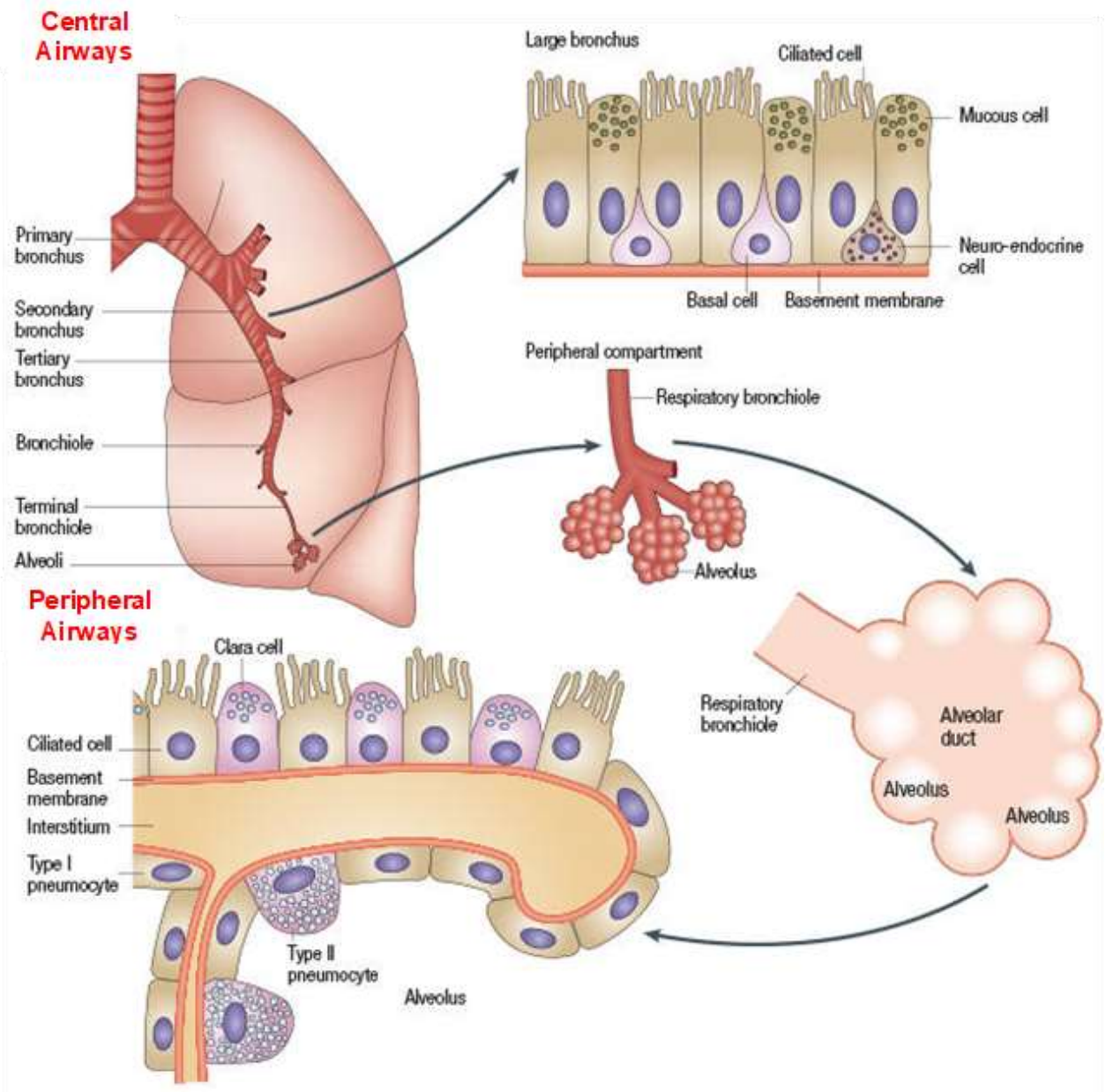


Figure 1.3. Graphic illustrations of cell types in peripheral airways and central airways. Peripheral airways comprise of Clara cells, Type I and II pneumocytes. Majority surface area of the lung is covered

by Type I cell pneumocytes. Central airways comprise primarily of basal cells, goblet cells, ciliated pseudostratified epithelium, and rare pulmonary neuroendocrine cells (PNECs). Adapted (Sun, Schiller, & Gazdar, 2007).

The connective tissue is a supporting layer beneath the epithelium and surrounding the blood vessels of the alveolar wall. The structural support provided by these connective tissues provides the framework for the lung. The supporting layer consists of fine reticular, collagenous and elastic fibers with occasional fibroblasts (Wheater & Burkitt, 1987).

The blood vessels are comprised of interconnected capillaries around each alveolus. The arrangement provides an interface of minimal thickness between alveolar air and blood (Wheater & Burkitt, 1987).

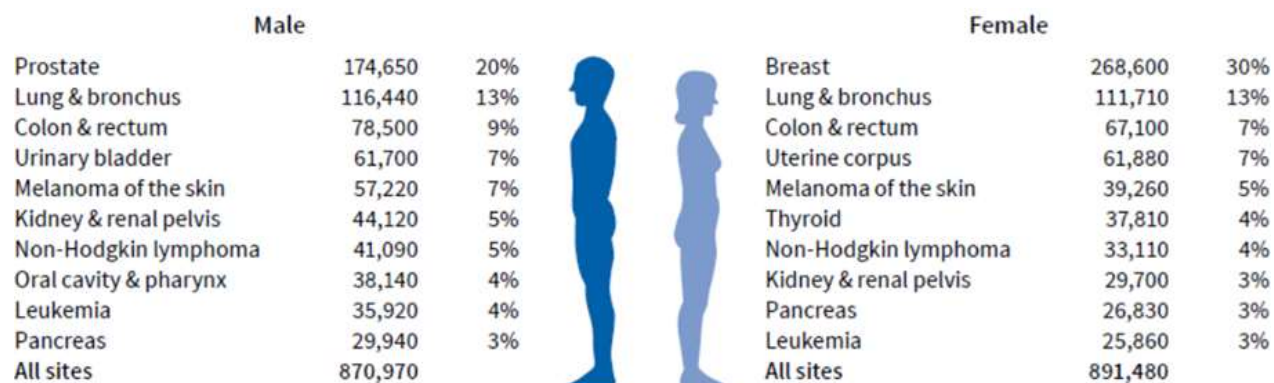
1.2 Cancer and Lung Cancer Statistics

In normal adult tissues, cell division is balanced by cell loss (cell death) and it is tightly regulated for proper tissue homeostasis thus maintaining normal tissue architecture and function. Tissues need maintenance throughout the repair of wounds and replacement of cells that have suffered abrasion by precise control of stem cells (Biteau, Hochmuth, & Jasper, 2011). Depending on the type of tissues, the turnover rates of cells can be very different. Under normal conditions, cell turnover in the lung is relatively low, at least compared with tissues such as the intestine and skin (Blenkinsopp, 1967; Rawlins, Ostrowski, Randell, & Hogan, 2007). The imbalance between cell division and failure of self-elimination can lead to uncontrolled cell division giving rise to a *neoplasm* (a new growth). As long as the neoplastic cells remain confined to its original location not invading the surrounding tissue it is called a benign tumor, and when cells have acquired the ability to invade the surrounding tissue then it is then called malignant (Alberts, 2015).

Carcinogenesis is considered as a multistep process in humans as a single alteration of either an oncogene or tumor suppressor by itself cannot lead to the formation of a tumor. It widely considered that cells accumulate multiple genetic alterations over an extended period of time resulting in molecular changes with the increasing capacity of cell proliferation, survival, invasion, and metastasis. It has been well documented such multistep process in breast cancer, colorectal cancer, and lung cancer as a series of increasingly abnormal stages ending with metastatic

cancer (Beckmann, Niederacher, Schnurch, Gusterson, & Bender, 1997; Fearon, 1991; Sato et al., 2013). In this multiple step process normal cells acquire traits such as sustaining proliferative signaling, evading growth suppressors, resisting cell death, enabling replicative immortality, activating invasion and metastasis, deregulating cellular energies, avoiding immune destruction and inducing angiogenesis which together transforms normal cells into a malignant tumor enabled by genome instability and mutations as well as tumor-promoting inflammation signaling (Hanahan & Weinberg, 2011b).

Estimated New Cases



Estimated Deaths

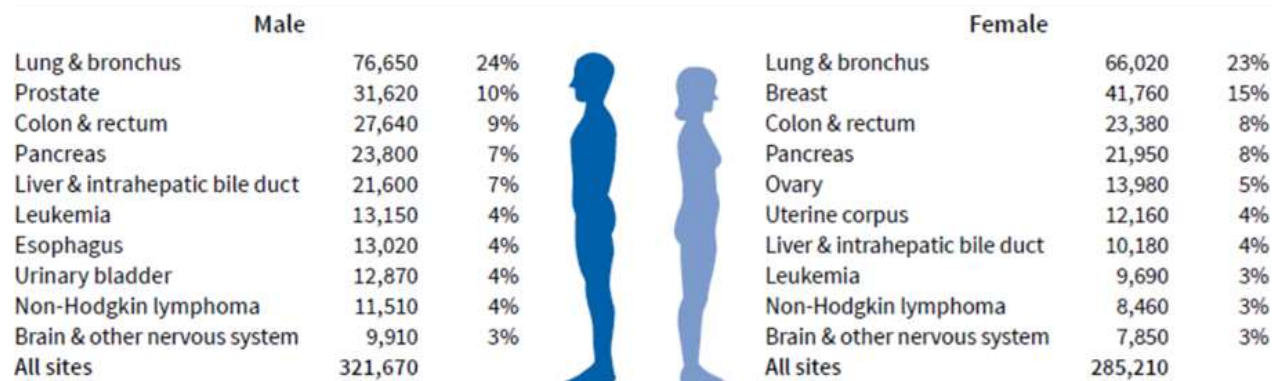
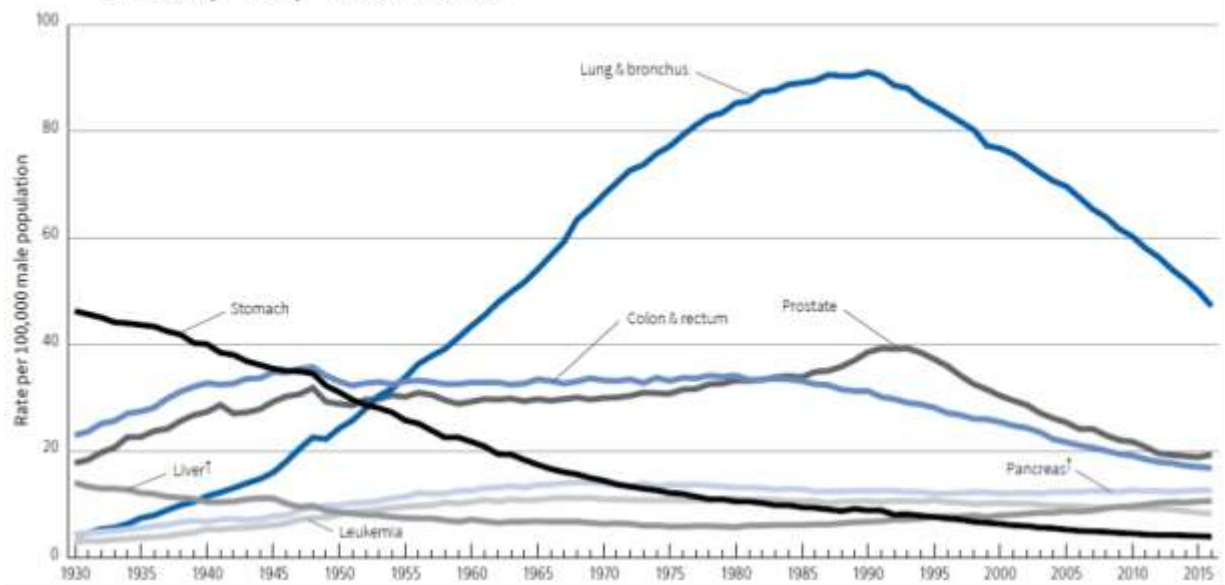


Table 1.1. Estimated new cancer cases and deaths in the United States in 2019. Adapted from American Cancer Society, 2019.

Cancer is considered as an age-related disease since 80% of all cancers diagnosed in the United States are among people 55 years age or older (ACS, 2019). It is estimated that 39 out of 100 men and 38 out of 100 women would develop cancer during their lifetime (Siegel, Miller, & Jemal, 2019b). Cancer is the second most common cause of death in the United States after heart disease. In 2019, it was estimated that there will be about 1.7 million new cases of cancer diagnosed, and approximately 606,880 people are expected to die due (Siegel, Miller, & Jemal, 2019a)to cancer. Prostate cancer is the most common cancer among males with 174,650 (20%) whereas breast cancer is the most common among females with 268,600 (30%) **(Table 1.1)**.

Lung and bronchus cancer is the second highest newly diagnosed cases in both male and female population (ACS, 2019)(Siegel et al., 2019a). An estimated 228,150 new cases of lung cancers will be diagnosed accounting for 14% and 13% of all new cases in males and females respectively in the United States. The average age for lung cancer diagnosis is between 68 to 70 years (Latimer & Mott, 2015). Lung cancer is the leading cause of cancer-related death in the US as of 2018 among both males and female population. It is estimated that approximately 142,670 deaths will occur from lung cancer (ACS, 2019). According to the American Cancer Society, the combined 5-year relative survival rate for lung cancer is 19% (16% for men and 22% for women).

Trends in Age-adjusted Cancer Death Rates Males, US, 1930-2016



Trends in Age-adjusted Cancer Death Rates Females, US, 1930-2016

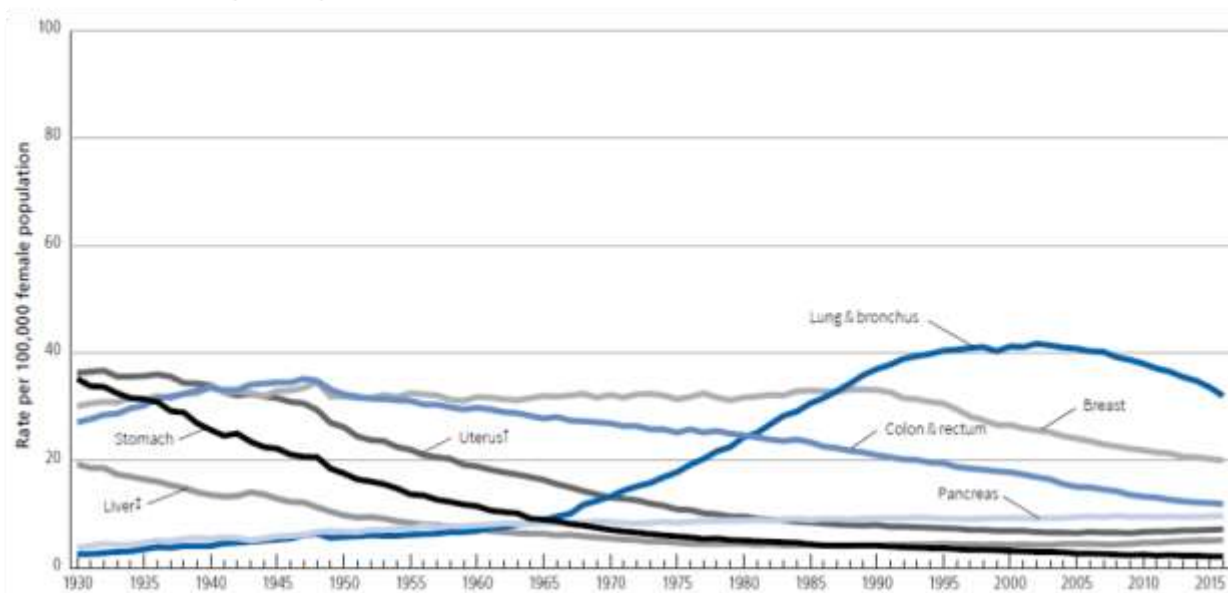


Figure 1.4. Trends in cancer death by sex. Adapted from American Cancer Society, 2019

The 5-year survival rate for lung cancer that is at the localized stage is 56% which drastically decreases to 5% if cancer is located at a distant site during diagnosis (**Table 1.2**) (ACS, 2019). The local stage is characterized with malignant cancer confined entirely to the organ of origin, regional stage as characterized by malignant cancer which has extended beyond the limits of the organ of origin directly into surrounding tissue, involves regional lymph nodes and has both regional extension and involvement in the lymph nodes. Finally, the distant stage is characterized as malignant cancer that has spread to the parts of the body remote from the primary tumor. Several risk factors such as smoking, exposure to radon gas, asbestos, exposure to certain metals (chromium, cadmium, arsenic), exposure to secondhand smoke, radiation, and air pollution have been linked to an increased risk of lung cancer (de Groot & Munden, 2012). Cigarette smoking is the leading factor that has been associated with an increase in lung cancer as 81% of lung cancer cases in the United States are associated with smoking history. Lung cancer deaths have been in decline since 1980 among men and since the 2000s in women (**Figure 1.4**). Such a declining trend in cancer mortality is due to a reduction in smoking prevalence, advances, and improvement in early detection and treatment of cancer.

Stages	5-year Relative Survival Rates (%)
All Stages	19%
Local	56%
Regional	30%
Distant	5%

Table 1.2. Five-year Relative Survival Rates by Stage of Diagnosis, US (2008-2014). (Adapted from American Cancer Society, 2019)

1.3 Pathology of Lung Cancer

The lung tumor is the result of a number of molecular aberrations such as oncogenic alterations, epigenetic changes, telomere alterations, micro-RNA modifications and tumor-suppressing alterations (Ganti & Gerber, 2013). In whole genome studies of patient cohorts (never smokers and oligo-smoker) presented molecular aberrations that contributed to the development or progression of lung cancer (**Table 1.3**) (Kris et al., 2011). The development of lung cancer from normal lung parenchyma is a multistep process. Histologically, normal epithelial cells transform to atypical adenomatous hyperplasia, squamous dysplasia/carcinoma in situ or diffuse idiopathic pulmonary neuroendocrine cell hyperplasia – precursor for the development of both atypical and typical carcinoids, small cell lung cancer (SCLC), and large cell neuroendocrine carcinoma (Aguayo et al., 1992; Inamura, 2017).

Lung cancer is classified into two main histological categories: small cell lung carcinoma (SCLC) accounting for 15-20% of all lung cancers and non-small cell lung carcinoma (NSCLC) accounting for 80-85% for all lung cancers (Sher, Dy, & Adjei, 2008). NSCLS are further subcategorized into adenocarcinoma, squamous cell carcinoma (SCC), and large cell carcinoma (LCC). Adenocarcinoma accounts for approximately 40% of all lung cancer cases, and it is the most common subtype of lung cancer in nonsmokers (Ganti & Gerber, 2013). Adenocarcinomas are

characterized by glandular differentiation and or mucin production of malignant epithelial tumors.

Squamous cell carcinoma (SCC) accounts for approximately 30% of all lung cancer, and it tends to be found in the middle of the lungs as 60% of cases of SCC arise from the central bronchi (segmental, lobar, main) while the remaining arise in the peripheral lung (Ganti & Gerber, 2013; Heist et al., 2012). SCC is strongly associated with cigarette smoking compared to other lung cancer types (Ettinger et al., 2013)

Small cell lung carcinoma (SCLC) comprises 14% of all lung cancers in the US, and two-thirds of SCLC are present as a perihilar mass (Tanoue & Matthay, 2011). SCLC is an aggressive carcinoma characterized by its unique microscopic appearance as small tumor cells with negligible cytoplasm, nuclear molding, absence of inconspicuous nuclei, high nuclear /cytoplasmic (N/C) ratio, and high mitotic rate (Ganti & Gerber, 2013). SCLC is also strongly associated with cigarette smoking.

Large cell carcinoma (LCC) accounts for 3% of all lung cancer, and LCC mostly rise on the periphery of the lung (Weinberger, Cockrill, & Mandel, 2019). LCC is an undifferentiated NSCLC which lacks the features of adenocarcinoma or squamous cell carcinoma or small cell carcinoma. Similar to SCC and SCLC, LCC is also associated with smoking.

1.4 Molecular Aberrations in Lung Cancer

The most common molecular changes in lung cancer are *KRAS*, *EGFR*, *ALK* rearrangement, and *BRAF* (**Table 1.3**). *KRAS* is a member of the Ras family of GTPases that stimulate several pathways involved in cellular growth and cell survival (Ganti & Gerber, 2013). *KRAS* is the most commonly mutated member of RAS family in lung cancer, and only a few cancers have *HRAS* or *NRAS* mutated (Suzuki, Orita, Shiraishi, Hayashi, & Sekiya, 1990). *KRAS* acquires its tumorigenic ability when it is mutated resulting in constitutive activation causing a marked upregulation of kinases by RAS signaling. The activating mutation of the *KRAS* is strongly associated with tobacco smoking (Dogan et al., 2012; Luo & Lam, 2013). The incidence of *KRAS* mutations in NSCLC ranges from 8% to 24% (De Roock, De Vriendt, Normanno, Ciardiello, & Tejpar, 2011; Ganti & Gerber, 2013). To date, there are no targeted therapies available for NSCLC patients with *KRAS* mutations (Chan & Hughes, 2015).

The Epidermal growth factor receptor (EGFR) belongs to a family of transmembrane receptor tyrosine kinases (TK) presented on the surface of both normal cells as well as in lung cancer cells. Either through overexpression or molecular alteration, EGFR can activate the TK pathway. EGFR mutations initiate hyperactivation of EGFR tyrosine kinases without binding of specific ligands resulting in multiple cellular processes such as cell proliferation, cell survival, cell motility and cell invasion (Scaltriti & Baselga, 2006). EGFR-mutated lung cancers

account for 15% to 20% of all lung adenocarcinoma diagnosed in the United States (Keedy et al., 2011). Most mutations in EGFR clusters in exons 19 and 21 each accounting for approximately 45% of EGFR mutations (Ganti & Gerber, 2013). EGFR can be targeted for treatments in non-small cell lung cancers.

Gene	Molecular Aberrations
KRAS mutation	25%
EGFR mutation	23%
ALK rearrangement	6%
BRAF mutations	3%
PIK3CA mutation	3%
MET amplification	2%

Table 1.3. Driver mutations identified in lung adenocarcinoma of tumor specimens from 1,00 patients. (Kris et al., 2011)

The ALK (anaplastic lymphoma kinase) rearrangement has been identified in 5-6% of NSCLC cases as a driving mutation (**Table 1.3**) (Devarakonda, Morgensztern, & Govindan, 2015; Kris et al., 2011). ALK is a transmembrane tyrosine kinase receptor in the insulin receptor superfamily which can be activated constitutively by rearrangement, amplification and point mutation. Unlike EGFR and KRAS, ALK expression is low throughout adult human life and not expressed in normal lung tissues. This molecular aberration appears to be more common among young patients, never or light smokers diagnosed with adenocarcinoma mutually exclusivity with EGFR and KRAS mutations (Du, Shao, Qin, Tai, & Gao, 2018; Ganti & Gerber, 2013). Targeted therapies have shown clinical efficacy in treating NSCLC patients harboring ALK rearrangement compared to conventional chemotherapy (Shaw et al., 2013; Shaw et al., 2011).

BRAF mutations are present in approximately 2-4% of lung adenocarcinomas constitutively activating the cell signaling pathways (serine-threonine kinase) activating important cell functions, including cell proliferation and survival (**Table 1.3**) (Kris et al., 2011; Schmid et al., 2009). *BRAF* mutations among adenocarcinomas cases are more common among former and heavy smokers (Sasaki et al., 2012). The specific mutation (BRAF V600) is the most common mutation in *BRAF* among lung cancers cases, and treatment with dabrafenib and trametinib has shown to be very effective in the treatment of patients harboring the *BRAF* V600 mutation (Anguera & Majem, 2018).

MYC is one of the major downstream effectors of the RAS/RAF/MEK/MAPK pathways. As transcription factor *MYC* regulates a spectrum of cellular functions, and it belongs to the family to “super transcription factors” that potentially regulates the transcription of at least 15% of the entire genome (Dang et al., 2006). There are three members of the *MYC* family (*MYC*, *MYCL*, and *MYN*). The aberrant expression of *MYC* is commonly found in lung cancer, and in 30%-50% of small cell lung cancers (SCLC) have *MYC* overexpression (Johnson, Brennan, Ihde, & Gazdar, 1992; Lorenz, Friedberg, Paulus, Oesch, & Ferlinz, 1994; Sos et al., 2012). *MYC* amplification is associated with poor survival in patients with small cell lung cancer (Alves Rde, Meurer, & Roehe, 2014).

The loss of the tumor suppressor gene (TSG) function plays important roles in lung adenocarcinoma development either through genetic mutation or epigenetic silencing of the TSG. The commonly inactivated TSGs in lung cancer are *TP53*, *RB1*, *STK11*, *CDKNA2A*, *FHIT*, *RASSF1A*, and *PTEN*. The most frequently mutated TSG in lung cancer is *TP53*: 46% in lung adenocarcinoma and 81% in squamous cell carcinoma (Gibbons, Byers, & Kurie, 2014; Greulich, 2010). The p53 protein is a transcription factor which controls responses to cellular stresses including DNA damage, hypoxia, and oncogene activation. The mutations in *TP53* in lung cancer is associated with smoking history in patients. Retinoblastoma (*RB*) is also a tumor suppressor gene which is absent or mutated in lung cancer, approximately 90% of SCLCs have alterations in the regulation of RB protein (pRB) as compared to 10-15% of NSCLCs (Otterson, Kratzke, Coxon, Kim, & Kaye, 1994).

1.5 Risk Factors for Lung Cancer

There are several risk factors that are associated with lung cancer such as tobacco smoking and second-hand smoke. In addition exposure to agents such as asbestos, radon, arsenic, and radiation (Alberg & Nonemaker, 2008) are associated with an increased risk of lung cancer. Smoking is the number one risk for lung cancer as 85% of all lung cancers are related to cigarette smoking. People who smoke have a risk for lung cancer on average 10-fold higher than in never smokers. The second-hand exposure of nonsmokers to smoke in household results in a 30% increased likelihood of developing lung cancer compared to nonsmokers living with nonsmokers. The more recent decrease in the incidence of lung cancer-related deaths in the United States has been attributed to the decrease in smoking prevalence (**Figure 1.4**) (Ganti & Gerber, 2013).

The exposure to agents such as asbestos has also been associated with increased risk of lung cancer. Asbestos is a naturally occurring fiber found in rocks and soil. Asbestos is a well-known occupational carcinogen, and there are six distinct types of asbestos. The continuous inhalation of asbestos particles increases the risk of lung fibrosis, lung cancer, and pleural and peritoneal malignant mesothelioma (Mossman, Bignon, Corn, Seaton, & Gee, 1990; Robinson & Lake, 2005). The latency period from asbestos exposure can range from 10 to 40 years before the diagnosis of lung cancer (Heintz, Janssen-Heininger, & Mossman, 2010).

Radon is a radioactive gas which is produced naturally from decaying of uranium. When radon atoms spontaneously decay they emit both highly ionizing particle and sparsely ionizing gamma rays in the process (Lantz, Mendez, & Philbert, 2013; Scott, 2011). When radon gas is inhaled, it can result in damage to DNA of the respiratory epithelium. Radon exposure is the second leading cause of lung cancer, and the risk is higher for smokers than nonsmokers as 86% of radon-related lung cancer deaths are current and former smokers (Lubin & Boice, 1997). Small cell carcinoma and squamous cell carcinoma of the lung are strongly correlated with radon exposure (Krewski et al., 2005; Pershagen et al., 1994). The radon exposure in the general population is substantially less than the occupational exposure among the uranium miners (Ganti & Gerber, 2013).

More than half of cancer patients are treated with ionizing radiation (IR) during the course of their disease, and workers in hospitals and clinics are exposed to IR when performing diagnostic imaging exams for appropriate care. There is a strong correlation between radiation therapy in pediatric and young adults' patients and the development of secondary malignancies later in life (Manem, Kohandel, Hodgson, Sharpe, & Sivaloganathan, 2015; Ng & Shuryak, 2015). Additionally, several studies have demonstrated the association between exposure to ionizing radiation and lung cancer (Jacob et al., 2009). The Life Span Study (LSS) of Japanese atomic bomb survivors have provided a greater understanding of the risk of lung cancer due to ionizing radiation (Grant et al., 2017). The risk of lung cancer due to ionizing radiation is discussed in the following section.

1.6 Introduction to Radiation

Radiation is the emission or transmission of energy that comes from the originating source and travels through space or a medium in the form of waves or particulates. Radiation can be ionizing or non-ionizing depending on how it affects the matter. Radiation is called ionizing radiation if it carries sufficient energy to eject one or more orbital electrons from atoms or molecules (Hall & Giaccia, 2019). Ionizing radiation can be classified as either electromagnetic radiation or particulate radiation. Electromagnetic radiation consists of energy which is propagated through space or material in the form of electromagnetic waves such as radio waves, infrared waves, X-rays, and gamma-rays (γ). Particulate radiation consists of electrons, protons, α -particles, neutrons, and heavy charged particles (Hall & Giaccia, 2019). The energy carried by various forms of radiation is generally defined using linear energy transfer (LET) which refers to the amount of energy deposited per unit length ($\text{keV}/\mu\text{m}$). The LET of radiation depends on the charge and velocity of the ion. Radiation can be categorized as low LET (sparsely ionizing) or high LET radiation (densely ionizing) and in general LET values greater than $10 \text{ keV}/\mu\text{m}$ are considered high LET radiation (Okayasu, 2012).

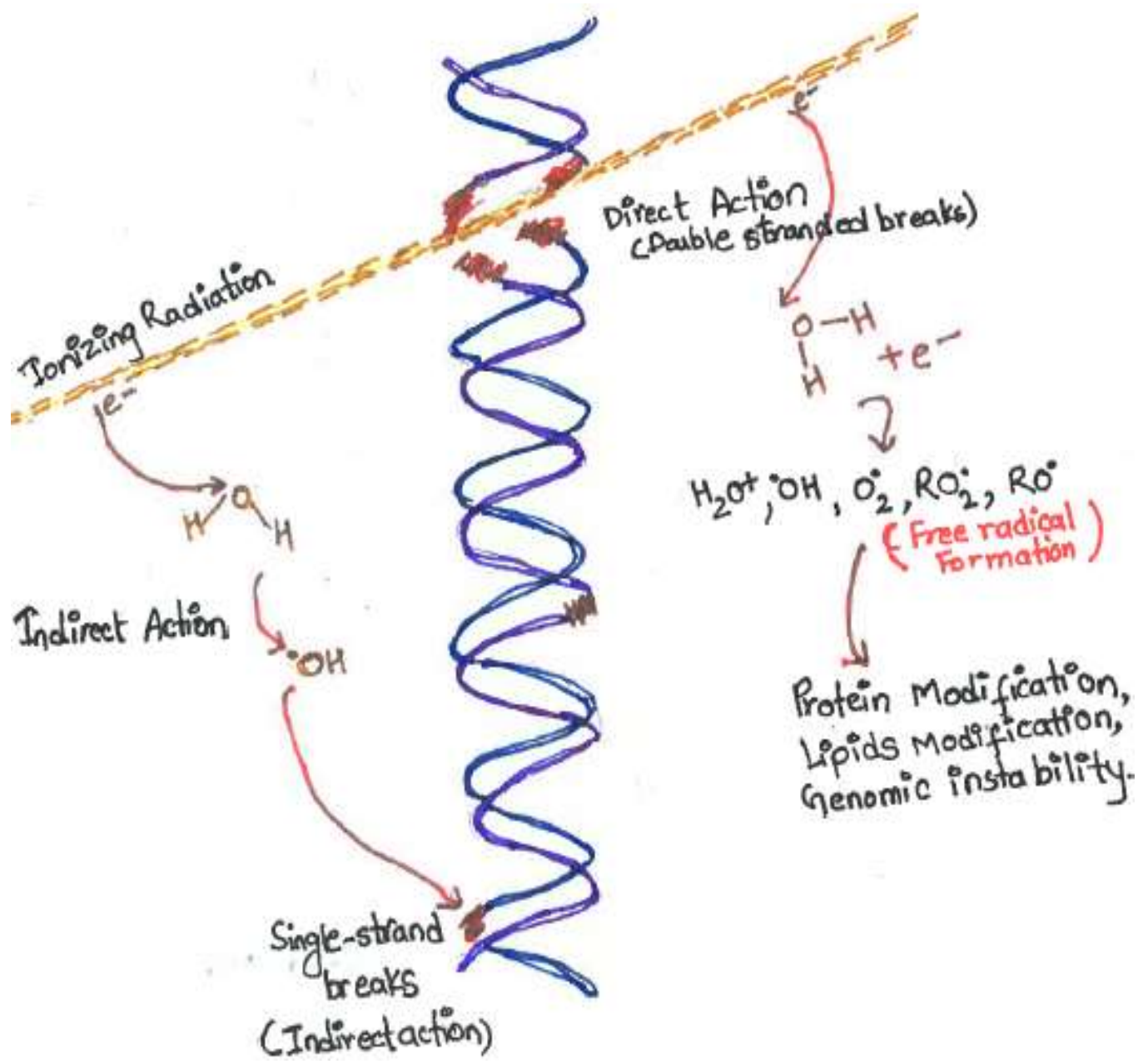


Figure 1.5. Direct and indirect action of ionizing radiation.

As the use of radiation in medicine is becoming more prevalent, it is important to understand how the absorbed dose of different types of radiation impacts the subsequent biological response. The main biological effects due to radiation exposure are caused by damage to deoxyribonucleic acid (DNA). When radiation is absorbed by biological material, it can interact directly with the critical cellular targets disrupting its molecular structure **(Figure 1.5)** (Hall & Giaccia, 2019). Through this direct action of radiation, it can induce base damage, single-strand breaks, double-strand breaks, and DNA protein cross-links. If irradiated cells do not repair correctly, it can induce carcinogenesis and other abnormalities (Baskar, Dai, Wenlong, Yeo, & Yeoh, 2014). The direct action of radiation is a dominant process when radiation exposure occurs with high linear energy transfer (LET) such as α -particles, neutrons, and high charge (Z) and energy E (HZE) particles.

Alternatively, the absorbed radiation in the cell may interact with other atoms and molecules within the cell producing free radicals and other reactive species (Hall & Giaccia, 2019). Most commonly water radiolysis can occur in the cells as 80% of a cell is composed of water. The ionization of water can produce hydroxyl radicals which can diffuse in the cells and damage other critical targets resulting in DNA damage. Low-LET ionizing radiations such as X-rays and γ -rays causes 60% the cellular damage by indirect effects **(Figure 1.5)** (Barcellos-Hoff, Park, & Wright, 2005). The oxidative DNA damage in tumor suppressors genes such as *TP53* and *RB* may induce malignancies in combination with other alterations (Hendry, 2001; Robles, Linke, & Harris, 2002).

The radiation-induced effect can occur within seconds to years depending on the consequences involved. Radiation-induced cell death may be expressed within an hour to days after radiation exposure while oncogenic damage may be delayed for years (**Figure 1.6**) (Hall & Giaccia, 2006; Olcina & Giaccia, 2016).

Classic Paradigm of Radiation Injury

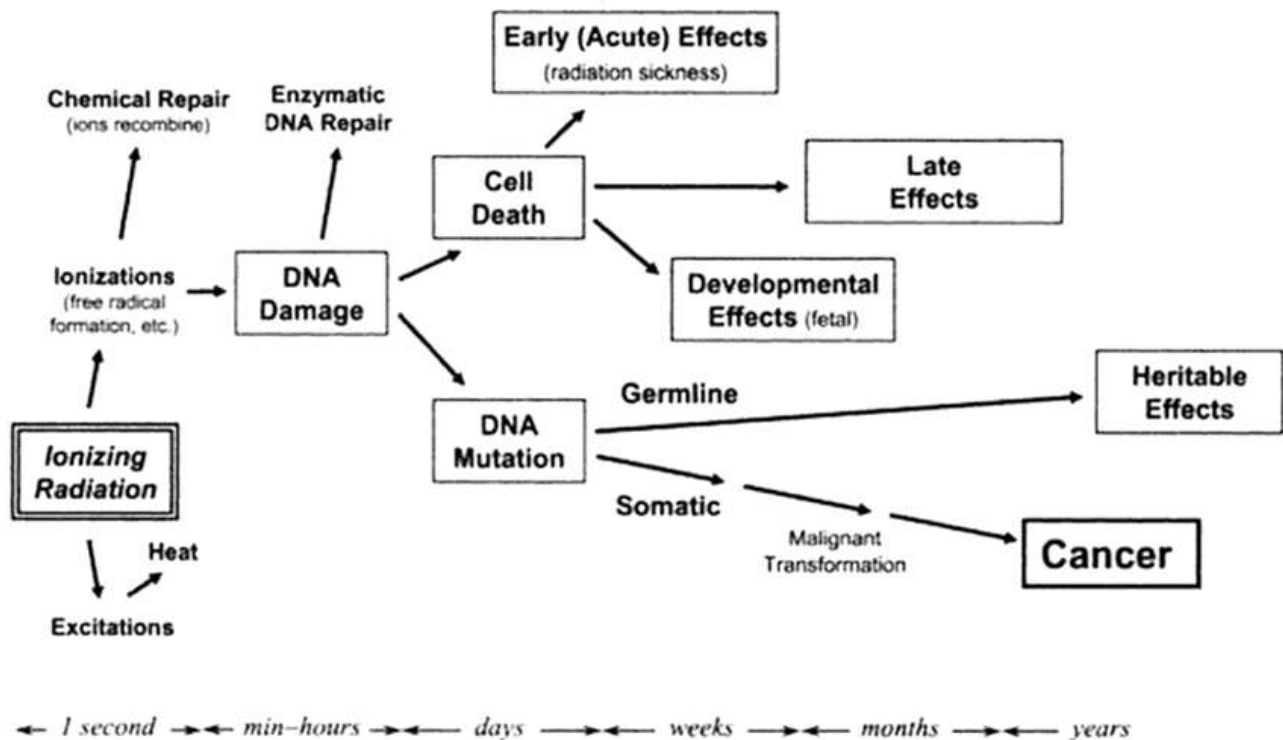


Figure 1.6. Illustration of the generally accepted biological effects after absorption of ionizing radiation. (Hall & Giaccia, 2006) modified.

1.7 Space Radiation and Risk of Lung Cancer

The health risks related to space radiation exposure such as carcinogenesis, degenerative diseases – cardiovascular, central nervous system damage, acute radiation syndrome on astronauts represent a major limiting factor for long-term space missions (Chancellor, Scott, & Sutton, 2014). Unlike terrestrial radiation, such as X-rays or β or γ -rays, space radiation composed of high-energy (E) protons and high charge (Z) particles (HZE) nuclei has the capacity to penetrate both shielding and human tissues. The main source of radiation in space includes galactic cosmic rays (GCR), solar particle events (SPE) and a secondary particle that arise from interactions of spacecraft shielding and tissues (**Figure 1.7**) (Sridharan et al., 2015). Ionizing radiation (IR) is a very well-known carcinogen and, radiation-induced carcinogenesis is considered one of the major health risks for long-duration human space missions beyond Low Earth orbit (LEO) (Norbury et al., 2016).

The GCRs, which are considered to originate from high-energy supernova explosions, consist of protons and HZE particles with charge number ranging from 1 to 28 and energies from $<10\text{MeV/u}$ to $>50\text{ GeV/u}$ (Cucinotta et al., 2001; M. Durante & Cucinotta, 2008). GCR consists of 2% electrons, 85.3% protons (hydrogen nuclei), 11.8% alpha particles (nuclei), and less than 1% of high charge (Z) and energy E (HZE) particles. Even though HZE particles account for less than 1% of GCR, they have high biological effectiveness as these heavy particles have high linear energy transfer (high-LET) values. HZE nuclei with enough energy can

penetrate a substantial thickness of shielding materials. The GCR exposure occurs at very low fluence rate: each cell in an astronaut's body being traversed by a proton and helium every few days and HZE nuclei about once every few months (Norbury et al., 2016). The irradiation of the mammalian cells with HZE particles can directly or indirectly damage biomolecules: lipids peroxidation, protein oxidation, oxidative alterations of mtDNA and nDNA as well as to results in inactivation of enzymes (M. Li et al., 2014).

The passage of HZE particles track has a unique pattern of energy deposition which induces clustered and complex DNA damage (double-stranded breaks (DSBs), single-stranded breaks (SSBs), and base damage) in the cells (**Figure1.8A**) (Simonsen, Wilson, Kim, & Cucinotta, 2000). The energy deposition by heavy ions is highly heterogeneous and dependent on the type and energy of the ion. These damages on DNA are hard to repair and can lead to genomic instability (Asaithamby et al., 2008; Li, Wang, Wang, Murnane, & Dynan, 2014). HZE particle radiation can give rise to secondary radiations from the atoms of the target as well as produce energetic electrons with its own tracks along the track of the primary particle on their own known as delta rays (δ -rays) (**Figure1.8B**) (Cucinotta, Wilson, Shinn, Badavi, & Badhwar, 1996). The range of δ -rays can vary depending on the velocity and mass of the particle, and δ -rays potentially can irradiate the adjacent cells to the cells directly irradiated by the primary particle track (**Figure1.8B**) (Cucinotta, Nikjoo, & Goodhead, 1998; Metting et al., 1988).

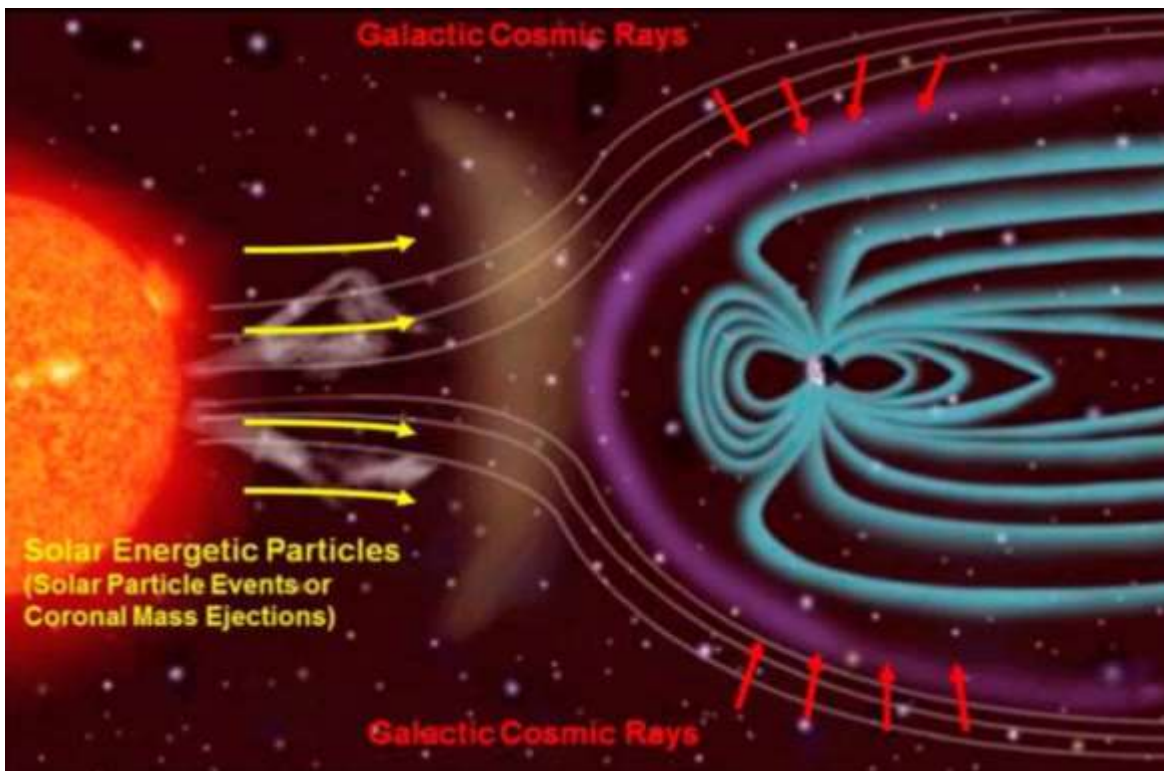


Figure 1.7. Space environment with a combination of galactic cosmic radiation (GCR) and (largely) proton radiation due to solar particle events (SPEs) (Chancellor et al., 2014).

Protons account for the vast majority of radiation in the space in the form of a Solar Particle Events (SPEs). Solar particle events (SPEs) are dangerous and unpredictable and can produce large quantities of energetic particles which can last from a few hours to several days, and the majority of the ejected particles consists of protons (McPhee, Charles, & United States. National Aeronautics and Space Administration., 2009). The majority of SPEs are harmless but SPEs with energies above 30MeV are a major concern to astronauts in shielded vehicles and habitats. SPEs exposures are intermittent and unpredictable whereas there is a constant presence of GCR in space. The high energetic SPE protons can also produce secondary intravehicular radiation similar to GCR (Chancellor et al., 2014).

The National Aeronautics and Space Administration (NASA) has set an acceptable level of risk at 3% for exposure-induced death for radiation carcinogenesis. The long-term space missions such as establishing a lunar colony and the Mars mission may exceed radiation risk limits beyond the acceptable levels of risk. (M. Durante & Cucinotta, 2008). In order to elucidate how space radiation exposure may translate into this increased carcinogenic risk, an understanding of how radiation impacts biological material is required. In different mouse models, investigators have demonstrated that high-LET radiation compared to low LET radiation result in a higher risk of tumorigenesis in the lung, liver, gastrointestinal tract and mammary gland (Delgado et al., 2014; Trani et al., 2014; Weil et al., 2009). The only available data from accidental exposure to ionizing radiation of survivors from Chernobyl accident and atomic bomb survivors showed increased risks of

cancers in different organs, and the greatest risk was for leukemia, lung, stomach, liver, and bladder cancer (Grant et al., 2017; Saenko, Thomas, & Yamashita, 2017).

As previously discussed radiation is one of the risk factors for lung cancer. The lung has a large surface area which makes it a prominent target for radiation exposure, and remarkably susceptible to radiation-induced cancer (Delgado et al., 2014; Luitel et al., 2018). There are considerable uncertainties of cancer risk estimates from chronic space radiation exposures, as the space radiation consists of a wide variety of ion species with a continuous range of energies. Therefore, experiments need to be designed using multiple ions with different energies to simulate the space environment to understand the potential health effects on astronauts.

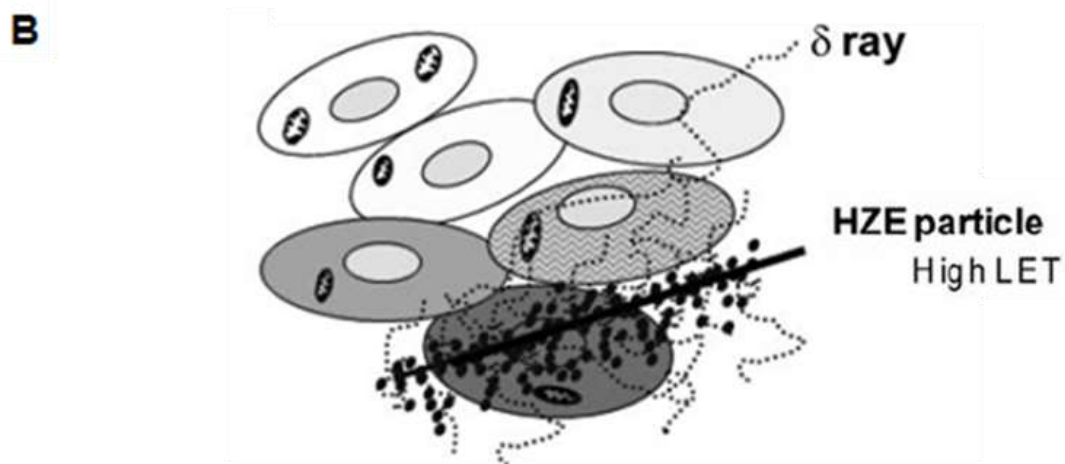
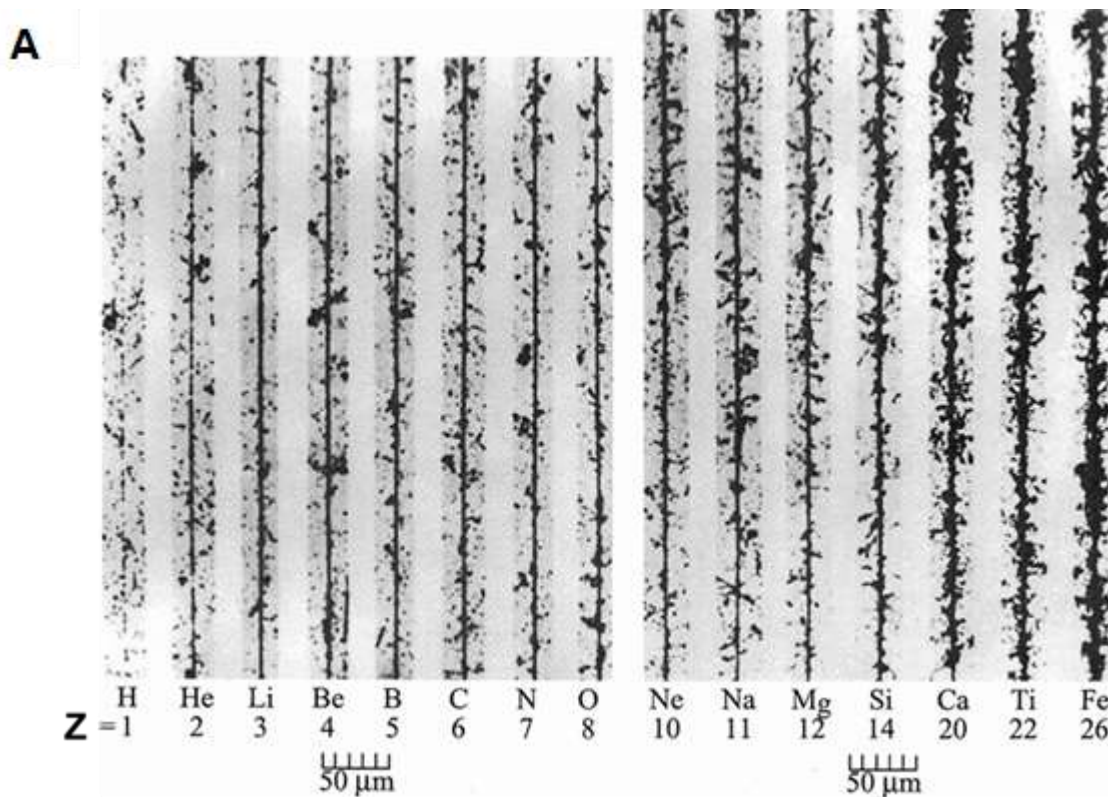


Figure 1.8. Comparison of particle tracks and delta (δ) rays from the primary track. (A) tracks from different ions, from protons to iron. (B) δ rays resulting from the interaction of primary HZE particles with the target materials. (M. Li et al., 2014).

1.8 Lung Cancer Mouse Model

Despite the evidence that terrestrial ionizing radiation can induce lung carcinogenesis, the mechanism of space radiation-induced lung cancer still remains an important area for research. Several mouse models of lung cancer have been developed by expressing oncogenes and deleting tumor suppressors to recapitulate human lung cancer progression, and they have been powerful experimental models to dissect the molecular pathways.

To understand the radiation-induced cancer risk we are using K-ras^{LA1} mouse model. Dr. Tyler Jacks and his colleagues reported this mouse model (K-ras^{LA1}) with a latent mutant K-ras gene in the endogenous gene locus. K-ras^{LA1} carries a targeted latent 'hit-and-run' allele that is activated by spontaneous *in vivo* recombination events. Thereby half of the recombination events result in normal *K-ras* alleles and the other half inactivated allele (*K-rasG12D*) (Leisa Johnson¹, 2001). In this model, there is a sporadic initiation of *K-ras* oncogene (through *in vivo* recombination) which gives rise to scattered cells that express the constitutively active *K-ras* gene within the authentic locus of the endogenous chromosomal site under normal physiological control. These mice develop lesions that are spontaneously activated, and progress into varying grades of tumors in alveolar type II cell lineage, forming hyperplasia/dysplasia, adenoma, adenoma with atypia, and invasive carcinoma (Figure 1.9 B).

With the activation of oncogenic K-ras, the life span of the LA1 mice significantly decrease compared to their wildtype littermates; most LA1 K-ras mice die by the age of 500 days in contrast to wildtype mice which can survive over 800 days (**Figure 1.9A**). This decrease in lifespan is most likely due to the significant tumor burden sustained by the lungs of LA1 K-ras mice even though the direct cause of death may be due to pneumonia or bronchial extensions. This model mimics human lung cancer progression starting from hyperplastic lesions and progressing to invasive carcinoma. Thus, the K-ras^{LA1} mouse model provides a platform to test how space radiation impacts stromal cells surrounding the initiated tumor, or how the microenvironment surrounding benign lesions may contribute to cancer promotion (**Figure 1.9 B**). When these mice are irradiated between the age of 8-15 weeks, most of them have initiated hyperplastic lesions but few adenomas. Although the expression of oncogenic K-ras is enough to induce adenomas in the K-ras^{LA1} mouse model, only 9% of the 129SV background mice with mutant (K-rasG12D) develop invasive carcinomas.

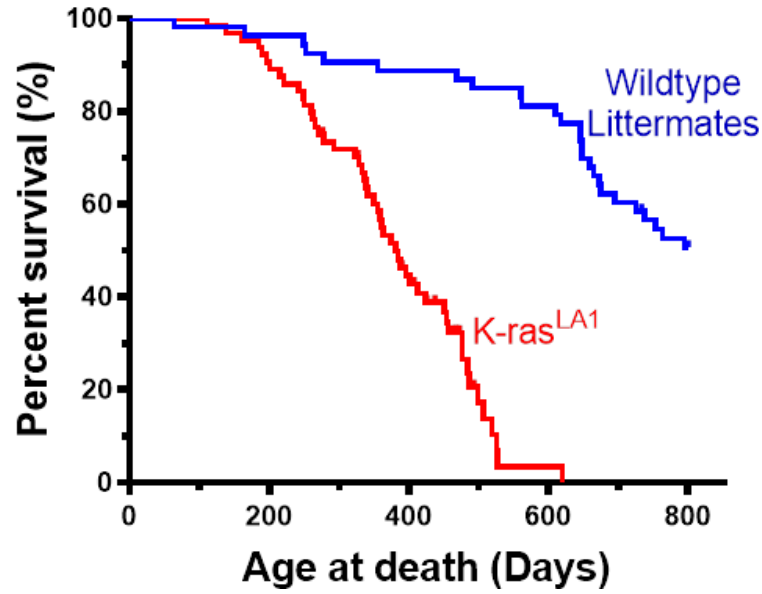
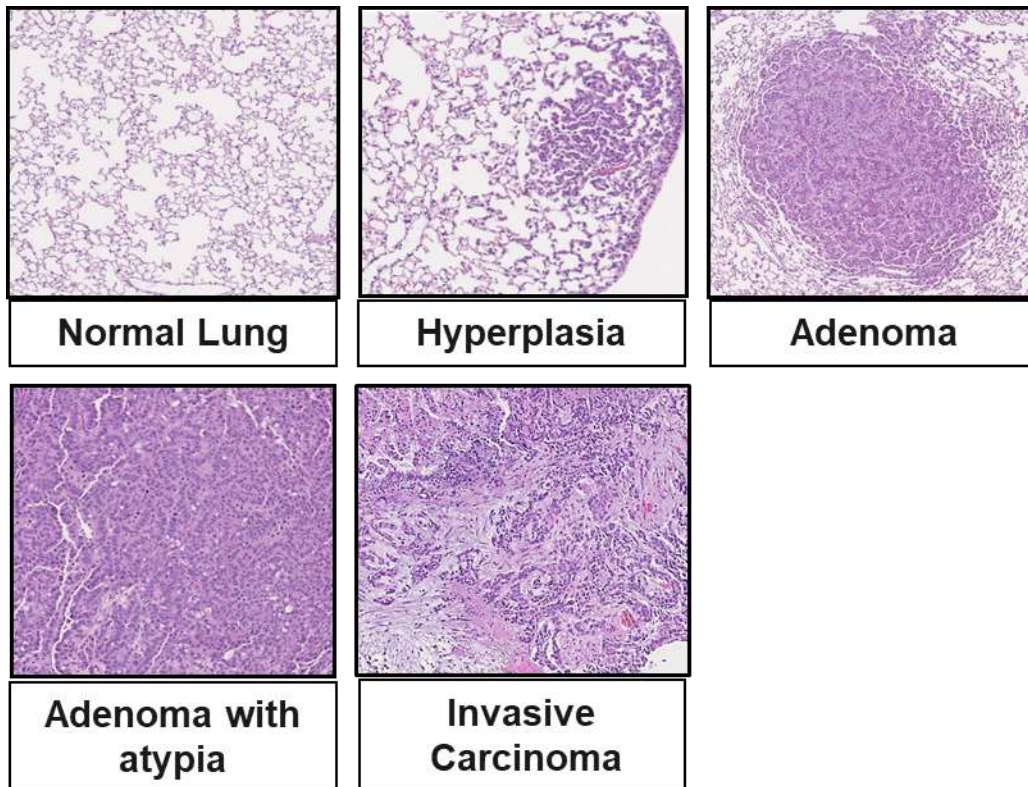
A**B**

Figure 1.9 Tumor progression in Kras^{LA1} mouse model. (A) Kaplan–Meier survival plot of Wildtype mice and Kras^{LA1} mice harboring (K-rasG12D) mutation. (B) Histopathology analysis of K-ras^{LA1} mice with Normal lung, hyperplastic lesion, adenoma, adenoma with atypia and invasive carcinoma.

Most lesions in these animals range from early lesions such as alveolar epithelial hyperplasia to well-defined adenomas suggesting that intact barriers to malignancy remain and additional alterations are required. These findings are consistent with human multi-step carcinogenesis. (Vogelstein & Kinzler, 1993). Exposing these mice to radiation such as is found in space could provide additional carcinogenic hits (such as genetic alteration or epigenetic changes) required to increase the incidence of invasive lung carcinoma. Thus, it is an ideal model to understand the effect of space radiation on the microenvironment of tumors and can potentially provide insights into the promotion of the benign lesions to more advanced stages of cancer.

CHAPTER TWO

Proton radiation-induced cancer progression

2.1 Introduction

Radiation-induced carcinogenesis remains a major concern for long-term deep space travel. Unlike terrestrial radiation which primarily is comprised of low-linear energy transfer (LET) radiations such as γ -rays, β , and X-rays, space radiation includes high LET radiation fields. Astronauts are exposed to Galactic Cosmic Rays (GCR) and Solar Particle Events (SPE) during deep space travel beyond the Low Earth Orbit (LEO) (Chancellor et al., 2014). The space environment contains a significant background of low and high energy protons fluxes as well as high charge and energy (HZE) nuclei. In addition, radiation is commonly used in medical imaging

as well as for cancer patients undergoing radiation therapy in the form of γ -rays or X-rays (photons). Due to superior targeting, minimal entrance dose, and with no exit dose has resulted in a large increase in particle radiotherapy for targeting solid cancers with more accuracy and potentially with fewer side effects. Worldwide there are ~75 particle radiation centers, and more than 170,000 patients undergoing proton or carbon radiation therapy for the treatment of various types of cancer (<https://www.ptcog.ch/>). Although the radiation side effects and risks due to γ -rays or X-rays have been studied over many decades, we still do not know much about the long-term effects of particle irradiation such as proton radiotherapy.

The lung has a large surface area which makes it a big target for radiation exposure. Lung cancer represents one of the most commonly diagnosed cancer types and it accounts for more cancer-related deaths than any other cancer type in both men and women (Cancer facts and figs 2018). Non-small cell lung cancer (NSCLC) is the most commonly diagnosed form of lung cancer, accounting for approximately 85% of all lung cancers, of which there is only a predicted 5-year survival rate of 16% for all patients (Ettinger et al., 2013). Risk factors for NSCLC include chemicals, air pollution, and radiation. Epidemiological data collected from individuals accidentally exposed to radiation (i.e. atomic bomb survivors, radon gas exposure in mine workers) demonstrate a positive correlation for increased risk of lung cancer development (Lubin et al., 1995; Preston, Shimizu, Pierce, Suyama, & Mabuchi, 2012). We previously reported that high-energy ^{56}Fe -particles irradiation given in fractionated doses enhanced the acceleration of lung cancer in a lung

cancer susceptible mouse model over single acute doses (Delgado et al., 2014). However, there have been limited studies evaluating the effects of proton radiation in the progression of lung cancer. Such studies might help in understanding the biological factors contributing to the incidence of secondary malignancies from radiation exposure. It will also help in estimating lung cancer risks for astronauts on long-term space missions since protons will be over 85% of the radiation exposure (National Research Council (U.S.). Task Group on the Biological Effects of Space Radiation. & National Research Council (U.S.). Commission on Physical Sciences Mathematics and Applications., 1996).

The purpose of the present study was to examine the effects of proton radiation in the progression of lung cancer. We used the K-ras^{LA1} mouse model which develops lesions in the lung spontaneously (Leisa Johnson¹, 2001). Using this genetically engineered mouse model, we studied survival and the progression of lung cancer after total body exposure to an acute proton with 50 MeV/n energy using a total dose 2.0 Gy at an average dose rate of 20 cGy/min. We also exposed mice to 2.0 Gy X-rays (250 kVp) at an average dose rate of 20 cGy/min as a reference radiation exposure. Here we report proton irradiation given acutely enhances the acceleration of lung cancer progression in the K-ras^{LA1} mouse model.

2.2 Materials and Methods

2.2.1 Mice and Irradiation

Animal experiments were reviewed and approved by the Institutional Animal Care and Use Committees (IACUC) at the University of Texas Southwestern Medical Center at Dallas (UTSW) and Brookhaven National Laboratory (BNL) (Upton, NY). Animals were housed and fed ad libitum diet following an approved husbandry protocol in ventilated micro isolator cages within a pathogen-free facility at UTSW. Transgenic K-ras^{LA1} mice on a 129S2 background as previously described (Leisa Johnson¹, 2001) were obtained from Dr. Jonathan Kurie (University of Texas M.D. Anderson Cancer Center, Houston, TX) and an in-house breeding colony was established. Heterozygous 129S2 K-ras^{LA1} breeding pairs were established to generate both heterozygous and wild-type littermate controls.

Both male and female transgenic K-ras^{LA1} mice, ages 8-15 weeks were total-body irradiated with different radiation protocols. Mice were exposed to a single acute dose of 2.0 Gy of proton ions at an energy of either 50 MeV/n or 150 MeV/n. All acute proton dose exposures were delivered at approximately 20 cGy/min. As a reference radiation, mice were also irradiated with 2.0 Gy of X-rays (250 kVp) at a dose rate of 20 cGy/min. As previously described (Kim, Zhang, Barron, & Shay, 2014), during the radiation exposure, mice were housed individually in plastic cuboid boxes (#530C, AMAC Plastic Products, Petaluma, CA). Animals subjected to proton

irradiation and unirradiated controls were used for both time points and survival studies and were transported via World Courier (New Hyde Park, NY) overnight delivery to Brookhaven National Laboratory and returned to UT Southwestern within 1 week after irradiation.

2.2.2 Premalignant Lesions, Invasive Carcinoma Assessment, and Mouse

Survival

Total body irradiated, and age-matched control mice were either sacrificed at indicated time-points or monitored until evidence of increased morbidity or death for survival study. All mice were necropsied, and lungs removed and inflated via intratracheal infusion with 10% neutral buffer formalin (NBF). The lungs were then clamped at the trachea and the entire tissue was immersed in 10% NBF overnight. Tissues were processed, paraffin-embedded, cut into 5 μm thick sections and stained with hematoxylin and eosin (H & E) for histopathological assessment using standard protocols. To analyze tumor grade and quantify lesions from survival cohorts with or without radiation treatment, three sections were cut 50 μm apart per animal. The stained sections were then analyzed; tumors graded, and other histopathological characteristics scored as either positive or negative for adenocarcinoma, adenoma with atypia, pneumonia, adenoma, hyperplasia, bronchial extension, and autolysis which were confirmed by a DVM/ Ph.D. pathologist specializing in mouse pathology (J.R.). Hyperplastic lesions were characterized as small lesions with proliferative non-inflammatory cells in the

alveolar epithelium, and as these hyperplasias grew they increase in size and are composed of a monomorphous population of airways epithelium pushing the surrounding airways which were then considered adenomas. The adenocarcinomas were characterized by tumor cells with the high-nuclear-to-cytoplasmic ratio, definite nuclear pleomorphism, having an undifferentiated appearance, and stromal interactions associated with the tumor along with inflammatory cells.

To quantify premalignant lesion sizes and number, we cut three sections of lungs per animal approximately 50- μ m apart and stained with hematoxylin and eosin (H&E). Images were taken using the Hamamatsu Nanozoomer 2.0-HT mounted CCD camera (Whole Brain Microscopy Facility at UTSW). The scanning software was NDPscanv2.3. The images were analyzed using the Nanozoom Digital Pathology Software.

2.2.3 Western Blot Analysis

For acute studies aged-matched 129S2 wild type mice were also shipped to Brookhaven National Laboratories (BNL) for experiments to be conducted at the National Space Radiation Laboratory (NSRL). Mice were irradiated with an acute dose of protons (energy of 50 MeV/n, the dose rate of 20cGy/min, the total dose of 2.0 Gy) or unirradiated. Additional mice were irradiated with X-rays with 2.0 Gy at a dose rate of 20 cGy/min at UTSW. Mice were sacrificed 4 hrs., 1 day, 2 days, 3 days. Whole mouse lungs were excised of which half was embedded in Tissue Tek O.C.T.

(Qiagen) for cryosectioning and the other half of the lung was snap frozen using liquid nitrogen. Frozen mouse lung tissue was disrupted using a liquid nitrogen-cooled mortar and pestle (Bel-Art™ Scienceware™, Fisher Scientific). Disrupted lung tissue was homogenized using a 18G needle and lysed in ice-cold lysis buffer (50mM Tris pH7.5, 150mM NaCl, 1% Triton X-100, and 1mM EDTA) containing protease and phosphatase inhibitor cocktails (Roche). Lysates were centrifuged, and supernatants used for protein assays. Proteins were separated by 4-15% Criterion TGX™ Precast Gel (Bio-Rad, CA), and transferred to a PVDF membrane using the Trans-Blot® Turbo™ Transfer System (Bio-Rad, CA). Phospho-histone H2A.X (Ser139) Cat#9718 was purchased from Cell Signaling Technology, Inc. (Danvers, MA, USA). Primary antibodies were used at 1:1000 dilution. Antibodies against beta-actin Cat# A1978 were purchased from Sigma Aldrich. HRP-conjugated goat anti-mouse or anti-rabbit (Jackson ImmunoResearch) were used as secondary antibodies at a 1:5000 dilution and detected with the SuperSignalWest Pico Chemiluminescent Substrate Kit (Thermo Scientific).

2.2.4 Oxyblot

Oxidized proteins were assessed using the OxyBlot™ protein oxidation detection kit (S7150, Millipore, Temecula, CA, USA). Snap-frozen half lungs of mice from acute studies were homogenized using a 18G needle and lysed in ice-cold lysis buffer (50mM Tris pH7.5, 150mM NaCl, 1% Triton X-100, and 1mM EDTA) containing 1% 2-mercaptoethanol. Denatured protein samples were mixed with 12%

SDS for a final concentration of 6% SDS. An equal amount of 1X dinitrophenylhydrazine (DNPH) solution was then added to the mix and incubated at room temperature for 15 min then the reaction was terminated by addition of a neutralization solution. Proteins were separated by 4-15% Criterion TGX™ Precast Gel (Bio-Rad, CA), and transferred to a PVDF membrane using the Trans-Blot® Turbo™ Transfer System (Bio-Rad, CA). Antibodies against DNPH-derivatized proteins were used for the detection (1:150 dilution), along with HRP-conjugated secondary antibodies (1:300 dilution). The chemiluminescent reagents were detected with the SuperSignalWest Pico Chemiluminescent Substrate Kit (Thermo Scientific).

2.2.5 Immunofluorescence

One half of each lung tissue was embedded in Tissue Tek O.C.T. (Qiagen) from the acute studies and then cryosectioned. Embedded blocks were cut into 5-10 µm sections using a cryostat microtome (Leica CM1950), and slides containing the sections were blocked for 1 hr. in PBS containing 10% goat serum. Primary antibodies such as 53BP1 (NB100-304, Novus Biologics) were diluted in blocking buffer and incubated overnight. Secondary antibodies were applied for 1 hr. at room temperature, washed, followed by slides being cover slipped using an antifade mounting medium with DAPI (Vector Laboratories). Images were captured on a Deltavision wide-field microscope using a 60X magnification oil immersion objective, and DNA damage foci were counted using Image J software (Schneider, Rasband,

& Eliceiri, 2012). To detect 8-oxo-dG, immunofluorescence was performed using an antibody obtained from Trevigen (Gaithersburg, MD) as per the manufacturer's instructions with minor modifications. Apoptosis was detected using an ApopTag Fluorescein In Situ Apoptosis Detection Kit (catalog no. S7110; Millipore) per manufacturer's protocol.

2.2.6 Quantitative Real-time PCR

Frozen mouse lung tissue from the acute studies was disrupted using a liquid nitrogen-cooled mortar and pestle (Bel-Art™ Scienceware™, Fisher Scientific), and RNA was extracted with Qiagen RNeasy Plus Kit (Qiagen) per the manufacturer's protocol. RNA (1ug) was used for reverse transcription, using the iScript cDNA synthesis kit (BioRad). Following cDNA synthesis, qRT-PCR was set up using SsoFast™ EvaGreen™ first-strand® Supermix (Biorad) in a LightCycler 480II (Roche Molecular biochemical). Primers used for the oxidative stress gene expression analyses were selected from Primer Bank (X. Wang, Spandidos, Wang, & Seed, 2012).

2.2.7 Immunohistochemistry

Formalin-fixed, paraffin-embedded tissues were used for immunohistochemistry. The extra sections obtained while taking 50 µm apart sections to measure tumor burden (sizes and numbers) were used for the

immunohistochemistry studies. Lung tissues sections (5- μ m thick) were deparaffinized, rehydrated and then antigens retrieved using citrate buffer in a pressure cooker (10 mmol/L sodium citrate, pH 6.0; 0.05% Tween 20). Hydrogen peroxide (3%) solution (Sigma-Aldrich) was used to block the endogenous peroxidase followed by Avidin/Biotin block (Vector Laboratories). The VECTASTAIN Elite ABC Kit (Vector Laboratories) was used per manufacturer's instructions to stain the protein of interest in the tissues. Primary antibodies Phospho-histone H2A.X (Ser139) (Cat#9718), Ki-67 (Cat#12202), CD8 α (Cat#98941), CD4 (Cat#25229), and FOXP3 (Cat#12653) were purchased from Cell Signaling Technology. The stained images were scanned using a Hamamatsu Nanozoomer 2.0-HT mounted CCD camera, and analyzed using Image J software. The scanning software used was NDPscanv2.3. Random (4-5) images of stained tumors per mouse were taken at 20X for the quantification of Ki-67, and random (4-5) images of stained lung tissues per mouse were taken at 40X for the quantification of Phospho-histone H2A.X. The quantification was done by counting positive cells as well as the total number of cells in each 20X field and reporting them as a percentage of positive cells. For the quantification of immune cells, after staining, whole sections were scanned, and the area of tumor margins was measured along with the number of infiltrating cells within the tumor margin. The quantification is reported as the number of infiltrating cells per millimeter square. All quantifications were performed before unblinding the code.

2.2.8 Malondialdehyde Assay on Serum

From aged-matched 129S2 mice, blood samples were collected in 0.5cc microcentrifuge tubes with 0.5M EDTA, and samples centrifuged for 15 min at 3,000 rpm at 4° C. From the centrifuged samples, the plasma was collected from the supernatant. MDA is a byproduct of lipid peroxidation. MDA levels in plasma were measured using TBARS Assay Kit (Cayman Chemical, 10009055) as per the manufacturer's instructions.

2.2.9 Statistical Analysis

Statistical analysis was performed using GraphPad Prism version 7.00 for Windows, (GraphPad Software, La Jolla California USA). At least 3-5 independent biological samples were used per radiation dose. Comparison between irradiated groups and controls were determined by using one-way ANOVA with Tukey correction along with pairwise comparisons for the P values. Differences were considered significant at $P < 0.05$. To determine statistical significance for Kaplan-Meier survival curves the Log-rank test (Mantel-Cox) was performed. Statistical analysis of the histopathology was performed using two-tailed Fisher exact (95% confidence interval, CI) or Chi-square test.

2.3 Results

2.3.1 Proton exposure causes complex and extensive DNA damage in the lung

We examined the extent of double-stranded DNA damage in mice irradiated (2.0 Gy) with either proton or X-rays after 4 hours, 1 day and 3 days. We observed proton radiation resulted in more complex DNA damage in the lungs of mice when compared to X-rays 4 hours post radiation, with more 53BP1 foci per cell. In proton irradiated mice more than 65% of 53BP1 positive lung cells had more than 5 foci per nucleus as compared only 38% of 53BP1 positive cells irradiated with X-rays (**Figure 2.1A and 2.1B**). We next examined the time course of DNA repair kinetics in the lung of the irradiated mice as complex DNA damage may take longer to repair (Asaithamby, Hu, Delgado, et al., 2011). Most of the DNA damage in the X-rays irradiated mice was repaired by 24 hours, but in the proton-irradiated mice, we observed that there was more than 20 percent of the cells with 53BP1 foci that persisted even 3 days post-irradiation (**Figure 2.1C and 2.1D**). Additionally, a significant amount of phosphorylated γ -H2AX remained in proton irradiated lungs compared to X-rays 3 days post-irradiation (**Figure 2.2A and 2.2B**). We next tested if the increased DNA damaged cells in proton irradiated animals resulted in increased apoptosis. Using Apotag, we did not observe any apoptotic cells in the lung tissues after 4 hours, 1 day or 3 days post-irradiation (data not shown).

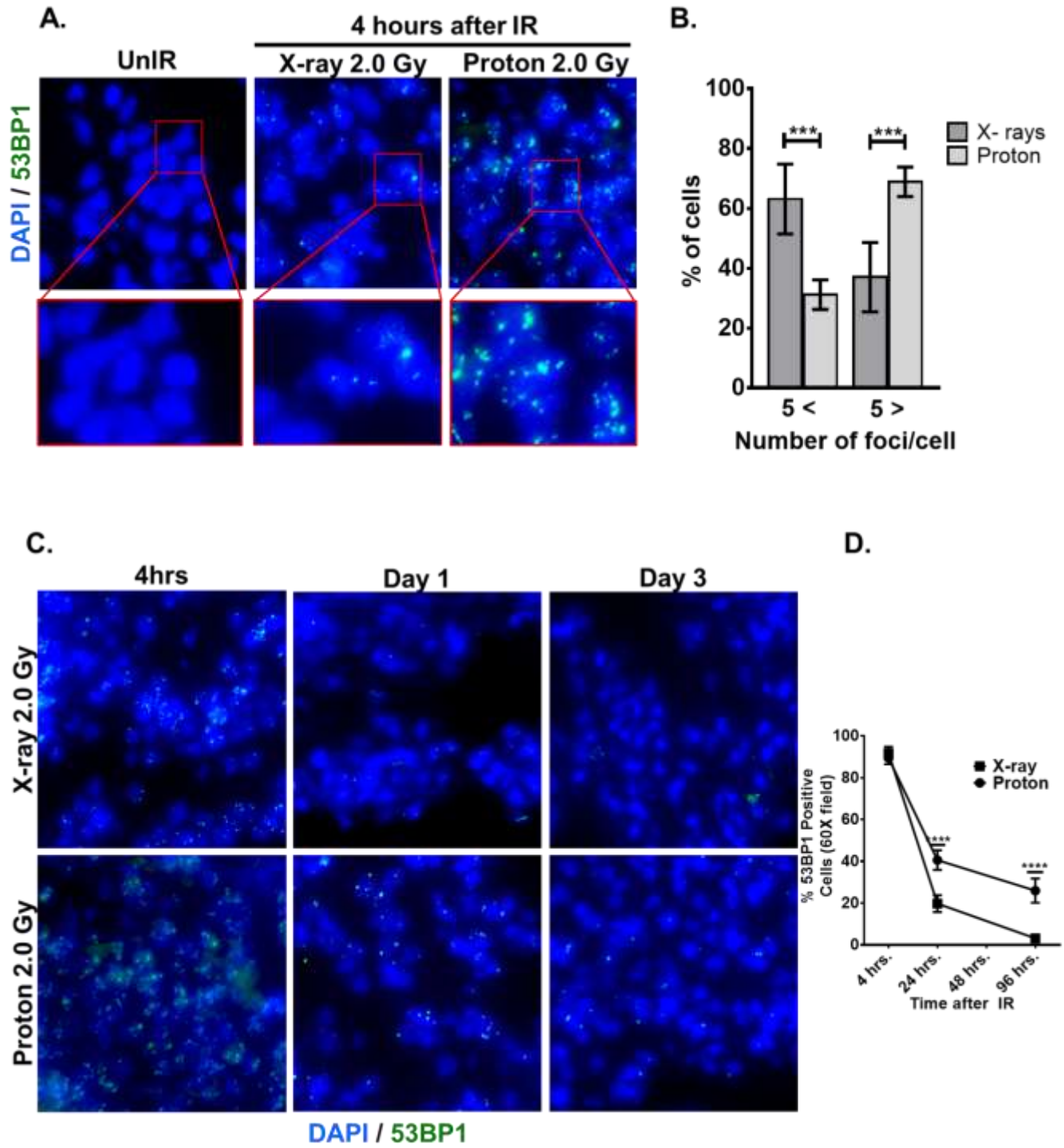


Figure 2.1. Proton-induced DNA damage responses in WT mouse lungs. (A) Representative immunofluorescence images of lung tissue sections of mice 4 hours post-irradiation with X-rays 2.0 Gy, protons (50 MeV/n) 2.0 Gy, and unirradiated controls stained with 53BP1 (green) and DAPI (blue). (B) 53BP1 foci per cell 4 hours post-irradiation were counted using a 60X objective. More than 100 cells were counted and scored as less than 5 foci per nucleus, or more than 5 foci per nucleus. (n=3 mice per group) *** $P < 0.001$ (proton compared with x-rays) in unpaired Student's t-test. (C) Representative images showing 53BP1 (green) and DAPI (blue) after indicated radiations (X-rays 2.0 Gy and protons (50 MeV/n) 2.0 Gy) at different time points 4 hours, 1 day, and 3 days post-irradiation. (D) The number of 53BP1 (green) positive foci per 60X field. More than 100 cells were counted per each field. (n=3 mice per group) **** $P < 0.0001$ (proton compared with X-rays) in the unpaired Student's t-test. The error bars represent standard errors.

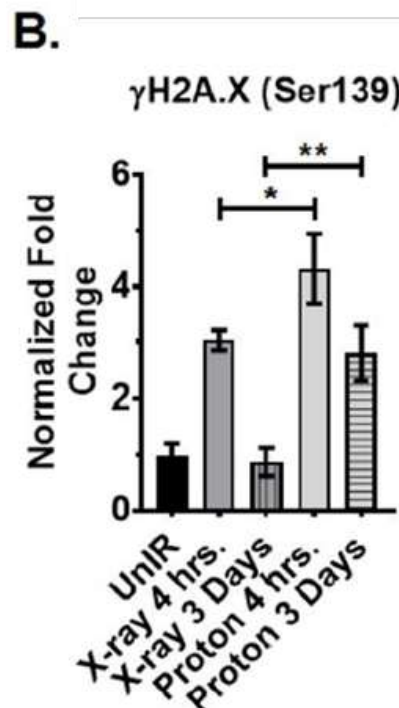
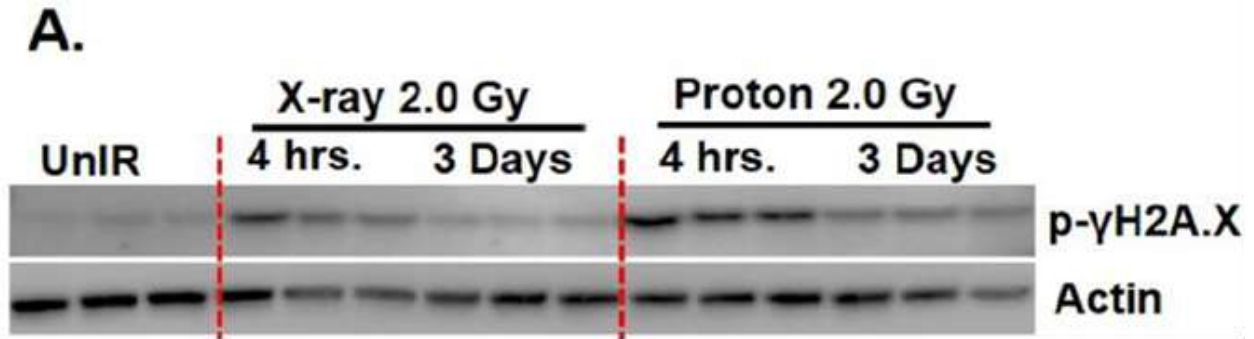


Figure 2.2. Proton-induced DNA damage responses in WT mouse lungs. (A) Western blots for phosphorylated γ -H2AX (Ser139) in lung tissues 4 hours and 3 days post-irradiation either with X-rays 2.0 Gy or protons (50 MeV/n) 2.0 Gy, and unirradiated controls. β -actin was probed as a normal protein loading control of samples. (B) Quantitative data indicating mean protein levels 4 hours and 3 days post-irradiation either with X-rays 2.0 Gy or protons (50 MeV/n) 2.0 Gy, and unirradiated controls. **P=0.0011, *P=0.0184. Statistical significances differences were determined by one-way ANOVA with Tukey correction. The error bars represent standard errors.

2.3.2 Proton irradiation causes both acute and chronic oxidative stress

Proton radiation can induce direct damage to DNA or indirectly through the generation of reactive oxygen species (ROS). Compared to X-rays, proton charged particles produce more ROS (Zhang et al., 2013). One possibility is that the increased number of 53BP1 foci that we observed in lung tissues (**Figure 2.1A and 2.1C**) could be caused by higher ROS. To test if there is higher oxidative stress in lung tissues post-irradiation, we determined the level of total protein oxidation in the tissue lysates. We observed that proton irradiated tissues have a higher amount of oxidized proteins as compared to X-irradiated tissues, and levels of oxidized proteins remained higher over a 3-day period in proton irradiated tissues but not in X-irradiated tissues (**Figure 2.3A and 2.3B**). In addition, immunoblots of lung tissues lysates showed phosphorylated Nrf2 (a stress response transcription factor) levels were higher in the proton-irradiated tissues and remained at the higher level 3 days post-irradiation. In contrast, levels of Nrf2 in X-irradiated lung tissues decreased 3 days post-irradiation (**Figure 2.3C and 2.3D**). In addition, we analyzed gene expressions related to oxidative stress. Using a p-value of <0.05 and fold change cutoff of 1.5, we found Nrf2, HO-1, Nqo1, Cat, Gpx2, Sod1, Prdx2, and Gpx8 were deregulated in proton irradiated tissues at 4 hours and at 3 days when compared to X-rays treated tissues (**Figure 2.4**).

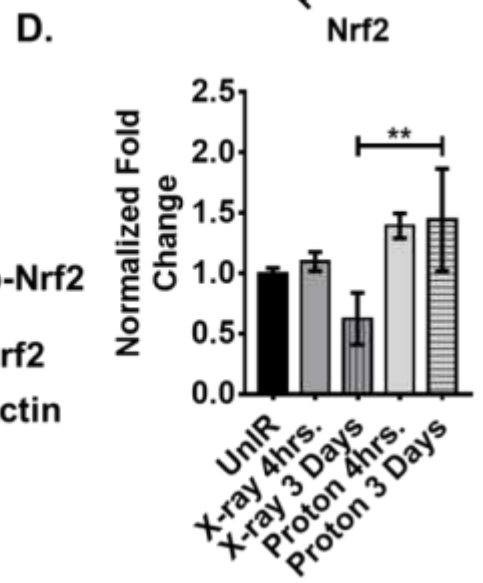
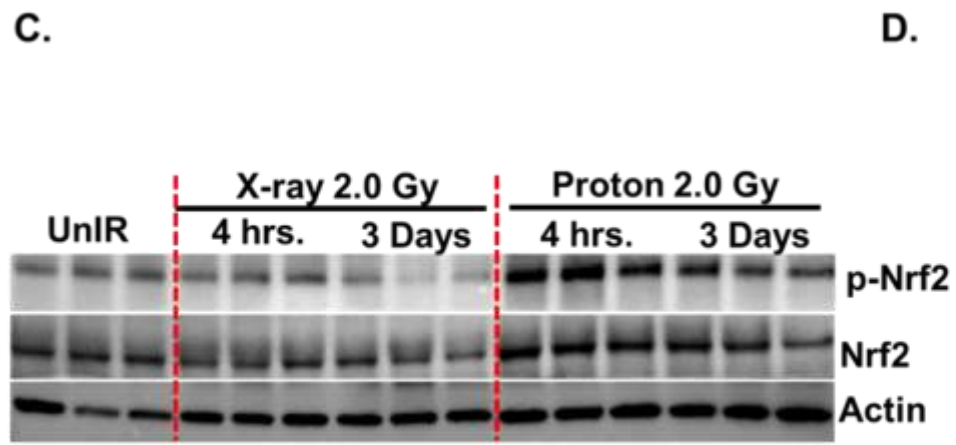
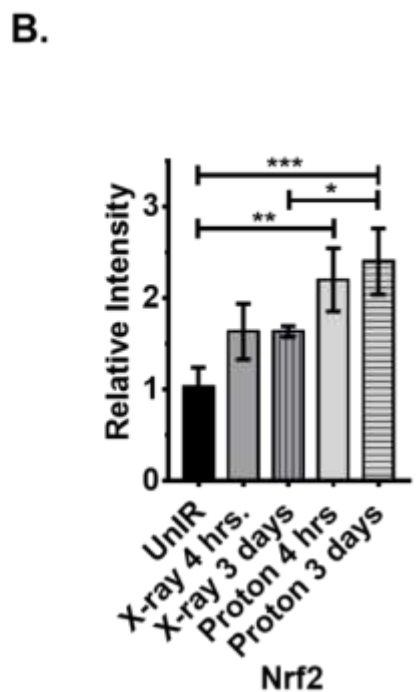
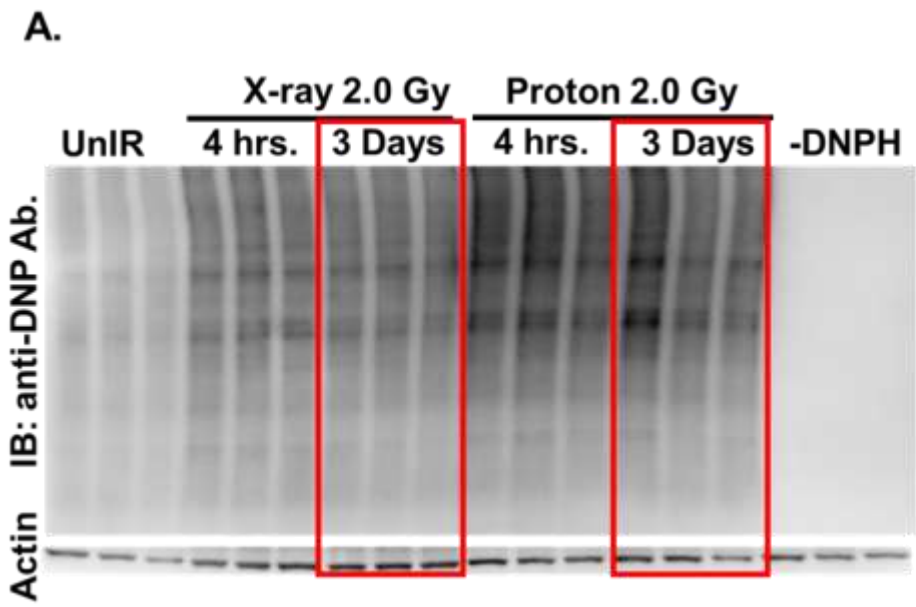


Figure 2.3. Proton exposure causes higher and extensive oxidative stress in WT mouse lungs. (A) Total protein oxidation immunoblot by oxyblot analyses of DNPH-derivatized lung tissue lysates of mouse 4 hours and 3 days post-irradiation with X-rays 2.0 Gy, protons (50 MeV/n) 2.0 Gy, unirradiated controls and (-) DNPH control. β -actin was probed as the normal protein loading for the samples. (B) The relative intensity of each band measured and normalized with β -actin and compared with the unirradiated control. (n=3 mice per group) * P=0.0448, *** P=0.0032 and *** P=0.0010. (C) Western blot analysis of Nrf2 protein expression following indicated radiations (X-rays 2.0 Gy and proton (50 MeV/n) 2.0 Gy) at different time points either 4 hours or 3 days post-irradiation. β -actin was probed as the normal protein loading for the samples (n=3 mice per group). (D) Quantification of western blot. ** P=0.0075. Statistical significance was determined by one-way ANOVA with Tukey correction. The error bars represent standard errors.

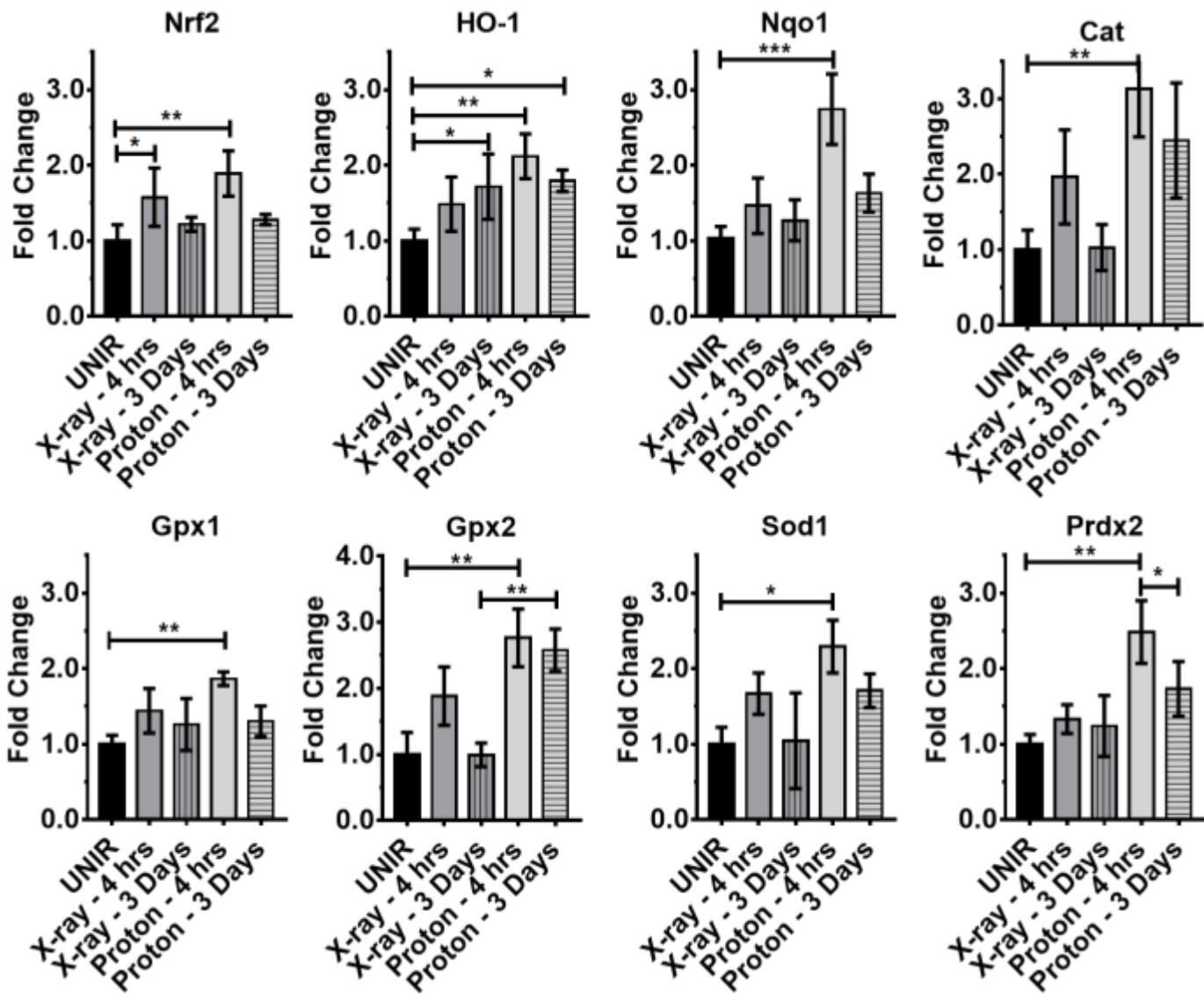


Figure 2.4. Radiation exposure altered expression of genes associated with oxidative stress. Differences were considered significant at $P < 0.05$. Statistical significances differences were determined by one-way ANOVA with Tukey correction. The error bars represent standard errors.

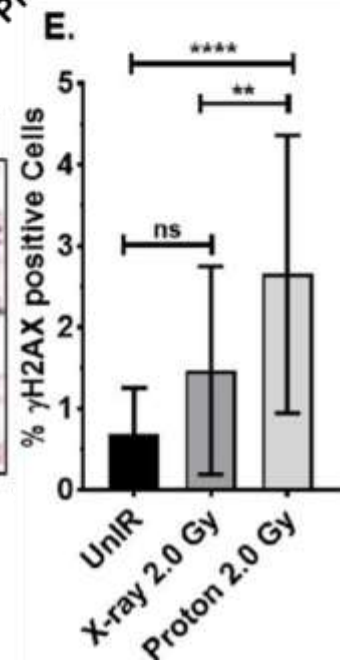
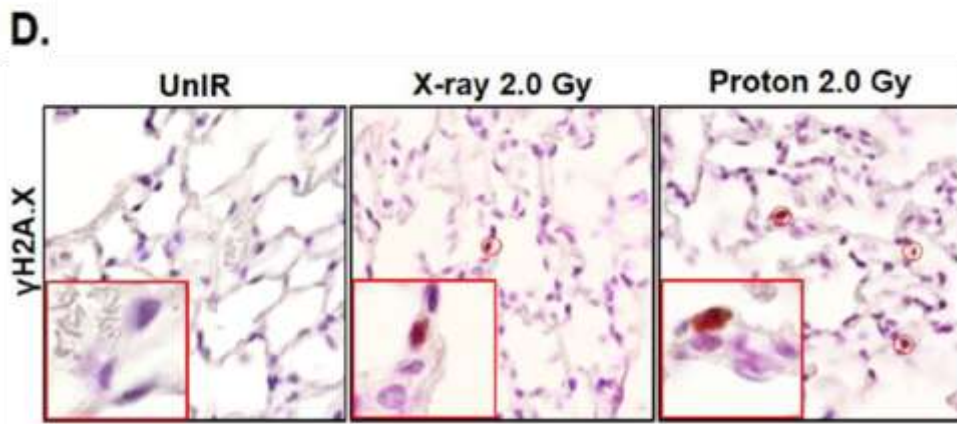
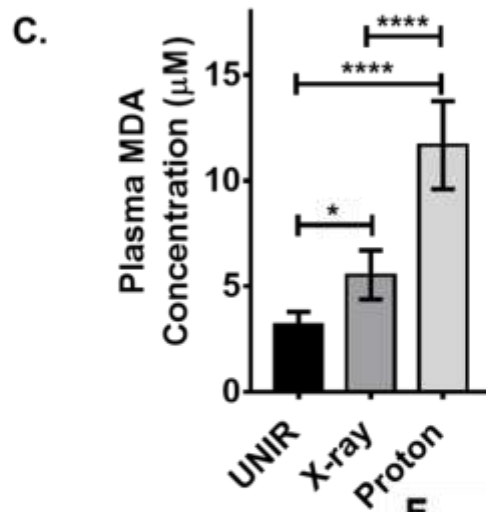
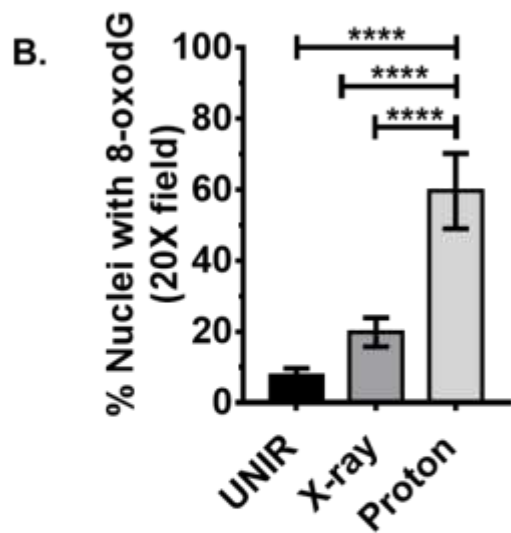
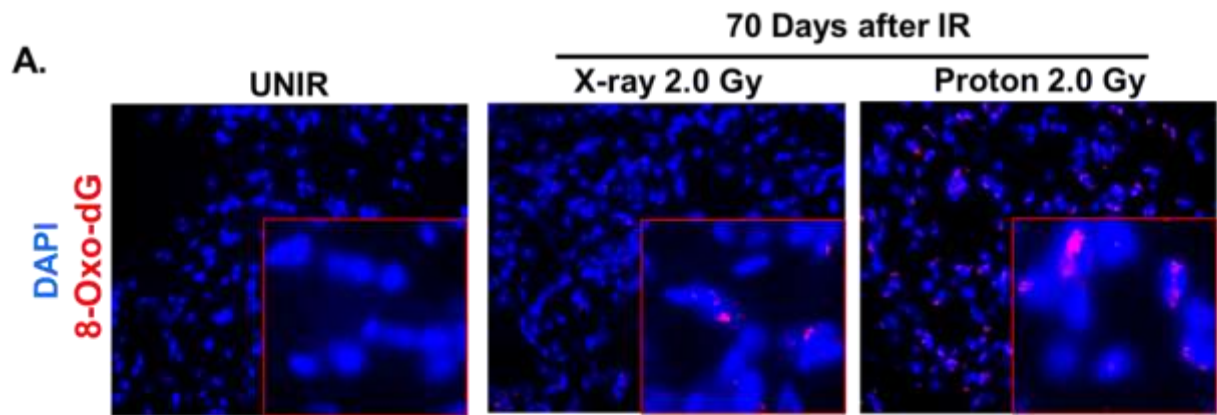


Figure 2.5. Proton exposure leads to chronic oxidative stress and DNA damage in WT mice. (A) Representative images of immunofluorescence staining of lung sections of age-matched mice 70 days post-irradiation with X-rays 2.0 Gy, protons (50 MeV/n) 2.0 Gy and unirradiated controls stained with 8-oxo-dG (red) and DAPI (blue). (B) Quantification of 8-oxo-dG staining in lung sections of WT mice (n = 5 mice per group) where all complete cells were counted scored for the 8-oxo-dG positive nucleus. **** P<0.0001. (C) Assay of MDA in the serum of WT aged matched mice 70 days post-irradiation with X-rays 2.0 Gy, protons (50 MeV/n) 2.0 Gy, and unirradiated controls. * P=0.0286, **** P<0.0001. (D) Representative immunostaining for phosphorylated γ -H2AX (Ser139) in mice lung 70 days post-irradiation with magnified images. (E) Quantification for phosphorylated γ -H2AX (Ser139) in lung sections of WT mice (n=5 per group). ****P<0.0001, **P=0.0032 Statistical significances differences were determined by one-way ANOVA with Tukey correction. The error bars represent standard errors.

These acute effects as well as chronic oxidative stress effects due to radiation have also been reported previously in different tissue types (Christofidou-Solomidou et al., 2015; Datta, Suman, Kallakury, & Fornace, 2012). To further assess persistent oxidative stress, we stained the lung sections with 8-oxo-2'-deoxyguanosine (8-oxo-dG) by immunohistochemistry 70 days post-irradiation. We observed there was markedly higher staining in the proton-irradiated lung tissues when compared to X-irradiated animals (**Figure 2.5A**). Compared to X-irradiated lung tissues, proton irradiated tissues had more than a 3-fold increase in 8-oxo-dG staining 70 days post-irradiation (**Figure 2.5B**). We also quantitated lipid peroxidation, by measuring the amount of MDA in the plasma. Malondialdehyde (MDA), together with 4-hydroxynonenal (4-HNE) are natural byproducts of lipid peroxidation. We observed that plasma collected had more than a 2-fold increased amount of MDA present in the proton-irradiated animals compared to X-irradiated mice (**Figure 2.5C**). Consistent with the observed oxidative stress, proton irradiated mice displayed a higher number of positive γ -H2AX foci in lung sections compared to X-irradiated mice or unirradiated controls (**Figure 2.5D and 2.5E**). Taken together, we interpret these data to demonstrate that even 70 days post-irradiation there is measurable oxidative stress and DNA damage present in proton irradiated mice.

2.3.3 Increases in number and sizes of premalignant lesions K-ras^{LA1} mouse model

To determine how radiation exposure affected the carcinogenic process, we compared premalignant lesions of aged-matched unirradiated control K-ras^{LA1} mouse lungs with X-rays and proton irradiated mouse lungs 100 days post-irradiation. We irradiated 8-15 weeks old K-ras^{LA1} mice with either 2.0 Gy X-rays or 2.0 Gy proton. At 8-15 weeks of age, K-ras^{LA1} mice have only a few smaller premalignant lesions. Compared with unirradiated K-ras^{LA1} mice, K-ras^{LA1} mice irradiated with either X-rays or protons developed higher numbers and larger lesions. Unirradiated animals had an average of 5 lesions with an average diameter of 0.26 mm, X-rays irradiated animals had average of 10 lesions with an average diameter of 0.38 mm, and proton irradiated animals had an average of 13 lesions with an average diameter of 0.45 mm (**Figure 2.6A and 2.6B**). The overall surface area of the lesions in the lung of unirradiated K-ras^{LA1} mice were 0.22 mm², while the lung of X-irradiated mice was 0.45 mm², and proton irradiated mice were 0.64 mm². Compared with the unirradiated and X-irradiated mice, proton irradiated mice also had a higher number of proliferative cells as determined by Ki-67 immunostaining (**Figure 2.6C and 2.6D**). Despite having a higher number of lesions and larger lesions, proton irradiated mice did not have any advanced adenomas or carcinomas 100 days post-irradiation.

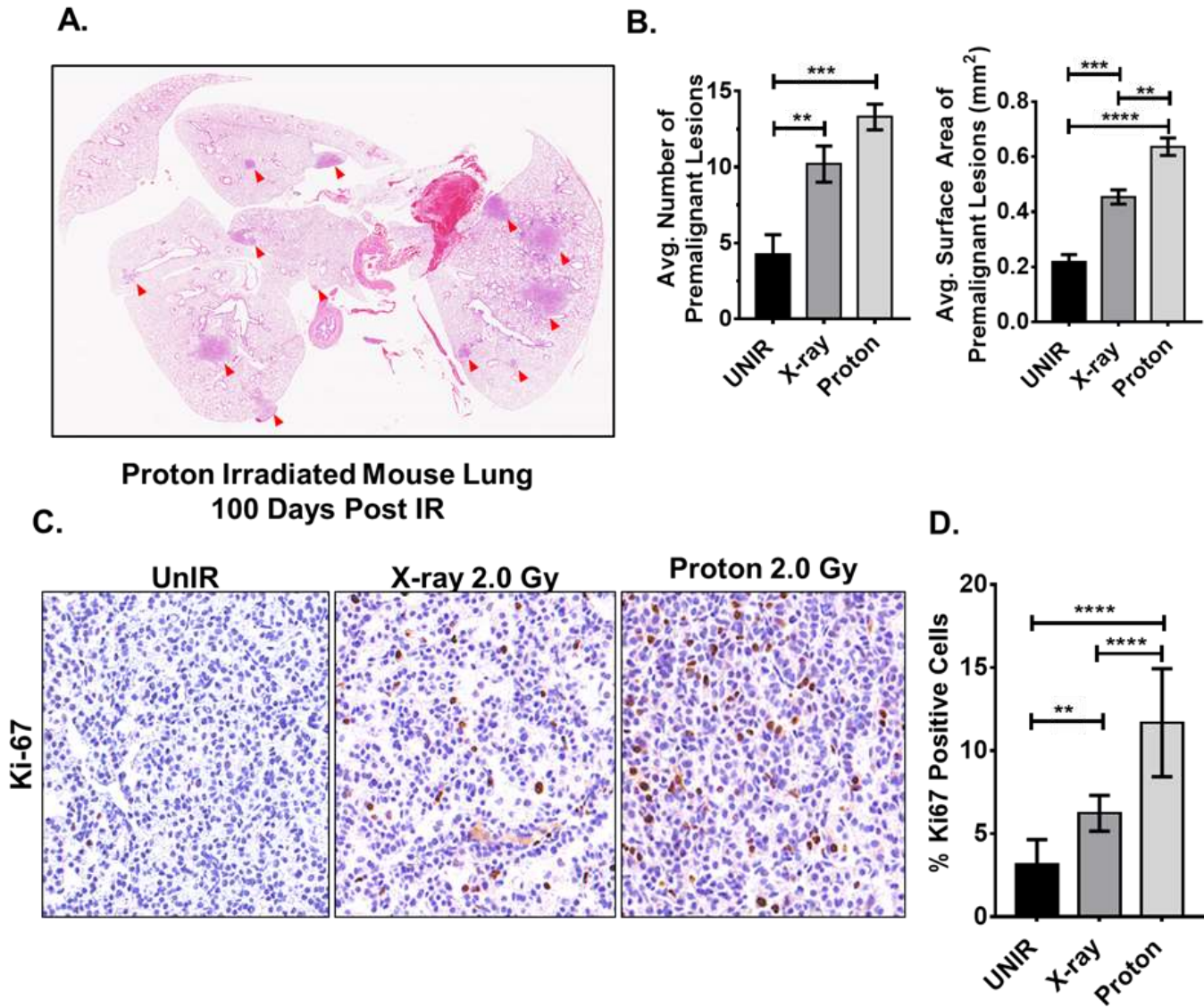


Figure 2.6. Proton irradiation increased the tumor burden in K-ras^{LA1} mice. (A) Representative hematoxylin and eosin (H&E) image of proton irradiated mouse lungs 100 days post-irradiation. (B) Quantification of overall number and size of pre-malignant lesions in age-matched K-ras^{LA1} lungs from 100 days post-irradiation with X-rays 2.0 Gy, protons (50 MeV/n) 2.0 Gy and unirradiated control (n = 5 mice per group). (5B, left) Differences in the number of the pre-malignant lesions. ** P=0.0088, *** P=0.0004. (5B, right) Differences in size (surface area) of pre-malignant lesions. *** P=0.0004, **** P<0.0001, and ** P=0.0018. (C) Representative

immunostaining for Ki-67 mouse lungs 100 days post-irradiation with magnified images. (n = 5 mice per group). (D) Quantification of Ki-67 staining in premalignant lesions. ** P=0.0053, **** P<0.0001. Statistical significances differences were determined by one-way ANOVA with Tukey correction. The error bars represent standard errors.

2.3.4 Inflammatory cells infiltration in the premalignant lesions

The tumor microenvironment is known to change throughout the carcinogenic process and contribute to tumor development and progression (Hanahan & Coussens, 2012; Hanahan & Weinberg, 2011a). The tumor microenvironment consists of a variety of inflammatory cells, and enhanced T cells infiltration has been reported previously (Burnette & Weichselbaum, 2013). We analyzed H&E stained premalignant lesions of aged-matched unirradiated control K-ras^{LA1} lungs and compared them with X-rays or proton irradiated lungs 100 days post-irradiation. We observed that proton irradiated mice lung at 100 days post-irradiation had pockets of inflammatory cells around the premalignant lesions in 3/5 mice while these were not observed in unirradiated mice. Only 1/5 mice irradiated with X-rays had any inflammatory cells present. Overall, infiltrating inflammatory cells were enhanced in the proton-irradiated tissues while only a few inflammatory cells were observed in the X-rays survival cohort and these were associated with higher grade tumors

(adenoma with atypia). Using immunohistochemistry, we analyzed a subset of immune cell types such as macrophages, neutrophils, and T cells in the premalignant lesions. There were no significant differences in the number of macrophages and neutrophils in the lungs. Furthermore, when we analyzed T cells, we found there were no significant differences among CD8⁺ T cytotoxic cells in premalignant lesions 100 days post-irradiation. On average there were around 10-11 CD8⁺ T cells/mm² in lung sections of irradiated mice as well as unirradiated mice **(Figure 2.5A and 2.5B)**. In contrast, CD4⁺ T cells and Foxp3⁺ cells were significantly higher in proton irradiated premalignant lesions compared to both X-irradiated mice and controls. There was an average of 13, 33 and 57 CD4⁺ T cells/mm² in premalignant lesions in unirradiated control, X- irradiated mice and proton irradiated mice respectively **(Figure 2.5C and 2.5D)**. Similarly, there was an average of 14, 23, and 57 Foxp3⁺ cells/mm² of premalignant lesions in unirradiated control, X-irradiated mice and proton irradiated mice respectively **(Figure 2.5E and 2.5F)**. Foxp3⁺ regulatory cells have been implicated in K-ras mediated lung tumorigenesis in mice (Granville et al., 2009; Zdanov et al., 2016).

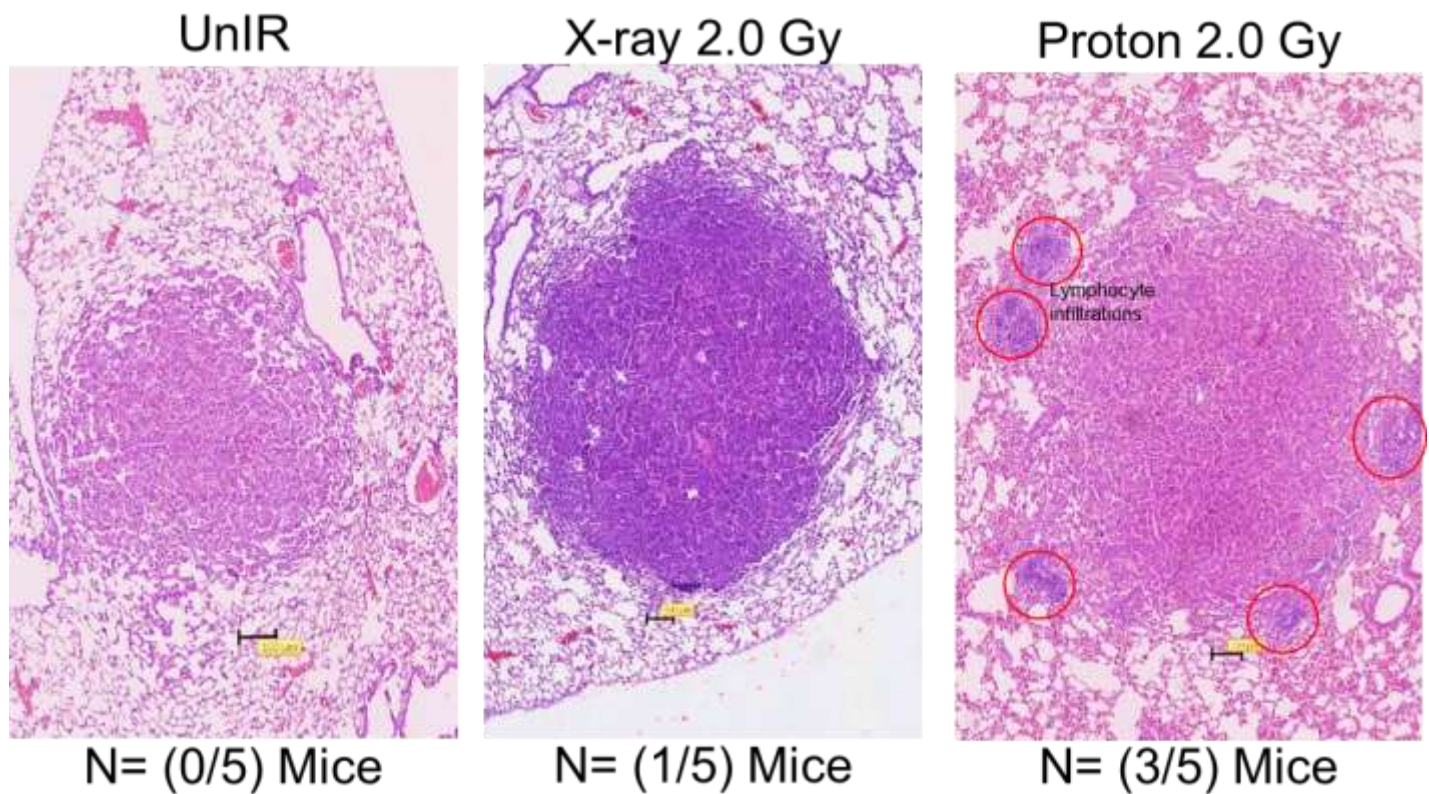


Figure 2.7. Representative images (H and E) of lung tissues irradiated with either X-rays or proton or unirradiated control showing the pockets of inflammatory cells near to the premalignant lesions of similar sizes 100 days post-irradiation. None of the premalignant lesions of unirradiated control (n=5) showed pockets of inflammatory cells whereas only one mice irradiated with X-rays has premalignant lesions with inflammatory cells, and proton irradiated has three mice with premalignant lesions with inflammatory cells (n=5).

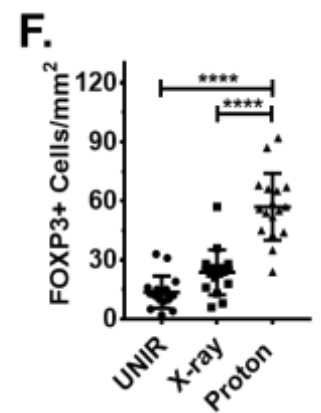
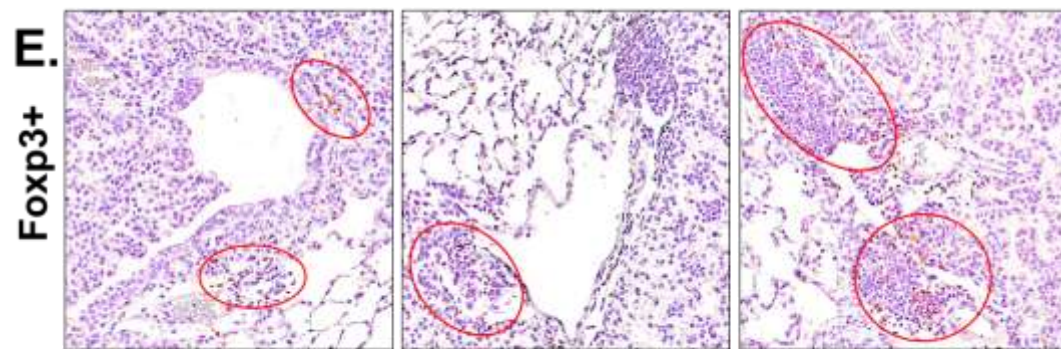
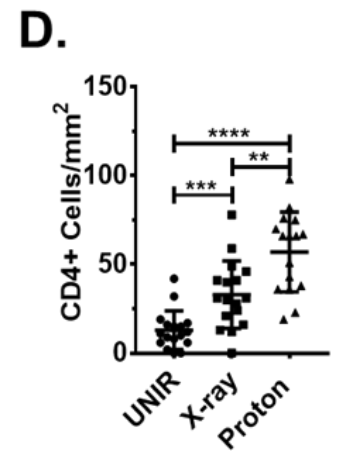
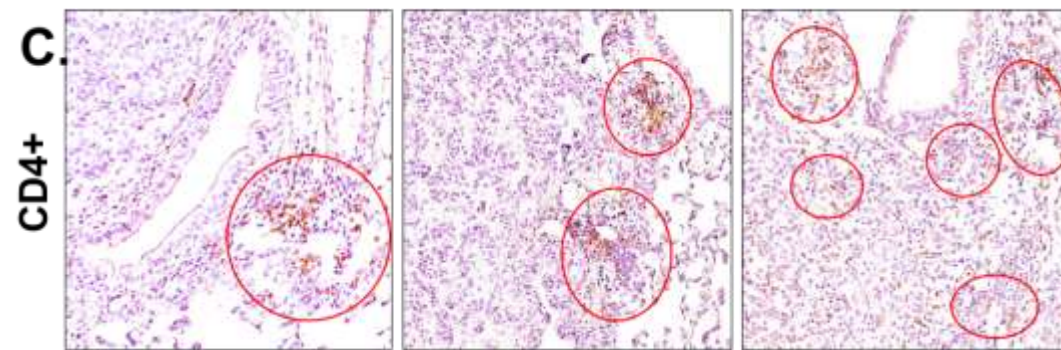
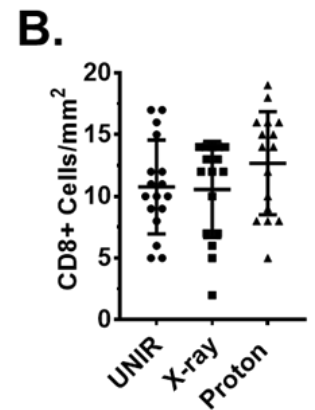
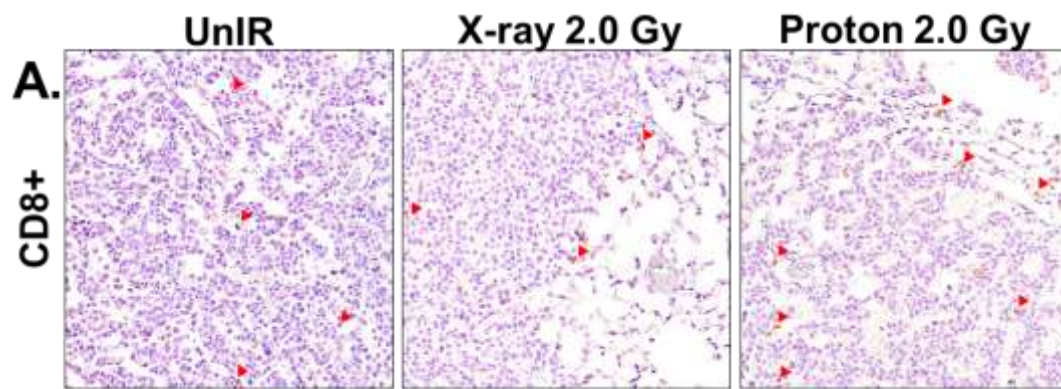
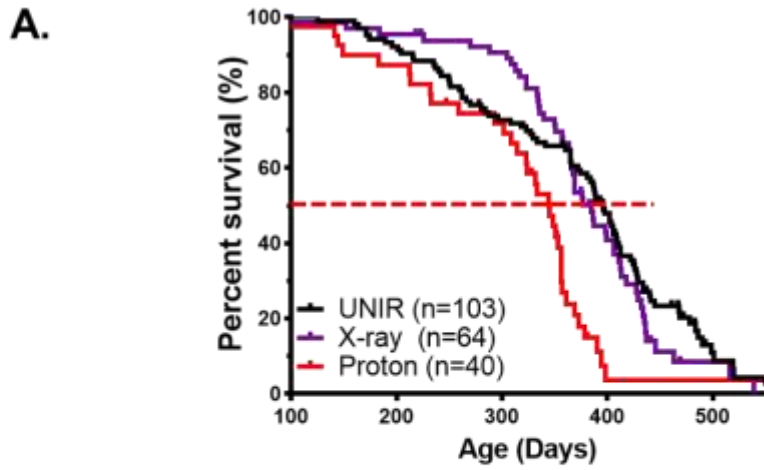


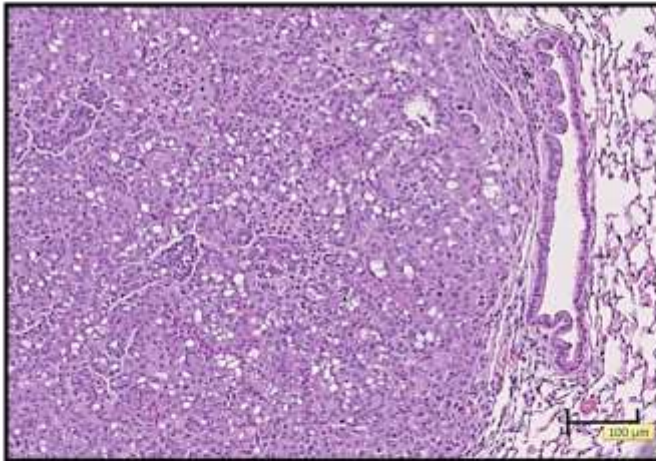
Figure 2.8. Immune cells infiltrations into premalignant lesions. (A)(C)(E) Representative images of premalignant lesions of irradiated mouse lungs stained for CD8 T cells, CD4 T cells, and Foxp3 cells respectively. (B) Number of CD8⁺ T cells per millimeter square as assessed by immunohistochemistry (n =5 animals per group). (D) Number of CD4⁺ T cells per millimeter square as assessed by immunohistochemistry (n =5 animals per group). ** P=0.0062, **** P<0.0001, **P=0.0011. (E) Number of CD8⁺ T cells per millimeter square as assessed by immunohistochemistry (n =5 animals per group). **** P<0.0001. Statistical significances differences were determined by one-way ANOVA with Tukey correction. The error bars represent standard errors.

2.3.5 Proton exposure reduces lifespan and increases invasive carcinoma

To evaluate how energetic proton exposure influences tumor development and overall survival in the K-ras^{LA1} lung cancer mouse model, we exposed K-ras^{LA1} mice to either a single acute dose of protons (50 MeV/n) or X-rays. K-ras^{LA1} mice exposed to energetic protons exhibited shortened lifespan compared to unirradiated control mice or X-irradiated mice (**Figure 2.6A**). K-ras^{LA1} mice exposed to 2.0 Gy of a monoenergetic acute proton (50 MeV/n) also exhibited a significant decrease in median survival. Unirradiated control mice had a median survival of 396 days, whereas mice exposed to a single dose of 2.0 Gy proton (50 MeV/n) displayed a median survival of 345 days, and mice exposed to an X-rays 2.0 Gy displayed a median survival of 385 days very similar to unirradiated controls. To further determine disease progression following radiation exposure, K-ras^{LA1} mice that were irradiated with acute proton or X-rays were evaluated histologically for the appearance of adenomas with atypia and invasive carcinomas. K-ras^{LA1} mice exposed to 2.0 Gy of acute proton or X-rays exhibited a significant increase in adenoma with atypia (**Figure 2.6B and 2.6D**) and invasive carcinoma formation (**Figure 2.6C and 2.6 E**). Unirradiated Kras^{LA1} mice possess a background carcinoma incidence of approximately 10%, whereas mice exposed to 2.0 Gy of 50 MeV/n proton radiation displayed a significant (27.3%) increase in invasive carcinoma while X-rays exposed mice have (18.4%) increase in invasive carcinoma(**Figure 2.6E, Table 2.1**).



B. Adenoma with atypia (proton irradiated)



C. Adenocarcinoma (proton irradiated)

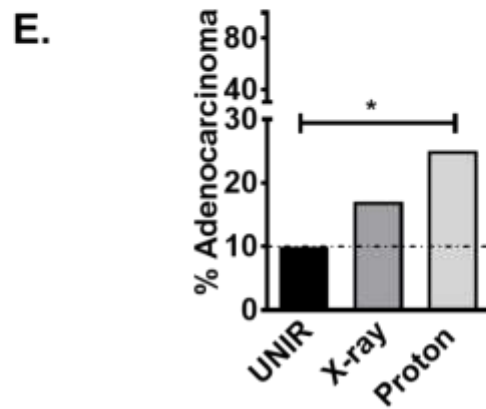
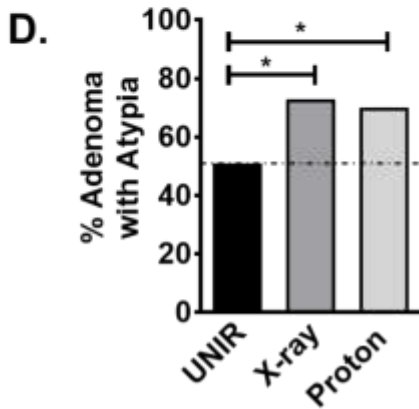
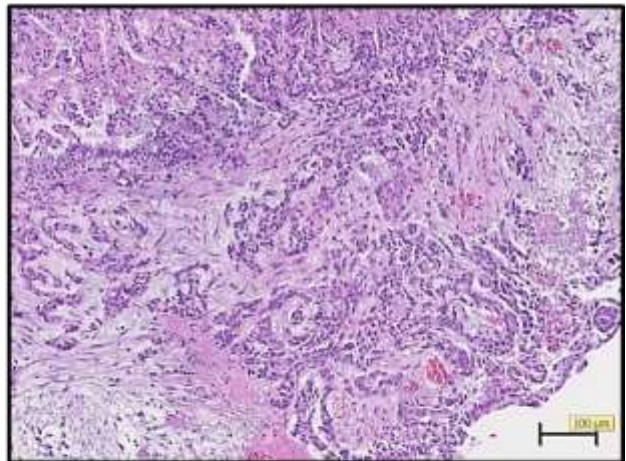


Figure 2.9. Tumorigenic effect of proton irradiation in the K-ras^{LA1} mouse model. (A) Kaplan–Meier survival plot of unirradiated compared to X-rays and proton irradiated K-ras^{LA1} mice. Unirradiated K-ras^{LA1} mice (black); acute protons (50MeV/n) irradiated mice (red); irradiated X-rays irradiated K-ras^{LA1} mice (purple). *** $P=0.0002$ in Log-rank (Mantel-Cox) test acute proton (50 MeV/n) compared with unirradiated K-ras^{LA1} mice survival. $P=0.4001$ in Log-rank (Mantel-Cox) X-rays compared with unirradiated K-ras^{LA1} mice survival. (B) Representative images of adenoma with atypia, and (C) adenocarcinoma found in the animals of the survival study. Scale bar, 100 μm . (D) Quantification of percent adenomas with atypia. * $P<0.05$ in contingency Chi-square test proton compared with UNIR. * $P<0.05$ in contingency Chi-square Test X-rays compared to UNIR. (E) Quantification of percent adenocarcinoma. $P<0.05$ in contingency table analysis protons with unirradiated control respectively.

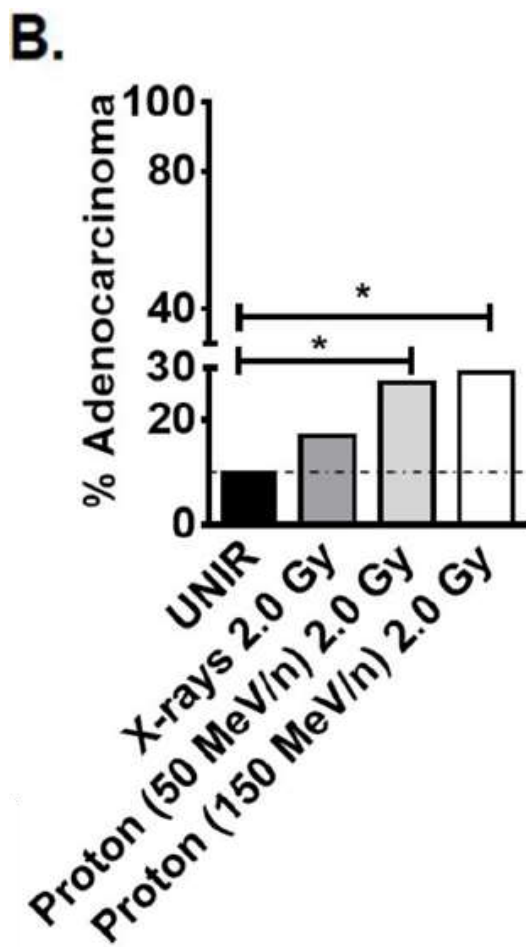
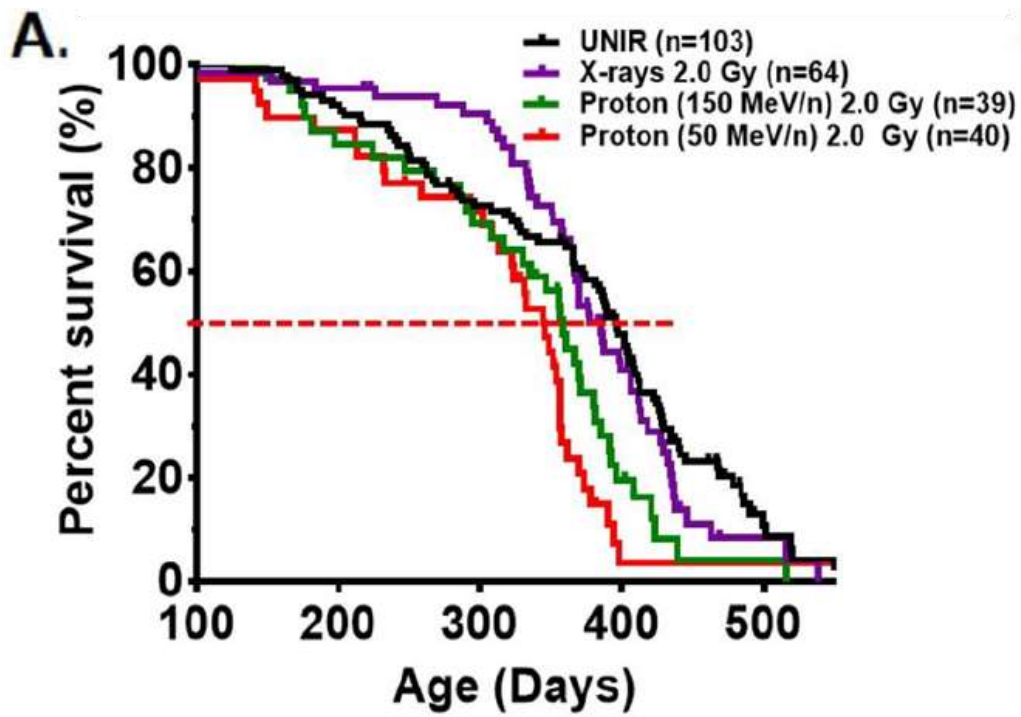


Figure 2.10. Tumorigenic effect of an acute proton (50 MeV/n) and proton (150 MeV/n) in K-ras^{LA1} mouse model. (A) Kaplan–Meier survival plot of unirradiated or irradiated K-ras^{LA1}. Unirradiated K-ras^{LA1} mice (black); acute proton (50MeV/n) irradiated mice (red); acute proton (50MeV/n) irradiated mice (green); irradiated X-rays irradiated K-ras^{LA1} mice (purple). *** $P=0.0002$ in Log-rank (Mantel-Cox) test acute proton (50 MeV/n) compared with unirradiated K-ras^{LA1} mice survival. *** $P=0.0037$ in Log-rank (Mantel-Cox) test acute proton (150 MeV/n) compared with unirradiated K-ras^{LA1} mice survival. $P=0.4001$ in Log-rank (Mantel-Cox) X-rays compared with unirradiated K-ras^{LA1} mice survival. (B) Quantification of adenocarcinoma in percent. . $P<0.05$ in contingency table analysis proton (50 MeV/n) with unirradiated control respectively. ** $P<0.05$ in contingency table analysis proton (150 MeV/n) with unirradiated control respectively.

<i>Radiation Type</i>	<i>Energy (MeV/n)</i>	<i>Dose rate (cGy/min)</i>	<i>Total dose (cGy)</i>	<i>Median Survival</i>	<i>Adenocarcinoma</i>
Unirradiated Control	0	0	0	396	10.1% (n=79)
X-rays	250 kVp	20	200	385	18.4% (n=38)
Proton acute	50	20	200	345	27.3% (n=35) ^{a, c}
Proton acute high	150	20	200	358	29.4% (n=33) ^{b, d}

^a P<0.05 in contingency table analysis compared with unirradiated control

^b P<0.05 in contingency table analysis compared with unirradiated control

^c P=0.40 in two-way contingency table analysis compared with X-ray.

^d P=0.18 in two-way contingency table analysis compared with X-ray.

Table 2.1. Effect of radiation exposure to K-ras^{LA1} mice.

2.4 Discussion

In the present study, we investigated if proton irradiation can lead to progression from preneoplastic lesions to invasive carcinomas of the lung and if this was different from X-irradiated mice. Radiation can cause DNA damage directly by breaking DNA strands or indirectly by the generation of reactive oxygen species (ROS). These types of damage are biologically significant as lack of or reduced repair can lead to genomic instability, cell death, and/or cancer progression. In the present studies, we observed that proton irradiation-induced DNA damage resulted in more premalignant lesions, but also the foci observed were larger in size compared to the control and X-rays exposed mice. Other investigators have demonstrated that proton irradiation leads to more potent acute DNA damage compared to γ -irradiation (Gerelchuluun et al., 2011). We were able to detect DNA damage foci 3 days post-irradiation only in the proton-irradiated mice as most of the DNA damage foci in X-irradiated mice were repaired within 24 hours post-irradiation (**Figure 2.1C, 2.1D, 2.2A, and 2.2B**). Along with DNA damage, radiation can elicit ROS that can cause oxidative damage to cells. The results obtained showed proton irradiated mice had extensive oxidative damage as observed by measuring oxidized proteins using the oxyblot method (**Figure 2.3A**). These results were in agreement with measured antioxidant genes in the lung tissues (**Figure 2.2C, 2.2D, and 2.4**).

It has been previously reported that proton irradiation can cause chronic oxidative stress in different organs post-irradiation (Christofidou-Solomidou et al.,

2015; Kim et al., 2016). Here, we also observed that there is chronic oxidative stress and DNA damage in the lungs as detected by measuring 8-oxo-dG nuclear foci and γ -H2AX respectively. In addition, we observed higher levels of peroxidized lipids in the plasma of the mice irradiated with protons (**Figure 2.5A, 2.5B, 2.5C, 2.5D, and 2.5E**). Next, we wanted to test the biological effect of chronic oxidative stress and DNA damage on tumor progression. For this, we irradiated 8-9 weeks old matched mice when they have only a small number of hyperplastic lesions or an occasional very small adenoma in the lung. We found that proton irradiated mice had a higher number and larger number of neoplastic lesions as compared to X-rays or unirradiated mice at 100 days post-irradiation (**Figure 2.6A and 2.6B**), and also there were more proliferating cells in the neoplastic lesions of proton irradiated tissues (**Figure 2.6C and 2.6D**). Similar, observations have been made by others when using high-LET radiation (Asselin-Labat et al., 2017). One possibility is that the radiation associated tumor progression observed after proton irradiation is through modulation of the tumor microenvironment. In the present studies, neoplastic lesions and the tumor microenvironment (inflammatory infiltrates) were different in proton versus X-irradiated lung tissues. Previously, we reported the upregulation of inflammatory genes in mice exposed to fractionated doses of ^{56}Fe 70 days post-irradiation (Delgado et al., 2014; Kitajima, Thummalapalli, & Barbie, 2016). Radiation has been implicated in modulating the immune system and chronic inflammation can enhance carcinogenesis process (Multhoff & Radons, 2012; Zhao & Robbins, 2009). In addition, inflammatory cell infiltration into the tumor

microenvironments is generally believed to be dose-dependent (Elgart et al., 2015; Hekim, Cetin, Nikitaki, Cort, & Saygili, 2015; Rodel, Frey, Multhoff, & Gaipf, 2015).

We further characterized the type of immune cells in the tumor stroma especially the presence of T cells as they may both promote and/or suppress tumor progression. It has been previously reported that tumor infiltration of lymphocytes in stage IA-IB non-small-cell lung cancer correlates with decreased risk of disease recurrence (Kilic, Landreneau, Luketich, Pennathur, & Schuchert, 2011). CD8⁺ T cells have antitumor effects by recognizing tumor-associated antigens resulting in cancer cell lysis. In addition, CD4⁺ T cells can promote CD8⁺ T cells in cytolytic functions. Regulatory T cells (Tregs) maintain self-tolerance and prevent autoimmune disease by immunosuppression and anti-inflammatory activity. Tregs are characterized by a master regulator transcription factor Forkhead box protein P3 (Foxp3) considered a crucial factor for immunosuppression (Hori, Nomura, & Sakaguchi, 2003). When infiltrated subsets of lymphocytes were examined in the tumor microenvironment, we found there was no significant difference in CD8⁺ T cells, but there were significant differences among CD4⁺ T cells and Foxp3⁺ cells (**Figure 2.8 A-F**). Having a high number of Tregs has been shown to modulate the tumor microenvironment and permit the tumor to escape immune surveillance, thus inhibiting anti-tumor responses (Erfani et al., 2012). Mutant K-ras has been shown to enhance the conversion of conventional T cells into regulatory T cells, and the requirement of Tregs for K-ras mediated lung tumorigenesis has been reported previously (Granville et al., 2009; Zdanov et al., 2016). Our data taken together can

be interpreted to suggest that proton irradiation can modulate tumor infiltration of lymphocytes and enhance the presence of Tregs in the tumor microenvironment. We also looked at the possibility of the senescence-associated secretory phenotype (SASP) involvement in modifying the tumor microenvironment, but we did not observe any evidence to support SASP involvement. Further experiments using different lung cancer mouse models such as mutations in EGFR would be necessary to understand the role of how proton radiation modulates tumor infiltration of lymphocytes in the tumor microenvironments or if it is specific to K-ras mutant mice.

Exposure to X-rays and proton radiation both increased cancer progression and decreased the median and overall survival as compared to unirradiated control mice. There were 1.5 times more carcinomas in proton-irradiated mice as compared to X-rays irradiated mice as accessed by histopathology at necropsy. The proton radiation with energy (50MeV/n) has a Bragg peak of around ~2.3 cm (total dose potentially stops inside the mouse body), so we used a different energy (150 MeV/n) proton radiation which has a Bragg peak around ~16.1 cm (total dose stops outside the mouse body) to examine its effects in cancer progression. With total dose of 2.0 Gy for whole-body proton irradiation with two different energies (50 MeV/n or 150 MeV/n) at 20 cGy/min, we observed an increased incidence of carcinoma 27.3% and 29.4% respectively compared to about 10% for unirradiated control mice **(Figure 2.10 A and 2.10B and Table 2.1)**. Despite having differences in where the proton irradiations deposited maximum total dose, whole body proton irradiation had similar outcomes in terms of increasing the invasive carcinoma incidence and a

decrease in median survival in the K-ras^{LA1} mouse model (**Figure 2.10A and 2.10B and Table 2.1**). More extensive biological studies will be required to understand the long-term risk of protons to normal tissues or tissues with early premalignant lesions.

In conclusion, whole body proton radiation can lead to several biological effects both acutely as well as chronically. These chronic effects of acute exposure to proton irradiation can modulate the tumor microenvironment leading to increases in tumor progression in the K-ras^{LA1} mouse model.

2.5 Future Directions:

Ongoing studies focus on understanding how low dose rate sSPE (low dose rate exposure of proton) affects lung carcinogenesis in K-ras^{LA-1} mice. In further studies, we will emphasize on understanding the carcinogenesis using high LET irradiation with different dose rate, total dose, and energies. We will be exploring the effect of Galactic Cosmic Radiation (GCR) in carcinoma incidence in the K-ras^{LA1} mice using multiple ions to simulate space environment (which has mixtures of radiation at the given time). Significant biological and mechanistically data obtained from these studies may help provide insights into molecular mechanisms which could be applicable by mitigating or preventing cancer initiation and progression during long-duration space travel. We will also be testing if the aspirin and CDDO-EA could be used to alleviate the effect of radiation as radiation seems to be the culprit enhancing the carcinogenesis.

Chapter Three

Triterpenoids (CDDO-EA): A Potent Radio-Protector Against Heavy Ion Radiation in A Lung Cancer Mouse Model

3.1 Introduction

Radiation-induced carcinogenesis is the major concern for astronauts on long-term space travel, as well as for cancer patients who are being treated with therapeutic radiation (Eskiocak et al., 2010). Space radiation consists of galactic cosmic rays (GCR) and solar particle radiation. GCR consists of 2% electron, 85.3% protons (hydrogen nuclei), 11.8% alpha particles (nuclei), and less than 1% of high charge (Z) and energy E (HZE) particles. Although HZE particles in deep space account for less than 1% of the GCR, it is believed to have higher carcinogenic effects compared to equivalent low energy terrestrial radiation (e.g. gamma-rays). At the present time astronaut's exposure to space radiation during exploration class missions represents a concerning and potentially unacceptable level of cancer risk.

While shielding protects against terrestrial radiation, shielding is not sufficient for space radiation as HZE particles can penetrate through the shielding (M. Durante & Cucinotta, 2008; Marco Durante & Cucinotta, 2011). Thus, there is a need for radioprotective drugs that could protect cells or tissues from biological damage caused by IR.

Unlike terrestrial radiation, which primarily consists of low-linear energy transfer (LET) radiation such as gamma, beta, and X-rays, high-LET space radiation particles are highly ionizing and penetrative. Both HZE particles and protons can directly ionize DNA or damages DNA and other cellular molecules through ionization of intermediary molecules, such as water (Hall & Giaccia, 2019). There is accumulating evidence that low dose radiation exposure induces oxidative stress and inflammation over time, where increased production of ROS/NOS leads to lipid peroxidation, oxidation of DNA and proteins as well as activation of pro-inflammatory factors. Mice exposed to IR exhibit persistently increased oxidant production and decreased anti-oxidant gene expression, leading to oxidative stress (Datta, Suman, & Fornace, 2014). Even two months after IR, Datta et al. reported a significant increase in 8-oxo-dG (marker of oxidative stress) staining in intestinal crypts relative to sham-irradiated controls. Additionally, our lab previously reported the upregulation of inflammatory genes in mice exposed to fractionated doses of ^{56}Fe 70 days post-irradiation (Delgado et al., 2014). Radiation has been implicated in modulating the immune system and chronic inflammation can enhance the carcinogenesis process (Multhoff & Radons, 2012) (Zhao & Robbins, 2009).

CDDO (2-cyano-3, 12-dioxooleana-1, 9-dien-28-oic acid) and its derivatives (methyl ester, CDDO-Me; ethyl amide, CDDO-EA; and imidazolide, CDDO-Im) (**Figure 3.1**) have become available for the prevention and treatment of inflammation and cancer (Suh et al., 1999). CDDO has been shown to have in the wide range of biological responses in a dose-dependent manner, and at lower concentrations, CDDO induces anti-inflammatory and anti-oxidant responses (Liby et al., 2007). CDDO-Me disrupts the interaction between Keap1 and Nrf2, leading to the release of Nrf2 (El-Ashmawy, Delgado, Cardente, Wright, & Shay, 2014). CDDO-Me can also bind to IKK β , which prevents the release of NF- κ B from its bound complex thus inhibiting the downstream pathways (Ahmad, Raina, Meyer, Kharbanda, & Kufe, 2006).

Our lab has reported that CDDO-Me protects colonic epithelial cells against IR-induced damage in an Nrf2-dependent manner, and also in part by enhancing signaling of DNA damage responses (**Figure 3.2 A**). In addition, CDDO-EA fed to mice before a lethal dose of total-body IR protected animals from DNA damage, acute gastrointestinal toxicity, and improved overall survival rate (**Figure 3.2 B**) (Kim et al., 2012). Recently, it was also demonstrated that a therapeutic window exists in which CDDO-Me that protects normal cells from radiation by activating the Nrf2 pathways but does not protect experimentally transformed or cancer cell lines (El-Ashmawy et al., 2014).

The aim of the current study is to investigate a synthetic triterpenoid (CDDO-EA) as a biological countermeasure (BCMs) that might improve the biological defenses to GCR as well as solar particle radiation exposure. For this study, we used the K-ras^{LA1} mouse model which mimics the human adenocarcinoma non-small cell lung cancer progression by spontaneous activation of mutant K-ras lesions. Mouse whole body irradiations were conducted with or without CDDO-EA (being provided in the chow 3 days prior to irradiation and for 1-day post-irradiation) with either 600 MeV/n ⁵⁶Fe or (50-150) MeV/n ¹H(SPE). K-ras^{LA-1} mice on CDDO-EA diet during fractionated ⁵⁶Fe-irradiation and SPE-irradiation resulted in a 2-3-fold decrease in the incidence of invasive carcinoma compared to mice on the control diet with no toxicities or side effects. Significant biological and mechanistically data obtained from these studies may help in space travel providing insights into molecular mechanisms which could be applicable by mitigating or preventing cancer initiation and progression during long-duration space travel with the help of orally available drug (CDDO-EA).

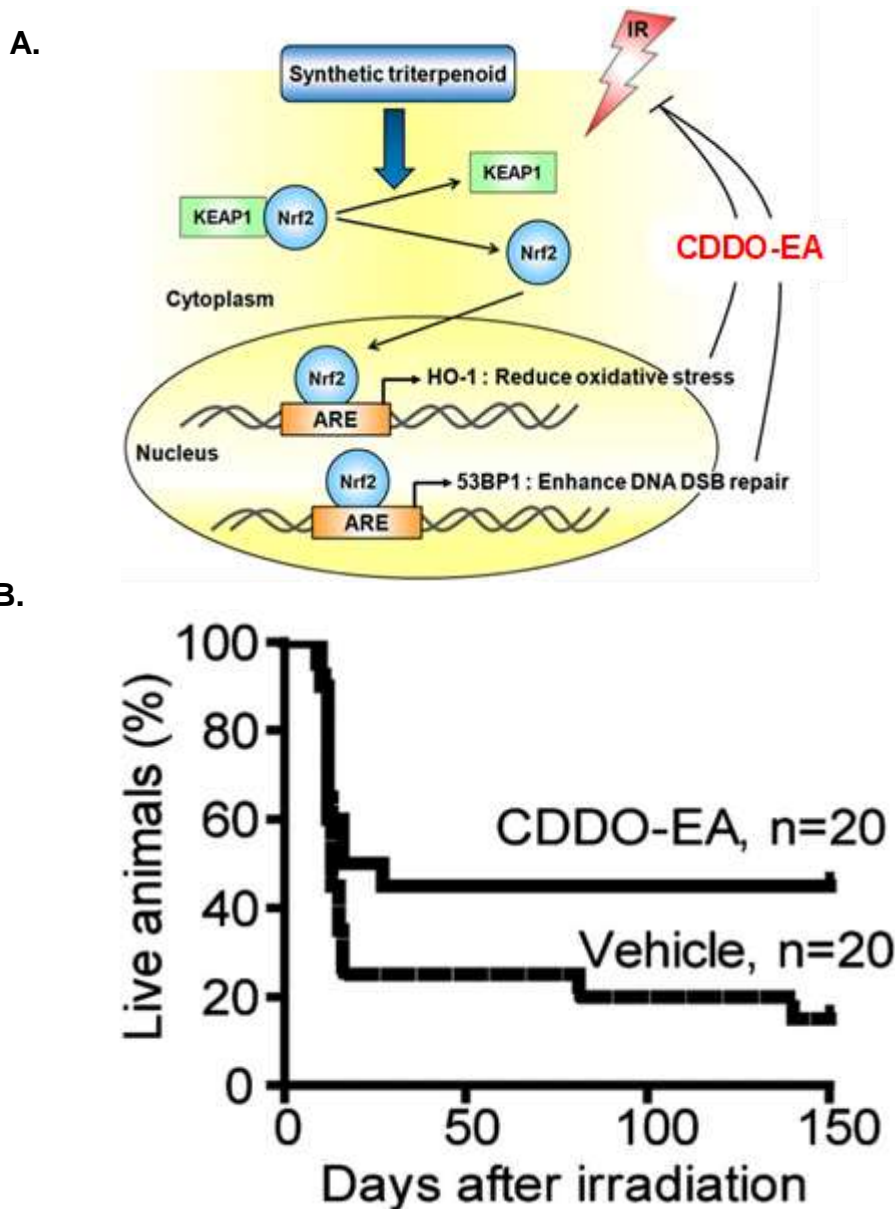


Figure 3.2. CDDO-EA as a radioprotector. (A) Schematic showing CDDO-EA pretreatment as a countermeasure before IR to activate Nrf2 regulating antioxidant enzyme and DNA repair protein. (B) Wild type female mice were fed the CDDO-EA diet or control diet 3 days before 7.5-Gy of whole-body irradiation pooled results from two independent experiments. CDDO treated animals have increased survival with a median survival in CDDO-EA treated mice 21.5 days in comparison to control mice 13 days with a median (95% confidence interval). Modified (Kim et al., 2012)

3.2 Materials and Methods

3.2.1 Mice and Irradiation

Male and female 8-15 weeks transgenic heterozygous K-ras^{LA1} mice were total-body irradiated with different radiation protocols: simulated solar particle event (sSPE) beam consisting of varying energies (50-150 MeV/n) using varying total doses (0.5-2.0 Gy) or 1.0 GeV/ nucleon ⁵⁶Fe-particles (5 daily doses of 0.2 Gy ⁵⁶Fe-particles). For ⁵⁶Fe-particles radiations animals were shipped to BNL, irradiated at the NASA Space Radiation Laboratory and returned to UTSW within 1 week after radiation via World Courier. All the animal experiments were reviewed and approved by IACUC at the UTSW at Dallas and BNL at Upton, NY. Animals were housed individually in plastic cuboid boxes subjected to either proton irradiation, ⁵⁶Fe-particles, and unirradiated control.

3.2.2 Lung Tumor Histopathology

Aged-matched both male and female heterozygous K-ras^{LA1} mice total body irradiated with radiation protocol (mentioned previously 3.2.1) were either sacrificed at indicated time-points or monitored until evidence of increased morbidity or death for survival study. For the histology, mice lungs were removed, inflated via intra-tracheal infusion with 10% neutral buffer formalin (NBF), clamped at the trachea and

immersed in 10% NBF overnight. Between 24-72 hrs. of necropsy, lung tissues were processed, paraffin-embedded, cut into 5 μm thick sections and stained with hematoxylin and eosin (H & E) for histopathological assessment using standard protocols. To analyze tumor grade and quantify lesions from survival cohorts with or without radiation treatment, three sections were cut 50 μm apart per animal. The stained sections were then analyzed; tumors graded, and other histopathological characteristics scored as either positive or negative as described previously in Chapter 2.2.2.

3.2.3 Experimental Design of CDDO-EA as a Countermeasure Experiment

To analyze CDDO-EA protection against ^{56}Fe 600 MeV/n (0.2 Gy x 5), 8-12 weeks old mice were given CDDO-EA or control diet 3 days prior to irradiation and 1-day post-irradiation. Similarly, to analyze CDDO-EA as a potential countermeasure against sSPE aged matched mice were given CDDO-EA or control diet 3 days prior to irradiation and 1-day post-irradiation. In both irradiation protocol, mice were either sacrificed at indicated time-points or monitored until evidence of increased morbidity or death for survival study (**Figure 3.3B**).

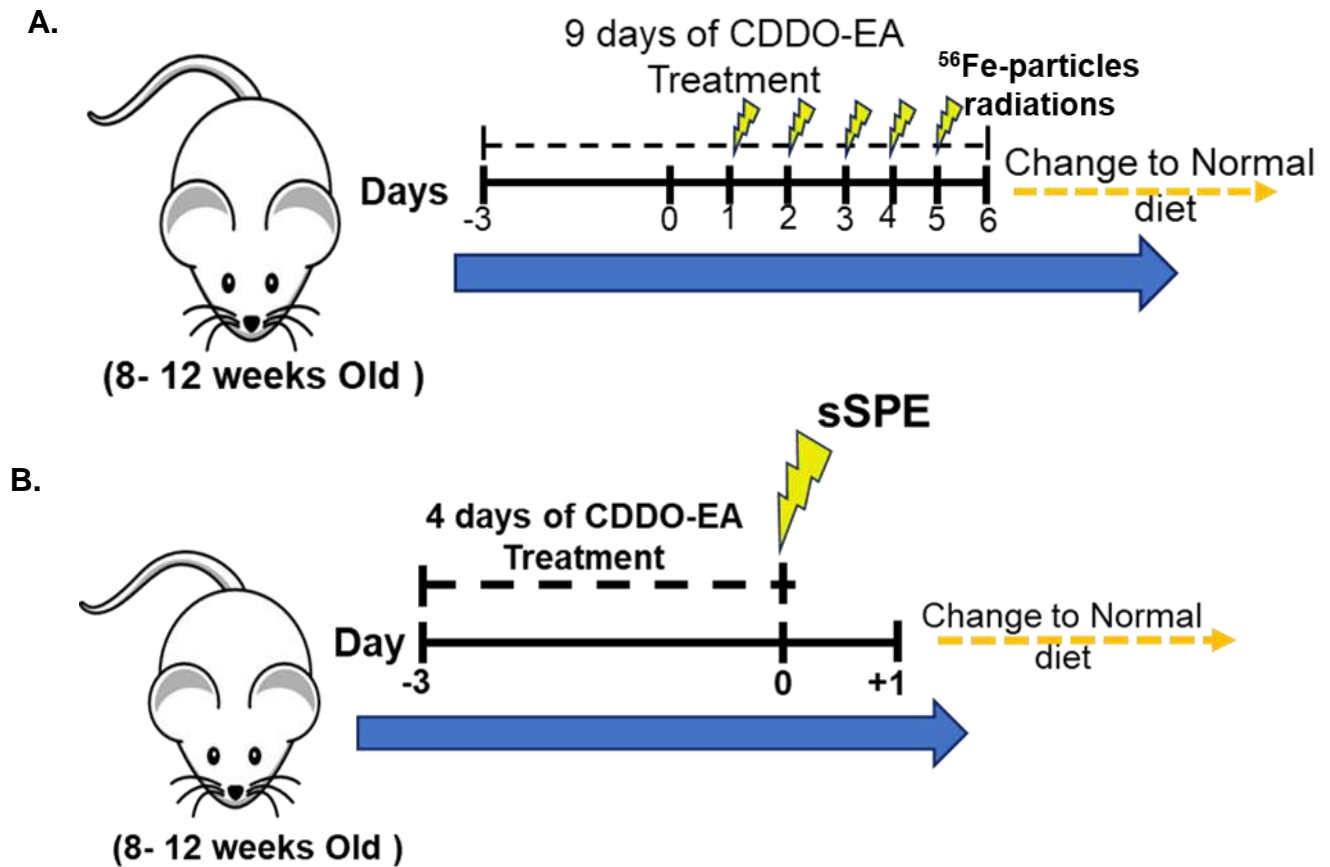


Figure 3.3. Experimental design - CDDO-EA as a radioprotector. Mouse whole body irradiations were conducted with or without CDDO-EA (being provided in the chow 3 days prior to irradiation and for 1-day post-irradiation) with either **(A)** 600 MeV/n ^{56}Fe or **(B)** (50-150) MeV/n (sSPE).

3.2.4 Western Blot Analysis

Frozen mouse lung tissues from the time-point experiments both 100 days for post IR (^{56}Fe) and CDOO-EA feed animals were disrupted using a liquid nitrogen-cooled mortar and pestle (Bel-ArtTM SciencewareTM, Fisher Scientific). Disrupted lung tissues were homogenized using an 18G needle and lysed in ice-cold lysis buffer (50mM Tris pH7.5, 150mM NaCl, 1% Triton X-100, and 1mM EDTA) containing protease and phosphatase inhibitor cocktails (Roche). Lysates were centrifuged, and supernatants used for protein assays. Proteins were separated by 4-15% Criterion TGXTM Precast Gel (Bio-Rad, CA), and transferred to a PVDF membrane using the Trans-Blot[®] TurboTM Transfer System (Bio-Rad, CA). Phospho- NF- κ B (s866/870) Cat #4810, NF- κ B Cat #8242, STAT3 Cat #9139, phospho-STAT3(y705) Cat #9145, and Nrf2 Cat #12721 were purchased from Cell Signaling Technology, Inc. (Danvers, MA, USA). Primary antibodies were used at 1:1000 dilution. Antibodies against beta-actin Cat #A1978, HO-1 Cat #Ab13248, phospho-Nrf2 Cat # Ab76026, and NQO1 Cat# Ab2346 were purchased from Sigma Aldrich. HRP-conjugated goat anti-mouse or anti-rabbit (Jackson ImmunoResearch) were used as secondary antibodies at a 1:5000 dilution and detected with the SuperSignalWest Pico Chemiluminescent Substrate Kit (Thermo Scientific), and quantified and analyzed using the Image J software.

3.2.5 Statistical Analysis

Statistical analysis was performed using GraphPad Prism version 7.00 (GraphPad Software, La Jolla California USA). To determine statistical significance for Survival analysis Kaplan-Meier curves were used the Log-rank test (Mantel-Cox) was performed. Statistical analysis of the histopathology was performed using two-tailed Fisher exact (95% confidence interval, CI) or Chi-square test. Comparison between irradiated groups with and without drug and controls were determined by using one-way ANOVA with Tukey correction along with pairwise comparisons for the P values. Comparison between groups with and without drug was done using Student's t-test. Differences were considered significant at $P < 0.05$.

3.3 Results

3.3.1 CDDO-EA diet reduces the progression of tumors in the K-ras^{LA1} mouse model

Previously CDDO-EA has been shown to be effective for chemoprevention of lung cancer induced by vinyl carbamate in A/J mice (Liby et al., 2007). So, we wanted to investigate how CDDO-EA affects tumor progression in K-ras^{LA1} mice. For this, we administered CDDO-EA (400mg/kg) or ctrl diet in chow to 12-15 weeks old to K-ras^{LA1} mice (**Figure 3.4A**). At this age, these mice only have small hyperplastic lesions and small adenomas. We treated these animals with CDDO-EA for 50 days, and after 50 days we analyzed the lung for tumor progression after necropsy. None of the animals in the CDDO-EA group developed any toxicity or adverse health effects. With the continuous 50 days CDDO-EA treatment of the K-ras^{LA1} mice, we found CDDO-EA decreased both initiations as well as progression in this mouse model. When we analyzed the lung, we found CDDO-EA-treated mice had a fewer number of hyperplastic lesions 50 days post-irradiation with the average of 3 lesions per mice as compared to 6 lesions per mice in control (**Figure 3.4C**). Similarly, the size of adenomas was smaller in CDDO-EA treated animals as compared to ctrl suggesting CDDO-EA is preventing the progression of the tumor (**Figure 3.4D**). Despite having the smaller sizes of adenoma, there was no difference in a number of adenomas suggesting that these CDDO-EA preventing or delaying in the progression of the adenoma but not eliminating them.

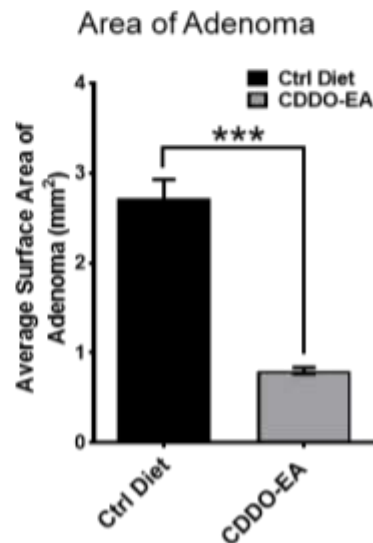
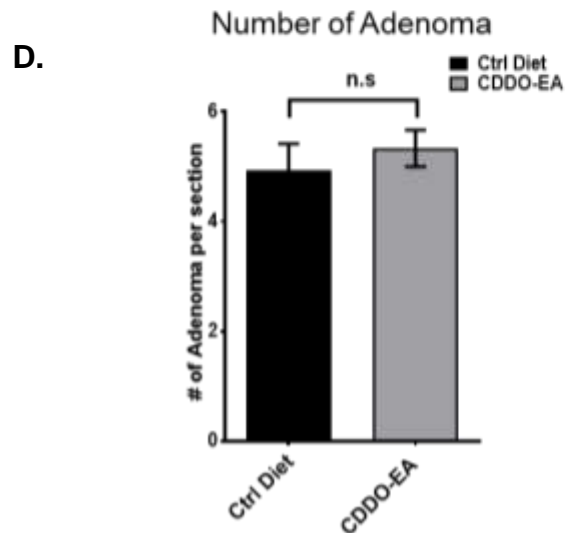
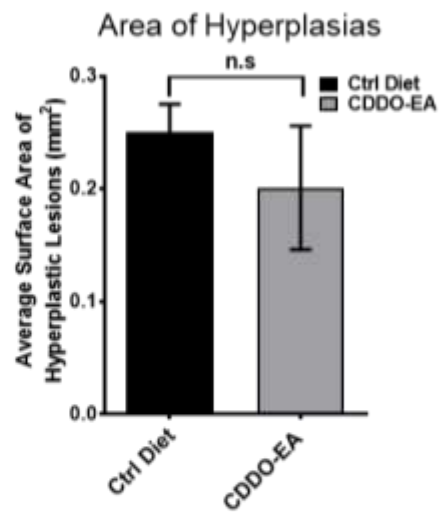
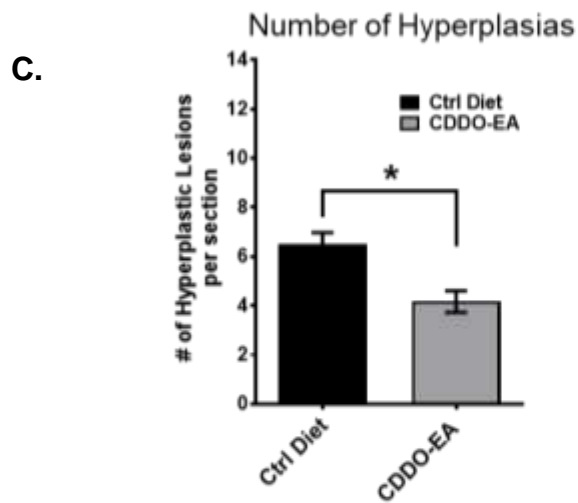
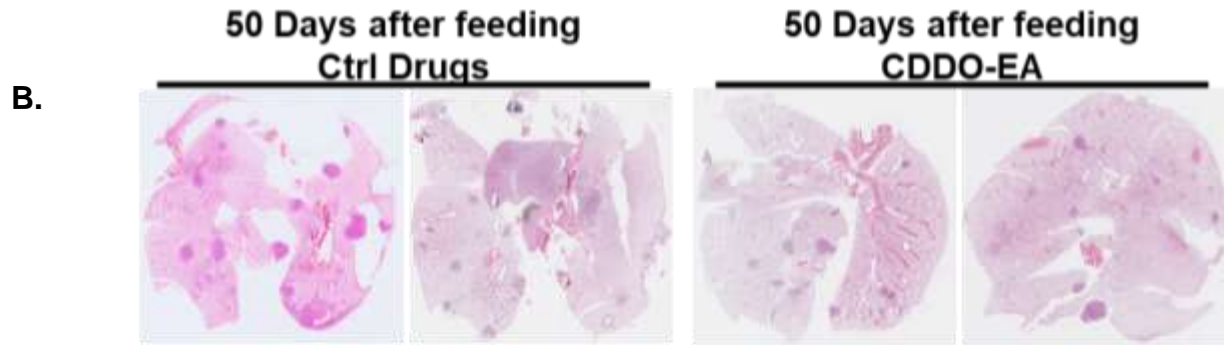
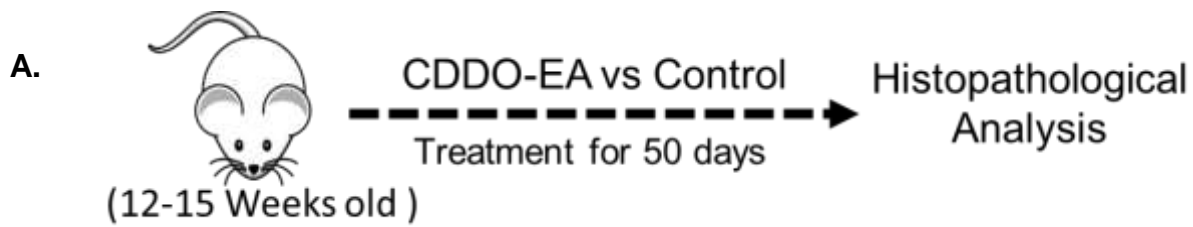


Figure 3.4. CDDO-EA diet reduces the progression of tumors in the K-ras^{LA1} mouse model. (A) Experimental design to analyze the effects of CDDO-EA on K-ras^{LA1} mice, 12-15 weeks old K-ras^{LA1} mice given diet containing CDDO-EA or control diet. (B) Representative hematoxylin and eosin (H and E) image performed after 50 days of continued treatment with and without CDDO-EA. (C) Quantification of overall number and size of hyperplasia's in age-matched K-ras^{LA1} lungs from after 50 days of treatment with and without CDDO-EA. * p=0.0233 (n = 5 mice per group) (D) Quantification of overall number and size of adenoma in age-matched K-ras^{LA1} lungs from after 50 days of treatment with and without CDDO-EA. *** p=0.0008 (n = 5 mice per group).

3.3.2. CDDO-EA as countermeasure sSPE radiation

To determine the radioprotective effect of the CDDO-EA, we irradiated 8-12 weeks K-ras^{LA1} mice with sSPE (simulated Solar Particle Events) or acute proton with 2.0 Gy and these mice were given diet containing CDDO-EA or control diet 3 days prior to irradiation and one-day post-irradiation (**Figure 3.3B**). To evaluate if CDDO-EA affected the tumor progression after radiation exposure, we compared premalignant lesions of aged-matched unirradiated control K-ras^{LA1} mouse lungs with proton irradiated mouse lungs as well as proton irradiated mouse CDDO-EA treated 100 days post-irradiation. Pretreatment of CDDO-EA prior to sSPE exposure did not significantly decrease the number or size of premalignant lesions (**Figure 3.5A and 3.5B**). Unirradiated control had an average of 6 lesions in mouse lung, proton irradiated mice had an average of 9 lesions in mouse lung, and proton irradiated with CDDO-EA treatment mice had an average of 7 lesions per section (**Figure 3.5A**). The overall surface area of the lesions in the lung of unirradiated K-ras^{LA1} mice were 0.24 mm², while the lung of proton-irradiated mice was 0.44 mm², and proton irradiated with CDDO-EA mice were 0.28 mm² (**Figure 3.5B**).

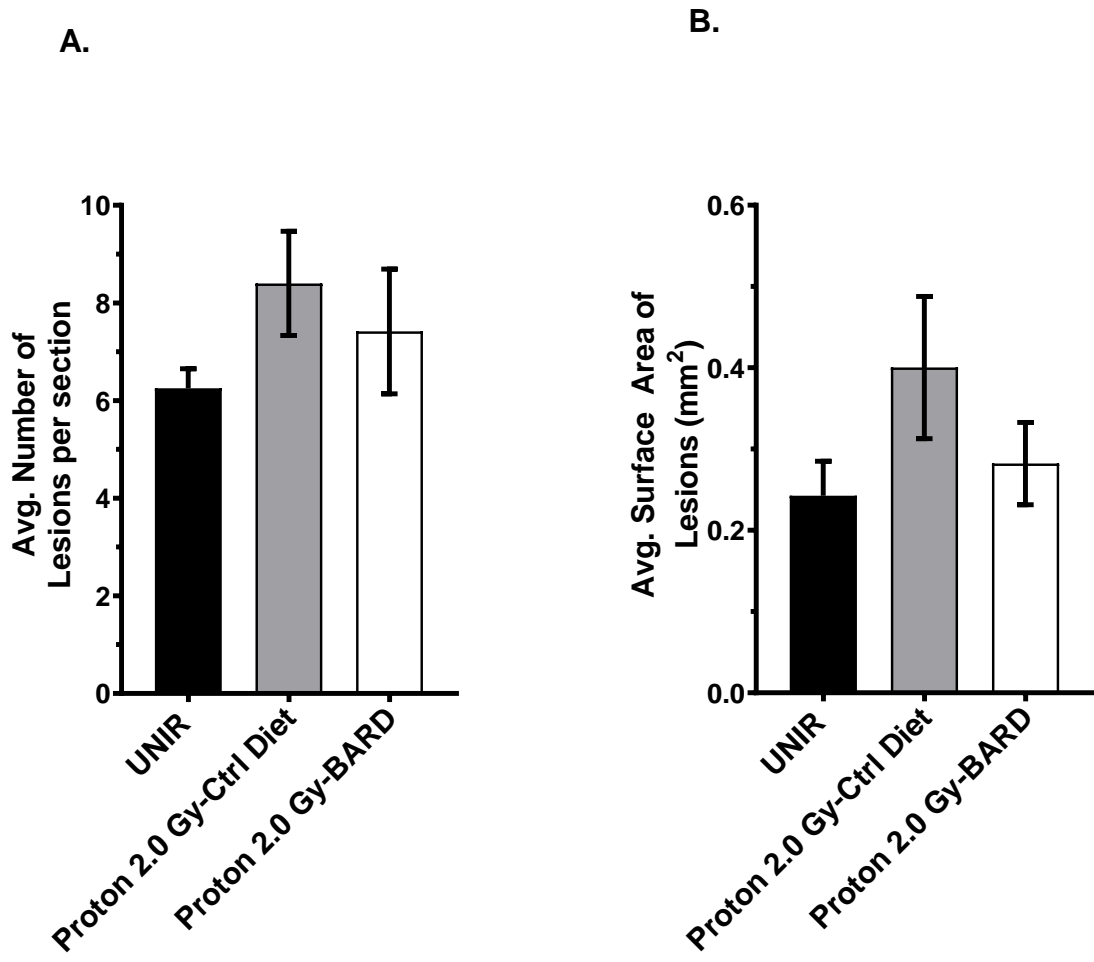


Figure 3.5. The decrease in number and sizes of premalignant lesions K-ras^{LA1} mouse model. (A) Quantification of overall number premalignant lesions in age-matched K-ras^{LA1} lungs from 70 days post-proton irradiation with and without CDDO-EA and unirradiated control. (B) Quantification of the overall area of premalignant lesions in age-matched K-ras^{LA1} lungs from 70 days post-proton irradiation with and without CDDO-EA and unirradiated control.

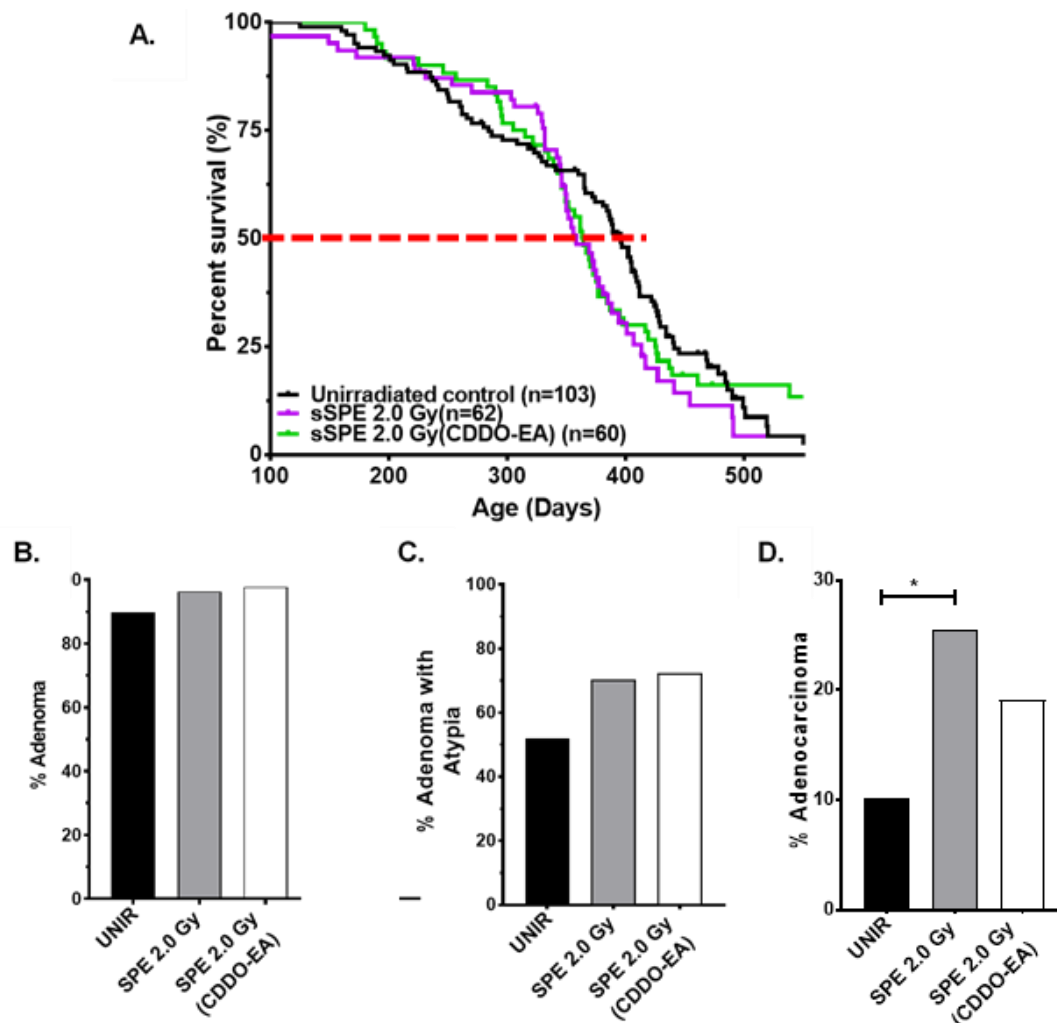


Figure 3.6. CDDO-EA decreases the incidence of invasive carcinoma in K-ras^{LA1} mice irradiated with a simulated solar particle event (50-150 MeV/n). (A) Kaplan–Meier survival plot of unirradiated, irradiated K-ras^{LA1} with and without CDDO-EA. Unirradiated K-ras^{LA1} mice (black); sSPE irradiated mice without drug (purple); sSPE irradiated mice with CDDO-EA (green). **P*=0.0443 in Log-rank (Mantel-Cox) test sSPE irradiated mice without drug compared with unirradiated K-ras^{LA1} mice survival. (B) Quantification of adenoma in percent. (C) Quantification of adenoma with atypia in percent. (D) Quantification of adenocarcinoma in percent. **P*<0.05 in contingency table analysis sSPE 2.0 Gy compared with unirradiated control respectively.

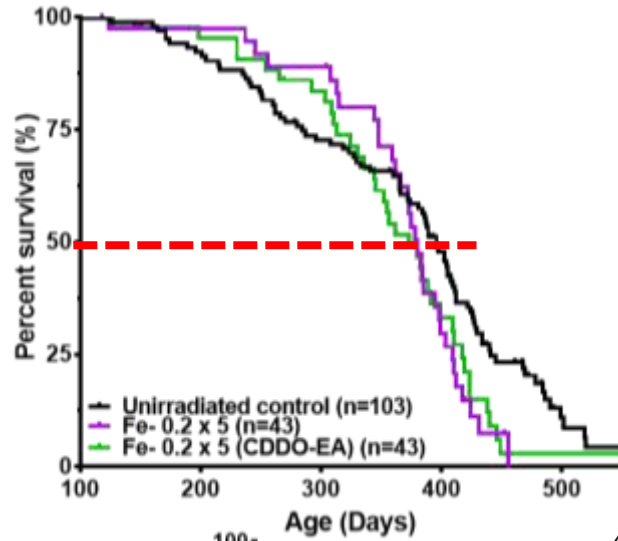
Similarly, we performed histopathological analysis on the survival of K-ras^{LA1} mice which were irradiated with sSPE and also treated with or without CDDO-EA. K-ras^{LA1} mice are susceptible to lung carcinoma as 10% of these develop invasive carcinoma. Unirradiated control mice had a median survival of 396 days, whereas mice exposed to an sSPE had a median survival of 358 days, and sSPE with CDDO-EA treatment displayed a median survival of 363 days. CDDO-EA did not significantly improve the median survival of sSPE treated animals (**Figure 3.6A**). As unirradiated Kras^{LA1} mice possess a background carcinoma incidence of approximately 10%, whereas mice exposed to 2.0 Gy of sSPE displayed a significant (25.5%) increase in invasive carcinoma while sSPE with CDDO-EA treatment displayed 19% incidence of carcinoma (**Figure 3.6D**). We did not observe a decrease in adenoma and adenoma with atypia with sSPE irradiation with CDDO-EA treatment (**Figure 3.6C & 3.6D**).

3.3.3. CDDO-EA as countermeasure HZE particles radiation

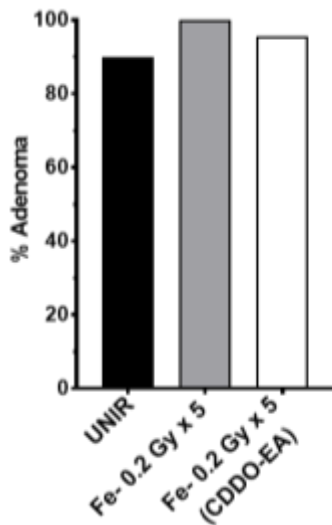
^{56}Fe - fractionated irradiation of 1.0 Gy decreased the lifespan of K-ras^{LA1} mice and resulted in an increased incidence of invasive carcinoma (**Figure 3.7**). K-ras^{LA1} mice on CDDO-EA diet during fractionated ^{56}Fe - irradiation exhibit a 2-fold decreased incidence in invasive carcinoma in comparison to mice on control diet. Despite the decrease of invasive carcinoma incidence, we did not see an increase in the lifespan of ^{56}Fe - irradiated mice on the CDDO-EA diet. The median survival of the unirradiated control mice was 396 days, ^{56}Fe - irradiated mice were 380 days and, ^{56}Fe - irradiated mice with CDDO-EA was 373 days (**Figure 3.7A**). We did not observe any difference in adenoma and adenoma with atypia among unirradiated control, ^{56}Fe - irradiated mice and ^{56}Fe - irradiated mice with CDDO-EA (**Figure 3.7B and 3.7C**). Approximately 17% of K-ras^{LA1} mice on the CDDO-EA diet during the ^{56}Fe -irradiation have invasive carcinoma in contrast to 34% in mice on the control diet (**Figure 3.7D**).

Previously our lab using fractionated ^{56}Fe have shown that inflammatory signaling may play an important role in radiation-induced carcinogenesis (Delgado et al., 2014). Using western blot analysis, we looked at the protein expression of inflammatory pathways such as STAT3 and NF- κ B (**Figure 3.8**). With the treatment of CDDO-EA prior to ^{56}Fe irradiation, we saw a decrease in activated STAT3 and NF- κ B 70 days post-irradiation (**Figure 3.8A, 3.8B & 3.8C**).

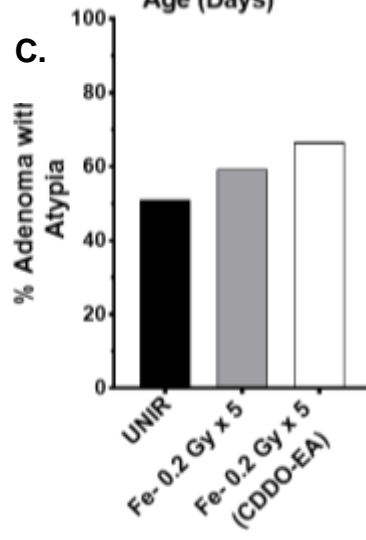
A.



B.



C.



D.

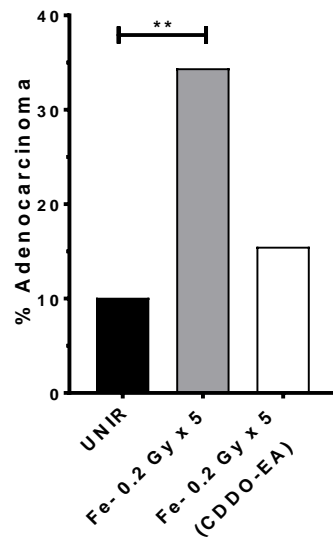
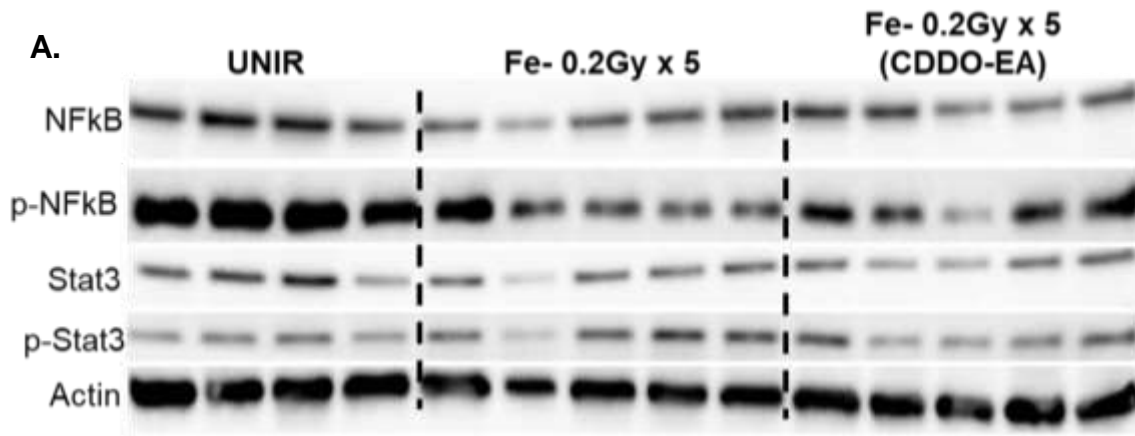
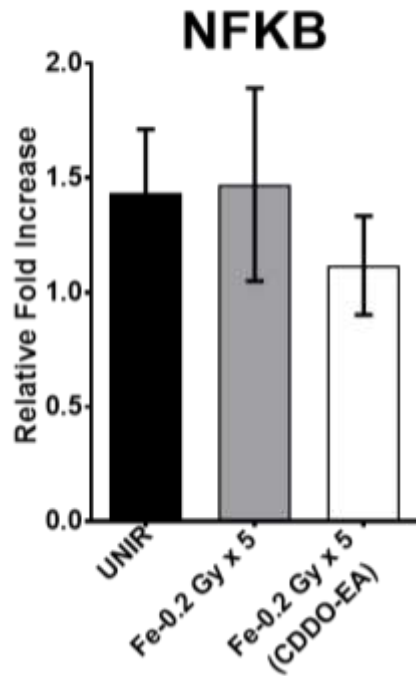


Figure 3.7. CDDO-EA decreases the incidence of invasive carcinoma in K-ras^{LA1} mice irradiated with ⁵⁶Fe (600MeV/n) 1.0 Gy. (A) Kaplan –Meier survival plot of unirradiated, irradiated K-ras^{LA1} with and without CDDO-EA. Unirradiated K-ras^{LA1} mice (black); ⁵⁶Fe irradiated mice without drug (purple); ⁵⁶Fe irradiated mice with CDDO-EA (green). *P=0.0481 in Log-rank (Mantel-Cox) test ⁵⁶Fe irradiated mice without drug compared with unirradiated K-ras^{LA1} mice survival. (B) Quantification of adenoma in percent. (C) Quantification of adenoma with atypia in percent. (D) Quantification of adenocarcinoma in percent. **P<0.05 in contingency table analysis ⁵⁶Fe (600MeV/n) 1.0 Gy compared with unirradiated control respectively.



B.



C.

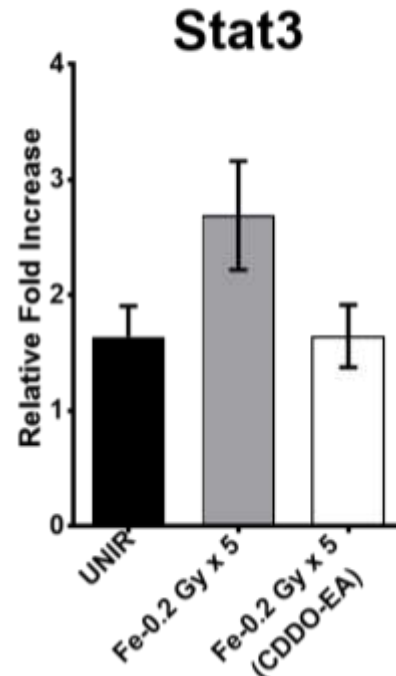


Figure 3.8. CDDO-EA modulates Inflammation-related signaling. (A) Western blot analysis of phosphorylated and total proteins such as STAT3 and NF- κ B. (B) Quantification of activated NF- κ B. (C) Quantification of activated STAT3.

3.3.4. CDDO-EA mitigator to radiation effect

To investigate the mitigating effect of CDDO-EA after irradiation, we initially administrated CDDO-EA to WT 129SV mice for 2 to 6 days, and then we measured antioxidant response proteins in the lung after different time point. With CDDO-EA treatment we saw an increase in transcription factors such as Nrf2 within 2 days after post-irradiation (**Figure 3.10A**), and we also saw an increase in HO-1 and NQO1 proteins in the lung detected by immunoblot (**Figure 3.10A**).

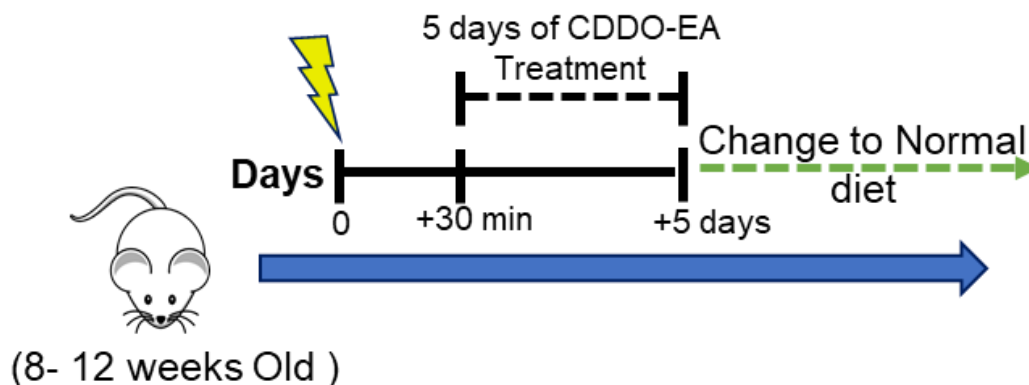


Figure 3.9. CDDO-EA as a mitigator. Mouse whole body irradiations were conducted with or without CDDO-EA (being provided in the chow up to 5 days post-irradiation).

Previously our lab has shown that CDDO-EA can be an effective radioprotector in mice when given 3 days before 7.5 Gy total body irradiation (TBI) (Kim et al., 2012). To further investigate the role of CDDO-EA in mitigation, we irradiated mice with 7.5 Gy total body irradiation (TBI) and then administered CDDO-EA 30 min post-irradiation to 5 days (**Figure 3.9**). Treatment with CDDO-EA starting 30 min post-irradiation did not improve the median survival of mice as compared to control treated mice (**Figure 3.10B**).

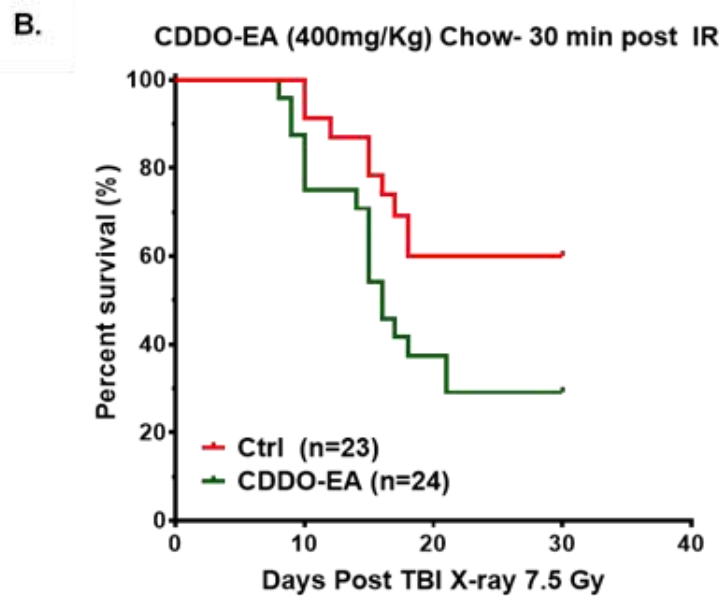
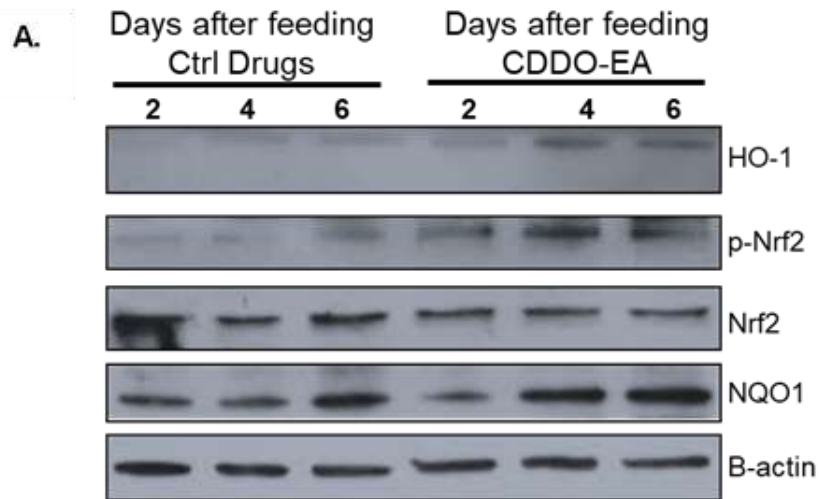


Figure 3.10. CDDO-EA decreases wild type mouse survival after an acute lethal dose of 7.5-Gy total body X-ray irradiation. (A) Western blot analysis of antioxidant protein in lungs lysate of wild type mice fed with CDDO-EA diet or control diet provided for 2,4 or 6 days. Total Nrf2, phospho-Nrf2 (p-Nrf2), NQO1 and HO-1 were detected by Western blot analysis. (B) Wild type female mice were fed the CDDO-EA diet or control diet for 5 days after 7.5-Gy TBI. Pooled results from two independent experiments are shown.

3.4 Discussion

Ionizing radiation (IR) carcinogenesis risk is a concern for patients receiving radiotherapy for cancer treatment, as well as for astronauts exposed to IR during long-term space travel. While shielding is effective protection against terrestrial radiation, shielding is ineffective against high-LET space radiation where particles can penetrate through the shielding (Chancellor et al., 2018). Therefore, there is mounting evidence that biological countermeasures may be required to ensure that the established limits of increased lifetime fatal cancer risks. In this study, we evaluated CDDO as a potential radiation countermeasure and mitigator both low and high LET radiation.

To analyze the effects of CDDO-EA in the tumor development in K-ras^{LA1} mouse model, 12-15 weeks old mice were fed either CDDO-EA or control diets continuously for 50 days as it has been shown previously that CDO-EA could regress vinyl carbamate induce K-ras mutations (Liby et al., 2009). After 50 days of continuous treatment, mice have few initiated hyperplastic lesion and smaller size adenomas in contrast to animals on a control diet (**Figure 3.4**). Although the role of reactive oxygen species (ROS) in cancer harboring oncogenic K-ras has not been fully understood, K-ras activation can lead to ROS production and increase oxidative stress (Trachootham et al., 2006), and ROS generation is required for K-ras induced tumorigenicity (Weinberg et al., 2010). Additionally, Human clinical data show that lung carcinomas harboring K-ras mutations are enriched with inflammatory cells

(Rekhtman, Ang, Riely, Ladanyi, & Moreira, 2013). In pancreatic ductile adenocarcinoma, *K-ras*-induced cancers in adult mice were reduced unless it was accompanied by injury or mild form of chronic inflammation (Guerra et al., 2007). These studies along with our study suggest CDDO-EA might have worked as an anti-inflammatory as antioxidant agent thus prolonging the onset of the tumors in the *K-ras*^{LA1} mouse model.

Previously using CPC; APC colon cancer-susceptible mice, we showed an increase in the incidence of invasive carcinoma ~250 days post solar particle irradiation simulations (sSPE). But the treatment of CPC; APC mice with CDDO-EA prior to sSPE not only exhibited fewer polyps ~100 days post-IR in comparison to mice on control diet but also exhibit a decreased incidence in invasive carcinoma in comparison to mice on control diet ~250 days post-IR. Our studies provide additional evidence that CDDO-EA can be used a countermeasure as we saw that with the administration of CDDO-EA 3 days prior to the sSPE decreased invasive carcinoma and increased median survival in *K-ras*^{LA1} mouse model. Additionally, CDDO-EA 3 days prior to the fractionated ⁵⁶Fe irradiation (HZE radiation), mice exhibited a decrease in invasive lung carcinoma in contrast to mice on the control diet. Even though we saw a decrease in invasive carcinoma with CDDO-EA treatment prior to fractionated ⁵⁶Fe irradiation but we did not observe an increase in median survival. We did not observe any differences among other tumor grade progression such as adenoma and adenoma with atypia with CDDO-EA treatment prior to the radiation.

Inflammation plays important role in the carcinogenic process as it can act as a tumor promotor by aiding in proliferation, simulating of angiogenesis, and altering the response to hormones and chemotherapy (Candido & Hagemann, 2013). We observed that there were a chronic oxidative stress and DNA damage in the lungs of mice irradiated with acute proton 2.0 Gy, and with low dose rate proton (sSPE) induces sets of SIR/PSIS gene expression (senescence-associated inflammatory responses / p53-suppressed invasiveness signature) (Kim et al., 2016; Luitel et al., 2018). Pretreatment with CDDO-EA in the CPC; APC mouse model reduced the initiation as well as the progression of colorectal cancer by inhibiting the induction of SIR/PSIS. Previously fractionated ⁵⁶Fe irradiation was shown to increase activation of inflammation-related network proteins such as NF- κβ and STAT3 which could be reduced by administering mice with CDDO-EA prior to radiation. These studies provide evidence that radiation-induced carcinogenesis can be reduced using short treatment of CDDO-EA prior to radiation, and it also suggests that CDDO-EA might be working by reducing the oxidative stress and increasing DNA repair post-irradiation. As CDDO-EA looked promising radioprotective drug, we tested if CDDO can act as a mitigator. Our preliminary data show that even with treatment of CDDO-EA within 30 minutes did not have any effect medial survival of the mice post-irradiation.

In summary, CDDO is an orally available anti-inflammatory/anti-oxidant modulator drug which could act as biological countermeasures to provide risk reduction for radiation.

3.5 Future Directions:

We will be doing extensive biological studies to examine DNA repair and oxidative stress both acutely and chronically as well as chronic modulation of inflammation with the treatment of CDDO-EA. We will evaluate if CDDO-EA treatment can decrease in cancer progression against low dose high LET radiation a such as silicon. Additional studies will be carried out before we rule out CDDO-EA as an effective mitigator for the radiation-induced biological effects. We will be exploring the use of CDDO-EA as a biological countermeasure for Official Galactic Cosmic Radiation (GCR) simulation developed at NSRL.

Chapter Four

Lung Cancer Progression Using Fast Switching Multiple Ion Beam Radiation and Countermeasure Prevention

4.1 Introduction

Human long-term interplanetary travel is currently limited due to uncertainties and concerns of serious health risk to astronauts associated with radiation in space (Chancellor et al., 2018; Cucinotta, To, & Cacao, 2017; M. Durante, 2014). Humans on earth and astronauts on the International Space Station are partially protected from galactic cosmic radiation (GCR) exposure by the Earth's magnetic field, but astronauts would be exposed to GCR during deep space missions even with shielding. The long-term health risks due to radiation exposure range from degeneration of central nervous system, cardiovascular disease, pulmonary disease and cancer risks to different organs such as lung, colon, stomach, and breast (M. Durante & Cucinotta, 2008). Unlike terrestrial radiation which is primarily composed

of low linear energy transfer (low-LET) photons such as x-rays and γ -rays, astronauts in space would be exposed to rare solar particle events (SPEs) and GCR which comprises mostly energetic protons, helium nuclei, and heavier atomic nuclei with high charge and energy (HZE) such as silicon (Mewaldt, 1994). Low-LET radiation is considered sparsely ionizing in contrast high-LET radiation that is considered highly ionizing and capable of producing secondary radiations known as δ -rays. Such radiation-induced DNA damage from high-LET radiation is difficult to repair, often leading to mutagenic repair and induction of genomic instability thus estimated to cause increases in tumorigenesis compared to equivalent doses of low-LET radiation, (Asaithamby, Hu, & Chen, 2011; Asaithamby, Hu, Delgado, et al., 2011; Li et al., 2013).

Previously, using different mouse models, other investigators have demonstrated that high-LET radiation compared to low LET radiation result in a higher risk of generation tumorigenesis in the lung, mammary gland, liver and gastrointestinal tract (Delgado et al., 2014; Trani et al., 2014; Weil et al., 2009). The lung has a large surface area which makes it a prominent target for radiation exposure, and remarkably susceptible to radiation-induced cancer (Delgado et al., 2014; Luitel et al., 2018). The analysis from the atomic bomb survivor cohort is evidence that the lung is one of the organs with a higher solid tumor incidence (Ozasa et al., 2012), and lung cancer accounts for more cancer-related deaths than any other cancer type among both men and women (Cancer facts and Fig. 2018) (Siegel et al., 2019a). While physical shielding may reduce some of the risks of cancer from space

radiation, there is mounting evidence that biological countermeasures may be required to ensure that the established limits of increased lifetime fatal cancer risks are not exceeded. In this study, we evaluated CDDO as a potential radiation countermeasure to a simplified GCR simulation. CDDO is an orally available anti-inflammatory/anti-oxidant modulator drug, and previously we showed CDDO provided in lab chow prior to a lethal dose of whole-body irradiation protected mice from acute gastrointestinal toxicity with enhanced DNA damage repair resulting in improved overall survival (Kim et al., 2012).

Most of the studies on radiation-induced cancer have been performed using either terrestrial (low-LET) radiation or single high LET ion type radiation which does not simulate the complex space radiation environment. To address this gap in how multiple ions might interact, we used three ions: protons (H), helium (He) and silicon (Si) to create a simplified fast switching ion beam GCR simulation. Using these three ions beams we exposed the lung cancer susceptible mouse model (K-ras^{LA-1}) at the NSRL (Brookhaven National Laboratory) with a total dose of 30 cGy (Leisa Johnson¹, 2001). We hypothesized mixed particle radiation would increase the incidence of invasive carcinoma, and CDDO would be a potential countermeasure reducing inflammation and carcinogenesis.

4.2 Material and Methods

4.2.1 Animals and Irradiation

All animal experiments were reviewed and approved by the Institutional Animal Care and Use Committees (IACUC) at the University of Texas Southwestern Medical Center at Dallas (UTSW) and Brookhaven National Laboratory (BNL) (Upton, NY). Mice were housed and bred following an approved husbandry protocol in ventilated micro isolator cages within a pathogen-free facility at UTSW. Transgenic K-ras^{LA1} mice on a 129S2 background as previously described (Leisa Johnson¹, 2001) were obtained from Dr. Jonathan Kurie (University of Texas M.D. Anderson Cancer Center, Houston, TX), and 129S2 K-ras^{LA1} breeding pairs were established to generate both heterozygous and wild-type littermate controls.

Both male and female transgenic K-ras^{LA1} mice, ages eight to twelve weeks old were total-body irradiated with different radiation protocols as shown in Fig **(4.1A)**. Animals subjected to irradiation and unirradiated controls for both time points and survival studies were transported via World Courier (New Hyde Park, NY) overnight delivery to Brookhaven National Laboratory and returned to UT Southwestern within 1 week after irradiation.

4.2.2. Synthetic Triterpenoid (CDDO) Treatment

To evaluate the ethyl amide derivative of CDDO (CDDO-EA) as a potential countermeasure against multiple ion beam radiations, we fed CDDO-EA or control chow to aged-matched 129S2 transgenic K-ras^{LA1} mice at Brookhaven National Laboratory. Both males and female mice were assigned randomly into the experimental cohorts. The concentration of CDDO-EA in the diet was 400mg/kg (provided by Reata Pharmaceuticals, Irving Texas) and prepared into chow pellets by Purina Mills). Animals were fed ad libum with CDDO-EA diet or control diet three days prior to the radiation, and the diet was changed to the normal diet one day after the radiation exposure.

4.3.3 Lung Tumor Evaluation and Histology

For the survival studies, mice were monitored until there was evidence of increased morbidity or sacrificed after 1-year post-irradiation. At the time of sacrifice or death, carcasses were necropsied and removed lungs were inflated by intra-tracheal infusion with 10% neutral buffered formalin (NBF), the trachea clamped, and the whole lung immersion-fixed overnight in 10% NBF. The lungs tissues were processed, paraffin embedded, cut at 5 microns thick sections, and stained with Hematoxylin and Eosin (H&E). To evaluate the grade and quantify lesions in the lung, two sections were cut 50µm apart per mouse. Tumor grades and other histopathological characteristics were described previously (Leisa Johnson¹, 2001) and included adenocarcinoma, adenoma with atypia, adenoma, hyperplasia,

pneumonia, bronchial extensions, and autolysis. All pathology was confirmed in a blinded fashion by a DVM/Ph.D. pathologist specializing in mouse pathology (J.R.).

To quantify premalignant lesions, sizes and numbers, a subset of aged-matched 129S2 mice were sacrificed one hundred days post-irradiation. Lungs tissues were removed, processed and paraffin embedded. We cut three sections of each lung per animal approximately 50 μm and stained with Hematoxylin and Eosin (H&E). Using a Hamamatsu Nanozoomer 2.0-HT mounted CCD camera (Whole Brain Microscopy Facility at UTSW) images were taken and analyzed using the Nanozoom Digital Pathology Software.

4.2.4 Malondialdehyde Assay on Serum

Aged-matched mice blood samples were collected in 0.5cc microcentrifuge tubes with 0.5M EDTA by the submandibular blood collection method from both unirradiated control and irradiated animals 100 days post-irradiation. The blood samples were then centrifuged 700-1000x G for 10 minutes at 4° C. From the centrifuged samples, the plasma (upper clear layer) was collected. MDA is a byproduct of lipid peroxidation. MDA levels in plasma were measured using the TBARS Assay Kit (Cayman Chemical, 10009055) as per the manufacturer's instructions.

4.2.5 Statistical Analysis

Statistical analyses were performed using GraphPad Prism version 7.00 for Windows, (GraphPad Software, La Jolla California USA). At least five independent biological samples were used per radiation dose. To make a comparison between irradiated and control groups one-way ANOVA with Tukey correction along with pairwise comparisons for the P values was used. Differences were considered significant at $P < 0.05$. Statistical analysis of the histopathology was performed using two-tailed Fisher exact (95% confidence interval, CI) or Chi-square test.

4.3 Results

4.3.1. Total Body Irradiation Using Multiple Ion Beam

In this study, we more closely simulated the space environment which is composed of heterogeneous radiation fields predominated with low background fluences of low-LET radiation and lower fluences of high-LET radiation. We used fast switching of protons (H), helium (He) and silicon (Si) particles to delivery mixed ion species to the approximate space environment. We delivered these particles 120 MeV/n protons (LET=0.64 keV/ μ m), 250 MeV/n helium ions (LET=0.40 keV/ μ m) and 300 MeV/n silicon ions (LET=76 keV/ μ m) in dose proportions of 66.7%: 16.67%: 16.67% respectively where silicon was used as a surrogate for particles of Z greater than 2. The total dose of 30cGy with a dose rate of 0.5cGy/min (measured at target) was delivered in approximately 60 minutes for this experiment including the time consumed in rapid switching between particle beams. We delivered these ions in two different orders: 3B-1 (H \rightarrow He \rightarrow Si) and 3B-2 (Si \rightarrow He \rightarrow H), and we used 30 cGy H as a single beam reference (**Figure 4.1A**). Small plastic boxes were used for the housing of mice during radiation, and we could fit 2-3 mice in a single box. These boxes had small holes drilled for the ventilation for the period of 60 minutes. Using 60cm x 60cm beam size 8-12 weeks old mice were arranged in the center of the field to assure the best uniformity for total body irradiation (TBI) (**Figure 4.1B**). During the irradiation, none of the animals showed any distress. Following irradiation, we had two different times, 100 days and 1-year post-irradiation, to measure biological outcome on K-ras^{LA1} mouse model.

A. 3B-1 : H-He-Si (30cGy)

Ion	Energy (MeV/n)	Total Dose (cGy)	Dose Rate (cGy/min)	Estimated time (min)
Proton (H) (66.66 %)	120	20	0.5	40
↓ Switch to He				~3
Helium (He) (16.67 %)	250	5	0.5	10
↓ Switch to Si				~3
Silicon (Si) (16.67%)	300	5	0.5	10

Total Dose = 30 cGy
Total Time ~66 min

3B-2 : Si-He-H (30cGy)

Ion	Energy (MeV/n)	Total Dose (cGy)	Dose Rate (cGy/min)	Estimated time (min)
Silicon (Si) (16.67%)	300	5	0.5	10
↓ Switch to He				~3
Helium (He) (16.67 %)	250	5	0.5	10
↓ Switch to H				~3
Proton (H) (66.66 %)	120	20	0.5	40

Total Dose = 30 cGy
Total Time ~66 min

H (30cGy)

Ion	Energy (MeV/n)	Total Dose (cGy)	Dose Rate (cGy/min)	Estimated time (min)
Proton (H) (66.66 %)	120	30	0.5	60

Total Dose = 30 cGy
Total Time 60 min

B.



C.

1. 3B-1 (30cGy)
2. 3B-2 (30cGy)
3. H (30cGy)



Age 8-12 Weeks



100 Days Post IR
Tissue Collection



1 year
Post IR

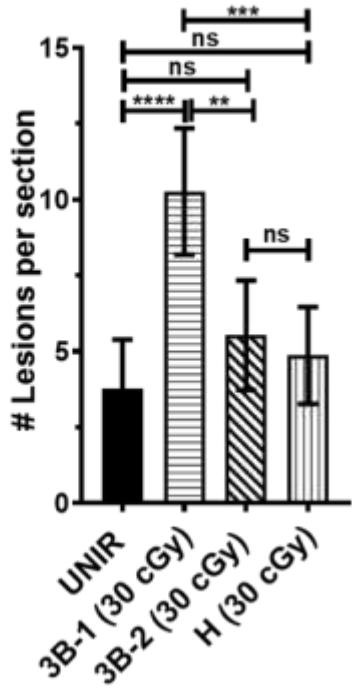
Figure 4.1. Experimental design for the three-beam radiation. (A) Different approaches for mixed beam radiation using Hydrogen, Helium and Silicon ions. (B) This figure shows the experimental setup of how mice were arranged in the beamline. (C) Schematic of experimental design for total body irradiation of mice.

4.3.2. Order of Particles in Multiple Ion Beam Radiation Matter

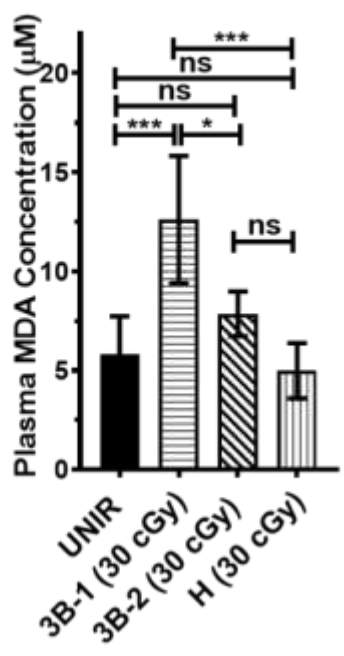
Initially, we hypothesized that both 3B-1 and 3B-2 irradiation protocol would equally induce lung cancer progression K-ras^{LA-1} mouse model compared to proton irradiation alone and unirradiated controls. But when we performed histopathological and chemical analyses in lung and plasma respectively of irradiated mouse and controls 100 days post-irradiation, we observed the 3B-1 radiation protocol appeared to be more damaging. To determine how multiple beam exposure affected the carcinogenic process, we compared premalignant lesions of aged-matched unirradiated control K-ras^{LA1} mouse lungs with proton irradiated mouse lungs or 3B-1 irradiation or 3B-2 irradiation 100 days post-irradiation. Compared with unirradiated or 3B-2 or proton only irradiation, K-ras^{LA1} mice irradiated with 3B-1 developed higher numbers of lesions. Unirradiated animals had an average of 4 lesions, 3B-1 irradiated mice had an average of 10 lesions, 3B-2 irradiated animals had an average of 6 lesions, and proton irradiated animals had an average of 5 lesions (**Figure 4.2A**). Similarly, our previous reports showed that exposure to higher dose proton (200 cGy) radiation was associated with an increase in oxidative stress in lung and plasma of the mice (Luitel et al., 2018). On analysis of blood plasma 100 day post-irradiation for lipid peroxidation as an indicator of oxidative stress, we observed plasma collected had more than a 2.5-fold increased amount of MDA present in the 3B-1 irradiated animals compared unirradiated controls. In comparison to 3B-1, 3B-2 and proton did not increase the MDA level in the plasma (**Figure 4.2.B**). Thus, the order of ion irradiation appeared to biologically matter.

To further determine disease progression following radiation exposure, one-year post-irradiation K-ras^{LA1} mice lung were evaluated histologically for the appearance of adenomas with atypia and invasive carcinomas. K-ras^{LA1} mice exposed to 3B-1 exhibited a significant increase (79%) in adenomas with atypia (**Figure 4.2C**) and an increase (28.6%) in invasive carcinoma formation (**Figure 4.2D**). Unirradiated Kras^{LA1} mice possess a background adenoma with atypia and carcinoma incidence of approximately 55% and 10% respectively. Mice exposed to 3B-2 and proton radiation did not display any significant increase in adenoma with atypia (54% for 3B-2 and 58% for proton irradiation) or invasive carcinoma (12.9 % for 3B-2 and 16.13 % for proton) one-year post-irradiation compared to the unirradiated control.

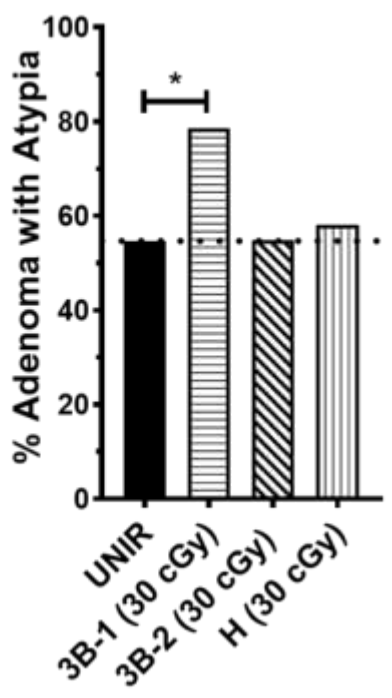
A. 100 Days Post IR



B. 100 Days Post IR



C. 1 Year Post IR



D. 1 Year Post IR

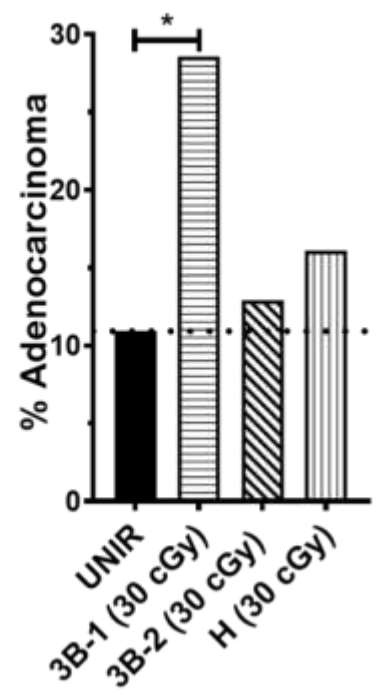


Figure 4.2. Tumorigenic effect of multiple ion radiation in K-ras^{LA1} mouse model. (A) Quantification of an overall number of premalignant lesions in age-matched K-ras^{LA1} lungs from 100 days post-irradiation with 3B-1 (30 cGy), 3B-2 (30 cGy), protons (30 cGy), and unirradiated controls (n = 5 mice per group). Differences in the number of the premalignant lesions. ** P=0.0020, *** P=0.0005, **** P<0.0001. (B) Assay of MDA in the serum of MT aged matched K-ras^{LA1} mice 100 days post-irradiation with 3B-1 (30 cGy), 3B-2 (30 cGy), protons (30 cGy), and unirradiated controls (n=6 mice per group). * P=0.0185, *** P=0.0002, *** P=0.0003. The error bars represent standard errors. (C) Representative images of adenoma with atypia, and quantification of percent adenomas with atypia from the survival cohort. * P=0.0299 in contingency Chi-square test 3B-1 compared with UNIR. (D) Representative images of invasive adenocarcinoma, and quantification of percent adenocarcinoma. * P=0.0351 in contingency Chi-square test 3B-1 compared with UNIR.

4.3.3. Skipping a Day for Silicon in 3B-1 Irradiation Protocol Attenuates Its Effect

Because we observed an increase in invasive carcinoma incidence in 3B-1 after histopathological analysis, we next evaluated if skipping a day for silicon irradiation would have any rescue effect due to DNA repair. We reasoned that even though we used 0.5 cGy per min dose rate, the dose rates in space are much lower and thus there could be time for proton and helium damage repair before exposing mice to Silicon. Thus, we modified the 3B-1 irradiation protocol where we delivered two particles 120 MeV/n protons and 250 MeV/n helium ions in day 1, and on the next day, after approximately 24 hrs. we delivered 300 MeV/n silicon ions in dose proportions of 66.7%: 16.67%: 16.67% respectively and we designated this modified protocol as “3B-1-1”. We also irradiated mice with two particles 120 MeV/n protons and 250 MeV/n helium ions only with the total dose of 25cGy. 3B-1-1 radiation exposure did not increase the number of lesions nor did it increase chronic lipid peroxidation levels in plasma as observed earlier with 3B-1 irradiation in K-ras^{LA1} mice 100 days post-irradiation (**Figure 4.3A**). 3B-1-1 irradiated mice had an average of 5 lesions, proton and helium only irradiated mice had an average of 4 lesions which are similar to unirradiated control whereas 3B-1 had an average of 10 lesions per animal (**Figure 4.3A**). The level of lipid peroxidation that we observed in 3B-1-1 irradiated mice was comparable to unirradiated mice and proton and helium only irradiated mice (**Figure 4.3B**). Taken together we interpret these results to suggest

that not only does the order of particle in multiple beam irradiation matter but also all particles must be given together acutely to increase cancer risks.

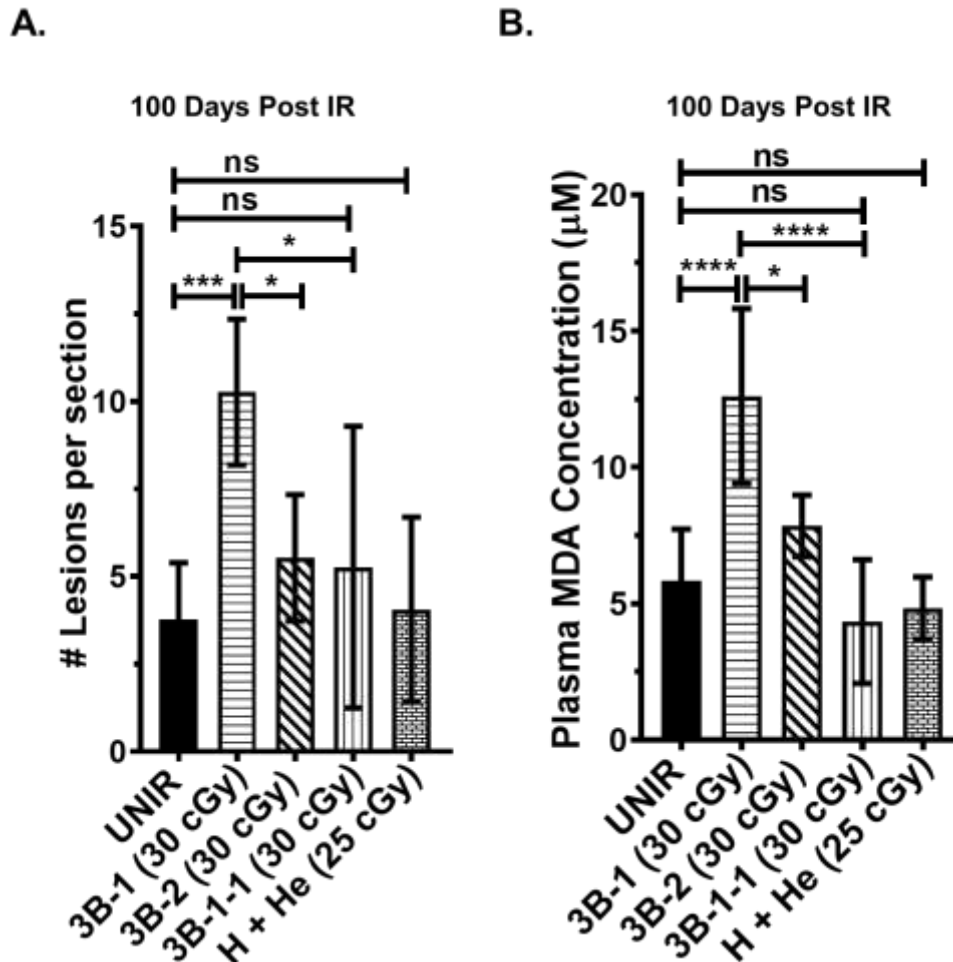


Figure 4.3. Skipping a day for silicon ion in 3B-1 total body irradiation rescues the biological damage in the mice. (A) Quantification of an overall number of premalignant lesions in age-matched K-ras^{LA1} lungs from 100 days post-irradiation with 3B-1 (30 cGy), 3B-2 (30 cGy), 3B-1-1 (30 cGy), proton and helium (25 cGy), and unirradiated controls (n = 5 mice per group). Differences in the number of the premalignant lesions. * P=0.0267, * P=0.0393, *** P=0.0006. (B) Assay of MDA in the serum of MT aged matched K-ras^{LA1} mice 100 days post-irradiation with 3B-1 (30 cGy), 3B-2 (30 cGy), 3B-1-1 (30 cGy), proton and helium (25 cGy), and unirradiated controls

(n=6 mice per group). * P=0.0198, **** P<0.0001, **** P<0.0001. The error bars represent standard errors.

4.3.4. CDDO as Countermeasure Against 3B-1 Irradiation

To determine the radioprotective effect of the CDDO-EA, 2-cyano-3,12-dioxooleana-1,9(11)-dien-28-oic acid–ethyl amide (CDDO-EA; a synthetic triterpenoid), on 3B-1 induced damage, groups of age-matched mice were fed ad libum a diet containing CDDO-EA (400 mg/kg diet) for 3 days continuously prior to 3B-1 irradiation till one-day post-irradiation (**Figure 4.4A**). The mice were on CDDO-EA diet for only a total of 4 days. Pretreatment of CDDO-EA prior to 3B-1 exposure decreased the number of premalignant lesions (**Figure 4.4B**) 100 days post-irradiation. The CDDO-EA treated mice had an average of 4 lesions compared to an average of 10 lesions and 4 lesions on 3B-1 irradiated mice with control diet and unirradiated control respectively (**Figure 4.4B**). Similarly, we also observed a reduction in the level of MDA concentration (lipid peroxidation) in the blood plasma of the CDDO-EA treated mice which were comparable to unirradiated mice (**Figure 4.4C**). These data substantiate the previous findings suggesting CDDO-EA could be a potential radioprotector (Kim et al., 2016; Kim et al., 2012).

4.3.5 Titration of Silicon total dose to better simulate the space environment

As reported above the order of particle in multiple beam irradiation given acutely affected the outcome of tumorigenesis of K-ras^{LA1} mice, and dose proportions of the proton, helium, and silicon was 66.7%, 16.67%, and 16.67% respectively. To better simulate the space environment, we made modification on the 3B-1 radiation protocol where we titrated the dose of silicon particle and helium particles. The modification of 3B-1 changed the dose proportion of the particles. The first titration protocol designated as 3B-1-2 irradiation included 120 MeV/n protons with 20 cGy, 250 MeV/n helium with 5 cGy and 300 MeV/n silicon ions with 2 cGy in dose proportions of 74.07%: 18.52%: 7.54% respectively with a total dose of 27 cGy. The second titration protocol designated 3B-1-3 irradiation included 120 MeV/n protons with 22 cGy, 250 MeV/n helium with 3 cGy and 300 MeV/n silicon ions with 0.5 cGy in dose proportions of 86.3%: 13.3%: 1.96% respectively with a total dose of 25.5 cGy (**Figure 4.5A**). With the titration of high-LET silicon particle, we saw a dose-dependent effect on cancer hallmarks in the K-ras^{LA1} mice. As we decreased the dose proportion of silicon, we observed a decrease in the average number of lesions in lungs as well as a decrease in the level of MDA concentration in blood plasma of K-ras^{LA1} mice 100 days post-irradiation (**Figure 4.5A and 4.5B**). 3B-1-2 irradiated mice had an average number of 8 lesions and 3B-1-3 had an average number of 7 lesions compared to 3B-1 had an average of 10 lesions per animal and unirradiated control mice had an average number of 5 lesions (**Figure 4.5B**). When we titrated the dose proportion of silicon on 3B-1 radiation even further, the MDA

level in plasma came down to background levels with dose proportion of silicon 7.54% and 1.96% in 3B-1-2 and 3B-1-3 respectively 100 days post-irradiation **(Figure 4.5C)**.

A.

3B-1-2 : H-He-Si (30cGy)

Ion	Energy (MeV/n)	Total Dose (cGy)	Dose Rate (cGy/min)	Estimated time (min)
Proton (H) (74.07 %)	120	20	0.5	40
↓ Switch to He				~3
Helium (He) (18.52 %)	250	5	0.5	10
↓ Switch to Si				~3
Silicon (7.54%)	300	2	0.5	4

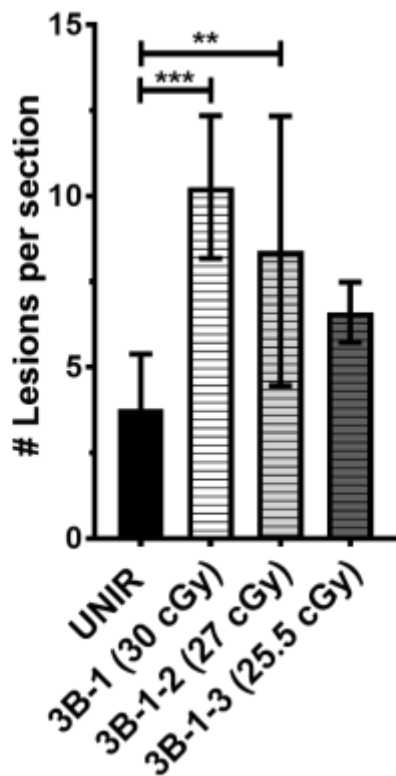
**Total Dose = 27 cGy
Total Time ~60 min**

3B-1-3 : H-He-Si (30cGy)

Ion	Energy (MeV/n)	Total Dose (cGy)	Dose Rate (cGy/min)	Estimated time (min)
Proton (H) (86.3 %)	120	22	0.5	44
↓ Switch to He				~3
Helium (He) (13.3 %)	250	3	0.5	6
↓ Switch to Si				~3
Silicon (1.96%)	300	0.5	0.5	1

**Total Dose = 25.5 cGy
Total Time ~57 min**

B. 100 Days Post IR



C. 100 Days Post IR

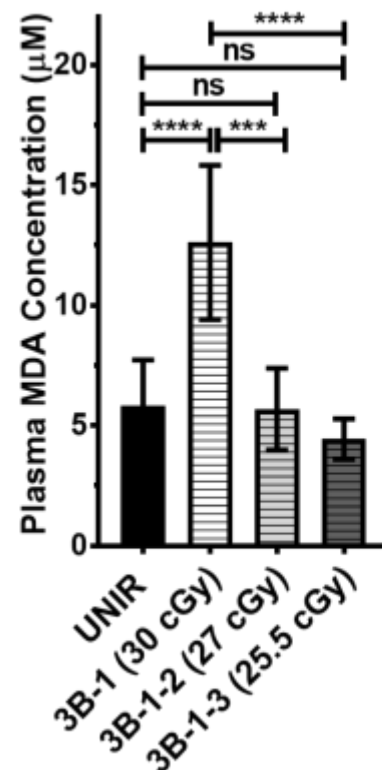


Figure 4.5. Titration of Silicon ion dose in 3B-1 irradiation shows dose response. (A) Illustration of mixed beam radiation using Hydrogen, Helium and Silicon ions. (B) Quantification of overall number of premalignant lesions in age-matched K-rasLA1 lungs from 100 days post-irradiation with 3B-1 (30 cGy): (H (20cGy) + He (5cGy) + Si (5cGy) (30 cGy)), 3B-1-2 (27 cGy): H (20cGy) + He (5cGy) + Si (2cGy), 3B-1-3 (25.5 cGy): H (22cGy) + He (3cGy) + Si (0.5cGy) and unirradiated controls (n = 5 mice per group). Differences in the number of the premalignant lesions. ** P=0.0064, *** P=0.0002. (C) Assay of MDA in the serum of MT aged matched K-rasLA1 mice 100 days post-irradiation with with 3B-1 (30 cGy):(H (20cGy) + He (5cGy) + Si (5cGy) (30 cGy)), H (20cGy) + He (5cGy) + Si (2cGy) (27 cGy), H (20cGy) + He (5cGy) + Si (0.5cGy) (25.5 cGy) and unirradiated controls (n=6 mice per group). *** P=0.0002, **** P<0.0001. (B) The error bars represent standard errors.

4.4 Discussions

In longer-term deep space missions, astronauts would be exposed to multiple ions with various ranges of energies. The health effects that could arise from such multiple continuous ion beam exposure represent a major limiting factor for long-term space missions beyond Low Earth Orbit (LEO). Galactic cosmic radiation (GCR) exposure occur at low fluence rates predominated by low background fluences of low-LET radiation with lower fluences of high-LET radiation that cannot be simulated on earth. It is estimated that individual cells in an astronaut would be traversed by a proton every three days, helium nuclei every few weeks, and high atomic number (Z) and energy (HZE) nuclei about every month (Norbury et al., 2016). Using fast ion switching we exposed mice to proton (H), helium (He) and silicon (Si) particles to delivery mixed ion species to more closely approximate the space environment. In the present study, we demonstrated that multiple ion beam radiation given in a specific order acutely is effective in causing lung cancer progression in K-ras^{LA1} mouse model. Previously studies have used the monoenergetic single ion beam exposure with either only low-LET or high-LET radiation to understand the risk of radiation-induced tumorigenesis in space (Asselin-Labat et al., 2017; Delgado et al., 2014; Luitel et al., 2018; J. Wang et al., 2016). Mono-energetic HZE particles (iron, silicon, and oxygen) have been shown to induce a dose-dependent higher incidence of lung tumorigenesis (X. Wang et al., 2015). To our knowledge, this is the first study in a mouse model of total body

exposure to relatively low doses of multiple ions with low-LET and high-LET together to evaluate the risk of radiation-induced lung cancer progression.

The main biological effects due to radiation exposure cause DNA damage either directly or indirectly through the generation of ROS from radiolysis of water. Through these actions, radiation can induce base damage, single-strand breaks, double-strand breaks, and DNA protein cross-links. If irradiated cells do not repair correctly, it can induce carcinogenesis and other abnormalities (Baskar et al., 2014). Additionally, it well established that high-energy particles cause clustered more complex DNA damage, and if the damage is not repaired correctly, it can induce carcinogenesis and other abnormalities (Asaithamby, Hu, Delgado, et al., 2011; Baskar et al., 2014; Li et al., 2013; Z. Li et al., 2014; Sridharan et al., 2015). In our 3B-1 irradiation protocol when we irradiated mice with proton initially, every cell nucleus in a mouse body is predicted to be traversed by a proton ion multiple times. It is well accepted that the following radiation, chromatin undergoes conformational change to allow access of DNA repair proteins, thus DSBs caused by secondary radiation may be impacted (Goodarzi, Noon, & Jeggo, 2009; Hada, Meador, Cucinotta, Gonda, & Wu, 2007; Mariotti et al., 2013; Xu & Price, 2011). Thus, in our protocol irradiating mice with second ion or third ion (helium and silicon a high-LET ion respectively) may have led to inefficient DNA damage repair following proton irradiation. In contrast, irradiating mice with the 3B-2 protocol with silicon a high-LET ion initially may have impacted only one-third of the nuclei in a mouse body, thus irradiating mice with the second or third ions (both low-LET) may not have

perturbated the DNA damage repair system similarly to 3B-1. Additionally, irradiating mice with proton and helium on day one followed by silicon irradiation after 24 hrs. reduced the biological impact that was previously seen in 3B-1 irradiation protocol **(Figure 4.3A and 4.3B)** perhaps due to the repair of DNA damage between irradiations. When we titrated the dose of HZE ion in 3B-1 irradiation protocol, we observed a dose-dependent effect of silicon ions delivered **(Figure 4.4A and 4.4B)** and observed reducing the total dose of silicon from 5 cGy to 2 and 0.5 cGy, progressively reduced cancer progression back to background rates. These results provide a possible mechanism that may have contributed to the observed carcinogenic effect due to multiple ion beam radiation given acutely in a specific order. Considering our findings, with previously published data, suggest proton irradiation followed with HZE-particle might be carcinogenic (Sutherland, Cuomo, & Bennett, 2005; Zhou, Bennett, Cutter, & Sutherland, 2006). Further studies are required to clarify the role of DNA repair mechanisms *in vivo* using a mixed radiation field.

There is accumulating evidence of an adaptive response role in low-LET radiation, such that a low priming dose of radiation results in an enhanced resistance to a second and larger dose of radiation (Bhattacharjee & Ito, 2001; Elmore et al., 2008). This may be important in understanding the risk in the space radiation environment as it is likely that every cell in an astronaut is more likely to be hit with proton ions multiple times before any HZE ions hits a cell. The studies on the adaptive response on high-LET radiation are mixed and have depended on the

model system used, as in some studies initial exposure would decrease biological damage while in others it would increase the subsequent damage following the second exposure (Bennett, Cutter, & Sutherland, 2007; Mitchel, Burchart, & Wyatt, 2008; Rodman et al., 2017). With 3B-1 irradiation protocol, all the cells in the mouse body were primed with proton ions before cells were shortly thereafter irradiated with a second or third ion. In our study priming with the proton irradiation prior to second and third irradiation caused more transformations given acutely, but such transformation was reduced to background level if the priming was done 24hr apart from the second radiation (**Figure 4.2A and 4.3A**). Similarly, the transformation was not observed when primed with silicon ions prior to helium and proton irradiation (**Figure 4.3A**). Similar findings have been reported previously in vitro experiments (Sutherland et al., 2005). As CDDO-EA has been previously shown to enhance DNA repair and act as radioprotective against, it could have provided protection against the 3B-1 exposure (Kim et al., 2012). CDDO is an anti-oxidant and anti-inflammatory modulator that is currently in Phase 3 clinical trials in patients with chronic kidney disease. Here we also demonstrated that prior treatment with CDDO-EA can protect mice and reduce tumor incidence against multiple ion beam exposure.

Our mixed beam studies highlight the limitations and difficulties in accurately assessing of health risk due to the mixed ions irradiation as outcomes seem to depend not only on the order of ions, but also energies and doses used and importantly the biological endpoints of the experiments.

CHAPTER FIVE

Discussion and Future Directions

Ionizing radiation has long been associated with cancer as it causes oxidative stress resulting in alteration of DNA, lipids, and proteins (Sandor et al., 2015). Lung cancer accounts for more cancer-related deaths than any other cancer types among both men and women. The lung is a radiation susceptible organ demonstrated by the epidemiological data obtained from atomic bomb survivors and uranium mine workers (Denman, Eatough, Gillmore, & Phillips, 2003; Preston et al., 2007). Thus, radiation-induced carcinogenesis is a major concern for both radiation therapy as well as for astronauts on long-term missions in deep space away from the earth's protective magnetic field. Therefore, understanding the cellular and molecular mechanisms that contribute to carcinogenic risk in the development of radiation-induced lung cancer could be applicable in mitigating or preventing cancer initiation and progression due to radiation.

In this body of work, I have shown total body irradiation of mice with 2.0 Gy of protons induces acute oxidative stress and DNA damage which could manifest

later into chronic oxidative stress and persistent DNA damage. I also showed that mice irradiated with protons developed an immunosuppressive tumor microenvironment in the lung, with larger premalignant lesions, and increased invasive carcinomas compared to mice exposed to an equal dose of terrestrial radiation (X-rays) or to unirradiated mice. Altogether these studies confirm that proton irradiation causes more biological damage compared to equal dose X-rays. These findings are important for risk assessment for astronauts exposed to either solar particle events (mostly protons) or to galactic cosmic rays (GCR) where protons are highly abundant. Additionally, this study also has applications to risks for secondary cancer development in patients who are treated by proton radiotherapy. However, it is still necessary to address the type of biological effects when proton radiation is more localized as compared to total body radiation conducted in the present studies.

I have also addressed important gaps in understanding of risks to humans traveling in space using a series of multiple ion beam irradiations. Most charged-particle radiation studies until now have been performed using monoenergetic single ion radiation exposures, but the deep space environment is composed of multiple ions with a wide range of energies. Data obtained in the multiple ion studies suggest that changes in the order in which the different ions are delivered to the mice can produce different biological impacts, i.e. the risks of exposure to multiple ions depend on the order in which they are delivered. When mice are irradiated with proton ions followed by helium ions then by silicon ions, an increase in systemic

oxidative stress and invasive carcinomas in the lung was observed. When the order of ions was changed to silicon first, then helium ions and protons last while keeping dose, energy and dose rates the same, no such increases in systemic oxidative stress or in invasive lung carcinoma was observed. These findings are important because in deep space, astronauts are exposed to a complex mixture of ions in the GCR, with protons as the most abundant ion, followed by He ions. The heavier ions are much less prevalent although important due to their ability to deposit large amounts of energy locally. It is most likely that humans in deep space would be exposed first to protons, then He, and last to a heavy ion such as silicon. This is exactly the order in which the highest levels of oxidative stress and the highest risk of the induction of advanced, aggressive lung tumors in the exposed mice was observed. However, when we irradiated mice with proton ions followed by helium ions then skipped 24 hrs. followed by silicon ions, we did not observe an increase in systemic oxidative stress and invasive lung carcinoma. Taking consideration of low dose rates of IR in space it is more likely that proton damage repair before exposure to other HZE particles. Thus, our skip a day data suggests that there might be reduced risk in of cancer in space because of low dose rates of IR. This information on risk is useful to NASA as it tries to determine how many days in deep space are safe for astronauts going on future missions.

Additional experiments using triterpenoids (CDDO) as a potential countermeasure and mitigator to proton irradiation were conducted. CDDO is an anti-oxidant and anti-inflammatory modulator that is currently in Phase 3 clinical

trials in patients with chronic kidney disease. The key observation from these studies is that CDDO given prior to radiation can dramatically reduce tumor progression in this same mouse model of susceptibility to lung cancer. These results are of possible use to NASA as it considers whether pharmaceutical measures can help protect astronauts against exposure to the galactic cosmic radiation and to solar particle events. We also looked at the possible use of triterpenoids as countermeasures against exposure to multiple ions. This work was done to determine if the countermeasure that was found to be effective at reducing the risks of proton-induced lung cancers might also be useful for more complex radiation fields in the GCR.

Furthermore, with the high energy and control upgrades at the NASA Space Radiation Laboratory (Brookhaven, NY), experiments can now be conducted to better simulate the deep space environment that would occur on a Mars mission. These experiments consist of chronic exposure up to 4-6 weeks irradiation (6-days per week) or acute one-day exposures with continuous exposure to background protons and helium and a sporadic heavy ion exposure. The delivery dose consists of 33 ions and energy mix to approximate deep space environment. Using GCR simulation the health risks can be approximated, especially the carcinogenic effect in the K-ras^{LA1} lung cancer susceptible mouse model. These studies may provide a better understanding of the underlying molecular mechanisms that are needed to quantify and model the risk of space radiation-induced carcinogenesis.

Bibliography:

- Aguayo, S. M., Miller, Y. E., Waldron, J. A., Jr., Bogin, R. M., Sunday, M. E., Staton, G. W., Jr., . . . King, T. E., Jr. (1992). Brief report: idiopathic diffuse hyperplasia of pulmonary neuroendocrine cells and airways disease. *N Engl J Med*, 327(18), 1285-1288. doi:10.1056/NEJM199210293271806
- Ahmad, R., Raina, D., Meyer, C., Kharbanda, S., & Kufe, D. (2006). Triterpenoid CDDO-Me blocks the NF-kappaB pathway by direct inhibition of IKKbeta on Cys-179. *J Biol Chem*, 281(47), 35764-35769. doi:10.1074/jbc.M607160200
- Alberg, A. J., & Nonemaker, J. (2008). Who is at high risk for lung cancer? Population-level and individual-level perspectives. *Semin Respir Crit Care Med*, 29(3), 223-232. doi:10.1055/s-2008-1076742
- Alberts, B. (2015). *Molecular biology of the cell* (Sixth edition. ed.). New York, NY: Garland Science, Taylor and Francis Group.
- Alves Rde, C., Meurer, R. T., & Roehe, A. V. (2014). MYC amplification is associated with poor survival in small cell lung cancer: a chromogenic in situ hybridization study. *J Cancer Res Clin Oncol*, 140(12), 2021-2025. doi:10.1007/s00432-014-1769-1
- Anguera, G., & Majem, M. (2018). BRAF inhibitors in metastatic non-small cell lung cancer. *J Thorac Dis*, 10(2), 589-592. doi:10.21037/jtd.2018.01.129
- Asaithamby, A., Hu, B., & Chen, D. J. (2011). Unrepaired clustered DNA lesions induce chromosome breakage in human cells. *Proc Natl Acad Sci U S A*, 108(20), 8293-8298. doi:10.1073/pnas.1016045108

Asaithamby, A., Hu, B., Delgado, O., Ding, L. H., Story, M. D., Minna, J. D., . . .

Chen, D. J. (2011). Irreparable complex DNA double-strand breaks induce chromosome breakage in organotypic three-dimensional human lung epithelial cell culture. *Nucleic Acids Res*, 39(13), 5474-5488. doi:10.1093/nar/gkr149

Asaithamby, A., Uematsu, N., Chatterjee, A., Story, M. D., Burma, S., & Chen, D. J.

(2008). Repair of HZE-particle-induced DNA double-strand breaks in normal human fibroblasts. *Radiat Res*, 169(4), 437-446. doi:10.1667/RR1165.1

Asselin-Labat, M. L., Rampersad, R., Xu, X., Ritchie, M. E., Michalski, J., Huang, L.,

& Onaitis, M. W. (2017). High-LET Radiation Increases Tumor Progression in a K-Ras-Driven Model of Lung Adenocarcinoma. *Radiat Res*, 188(5), 562-570. doi:10.1667/RR14794.1

Barcellos-Hoff, M. H., Park, C., & Wright, E. G. (2005). Radiation and the

microenvironment - tumorigenesis and therapy. *Nat Rev Cancer*, 5(11), 867-875. doi:10.1038/nrc1735

Baskar, R., Dai, J., Wenlong, N., Yeo, R., & Yeoh, K. W. (2014). Biological response

of cancer cells to radiation treatment. *Front Mol Biosci*, 1, 24. doi:10.3389/fmolb.2014.00024

Beckmann, M. W., Niederacher, D., Schnurch, H. G., Gusterson, B. A., & Bender,

H. G. (1997). Multistep carcinogenesis of breast cancer and tumour heterogeneity. *J Mol Med (Berl)*, 75(6), 429-439.

- Bennett, P. V., Cutter, N. C., & Sutherland, B. M. (2007). Split-dose exposures versus dual ion exposure in human cell neoplastic transformation. *Radiat Environ Biophys*, 46(2), 119-123. doi:10.1007/s00411-006-0091-y
- Bhattacharjee, D., & Ito, A. (2001). Deceleration of carcinogenic potential by adaptation with low dose gamma irradiation. *In Vivo*, 15(1), 87-92.
- Biteau, B., Hochmuth, C. E., & Jasper, H. (2011). Maintaining tissue homeostasis: dynamic control of somatic stem cell activity. *Cell Stem Cell*, 9(5), 402-411. doi:10.1016/j.stem.2011.10.004
- Blenkinsopp, W. K. (1967). Proliferation of respiratory tract epithelium in the rat. *Exp Cell Res*, 46(1), 144-154.
- Burnette, B., & Weichselbaum, R. R. (2013). Radiation as an immune modulator. *Semin Radiat Oncol*, 23(4), 273-280. doi:10.1016/j.semradonc.2013.05.009
- Candido, J., & Hagemann, T. (2013). Cancer-related inflammation. *J Clin Immunol*, 33 Suppl 1, S79-84. doi:10.1007/s10875-012-9847-0
- Chan, B. A., & Hughes, B. G. (2015). Targeted therapy for non-small cell lung cancer: current standards and the promise of the future. *Transl Lung Cancer Res*, 4(1), 36-54. doi:10.3978/j.issn.2218-6751.2014.05.01
- Chancellor, J. C., Blue, R. S., Cengel, K. A., Aunon-Chancellor, S. M., Rubins, K. H., Katzgraber, H. G., & Kennedy, A. R. (2018). Limitations in predicting the space radiation health risk for exploration astronauts. *NPJ Microgravity*, 4, 8. doi:10.1038/s41526-018-0043-2

- Chancellor, J. C., Scott, G. B., & Sutton, J. P. (2014). Space Radiation: The Number One Risk to Astronaut Health beyond Low Earth Orbit. *Life (Basel)*, 4(3), 491-510. doi:10.3390/life4030491
- Christofidou-Solomidou, M., Pietrofesa, R. A., Arguiri, E., Schweitzer, K. S., Berdyshev, E. V., McCarthy, M., . . . Petrache, I. (2015). Space radiation-associated lung injury in a murine model. *Am J Physiol Lung Cell Mol Physiol*, 308(5), L416-428. doi:10.1152/ajplung.00260.2014
- Cucinotta, F. A., Nikjoo, H., & Goodhead, D. T. (1998). The effects of delta rays on the number of particle-track traversals per cell in laboratory and space exposures. *Radiat Res*, 150(1), 115-119.
- Cucinotta, F. A., Schimmerling, W., Wilson, J. W., Peterson, L. E., Badhwar, G. D., Saganti, P. B., & Dicello, J. F. (2001). Space radiation cancer risks and uncertainties for Mars missions. *Radiat Res*, 156(5 Pt 2), 682-688.
- Cucinotta, F. A., To, K., & Cacao, E. (2017). Predictions of space radiation fatality risk for exploration missions. *Life Sci Space Res (Amst)*, 13, 1-11. doi:10.1016/j.lssr.2017.01.005
- Cucinotta, F. A., Wilson, J. W., Shinn, J. L., Badavi, F. F., & Badhwar, G. D. (1996). Effects of target fragmentation on evaluation of LET spectra from space radiations: implications for space radiation protection studies. *Radiat Meas*, 26(6), 923-934.

- Dang, C. V., O'Donnell, K. A., Zeller, K. I., Nguyen, T., Osthus, R. C., & Li, F. (2006). The c-Myc target gene network. *Semin Cancer Biol*, 16(4), 253-264. doi:10.1016/j.semcancer.2006.07.014
- Datta, K., Suman, S., & Fornace, A. J., Jr. (2014). Radiation persistently promoted oxidative stress, activated mTOR via PI3K/Akt, and downregulated autophagy pathway in mouse intestine. *Int J Biochem Cell Biol*, 57, 167-176. doi:10.1016/j.biocel.2014.10.022
- Datta, K., Suman, S., Kallakury, B. V., & Fornace, A. J., Jr. (2012). Exposure to heavy ion radiation induces persistent oxidative stress in mouse intestine. *PLoS One*, 7(8), e42224. doi:10.1371/journal.pone.0042224
- de Groot, P., & Munden, R. F. (2012). Lung cancer epidemiology, risk factors, and prevention. *Radiol Clin North Am*, 50(5), 863-876. doi:10.1016/j.rcl.2012.06.006
- De Roock, W., De Vriendt, V., Normanno, N., Ciardiello, F., & Tejpar, S. (2011). KRAS, BRAF, PIK3CA, and PTEN mutations: implications for targeted therapies in metastatic colorectal cancer. *Lancet Oncol*, 12(6), 594-603. doi:10.1016/S1470-2045(10)70209-6
- Delgado, O., Batten, K. G., Richardson, J. A., Xie, X. J., Gazdar, A. F., Kaisani, A. A., . . . Shay, J. W. (2014). Radiation-enhanced lung cancer progression in a transgenic mouse model of lung cancer is predictive of outcomes in human lung and breast cancer. *Clin Cancer Res*, 20(6), 1610-1622. doi:10.1158/1078-0432.CCR-13-2589

- Denman, A. R., Eatough, J. P., Gillmore, G., & Phillips, P. S. (2003). Assessment of health risks to skin and lung of elevated radon levels in abandoned mines. *Health Phys*, 85(6), 733-739.
- Devarakonda, S., Morgensztern, D., & Govindan, R. (2015). Genomic alterations in lung adenocarcinoma. *Lancet Oncol*, 16(7), e342-351. doi:10.1016/S1470-2045(15)00077-7
- Dogan, S., Shen, R., Ang, D. C., Johnson, M. L., D'Angelo, S. P., Paik, P. K., . . . Ladanyi, M. (2012). Molecular epidemiology of EGFR and KRAS mutations in 3,026 lung adenocarcinomas: higher susceptibility of women to smoking-related KRAS-mutant cancers. *Clin Cancer Res*, 18(22), 6169-6177. doi:10.1158/1078-0432.CCR-11-3265
- Du, X., Shao, Y., Qin, H. F., Tai, Y. H., & Gao, H. J. (2018). ALK-rearrangement in non-small-cell lung cancer (NSCLC). *Thorac Cancer*, 9(4), 423-430. doi:10.1111/1759-7714.12613
- Durante, M. (2014). Space radiation protection: Destination Mars. *Life Sci Space Res (Amst)*, 1, 2-9. doi:10.1016/j.lssr.2014.01.002
- Durante, M., & Cucinotta, F. A. (2008). Heavy ion carcinogenesis and human space exploration. *Nat Rev Cancer*, 8(6), 465-472. doi:10.1038/nrc2391
- Durante, M., & Cucinotta, F. A. (2011). Physical basis of radiation protection in space travel. *Reviews of Modern Physics*, 83(4), 1245-1281. doi:10.1103/RevModPhys.83.1245

El-Ashmawy, M., Delgado, O., Cardentey, A., Wright, W. E., & Shay, J. W. (2014). CDDO-Me Protects Normal Lung and Breast Epithelial Cells but Not Cancer Cells from Radiation. *PLoS One*, *9*(12). doi:ARTN e115600

DOI 10.1371/journal.pone.0115600

Elgart, S. R., Bostani, M., Mok, K. C., Adibi, A., Ruehm, S., Enzmann, D., . . . Iwamoto, K. S. (2015). Investigation of DNA Damage Dose-Response Kinetics after Ionizing Radiation Schemes Similar to CT Protocols. *Radiat Res*, *183*(6), 701-707. doi:10.1667/RR13752.1

Elmore, E., Lao, X. Y., Kapadia, R., Giedzinski, E., Limoli, C., & Redpath, J. L. (2008). Low doses of very low-dose-rate low-LET radiation suppress radiation-induced neoplastic transformation in vitro and induce an adaptive response. *Radiat Res*, *169*(3), 311-318. doi:10.1667/RR1199.1

Erfani, N., Mehrabadi, S. M., Ghayumi, M. A., Haghshenas, M. R., Mojtahedi, Z., Ghaderi, A., & Amani, D. (2012). Increase of regulatory T cells in metastatic stage and CTLA-4 over expression in lymphocytes of patients with non-small cell lung cancer (NSCLC). *Lung Cancer*, *77*(2), 306-311. doi:10.1016/j.lungcan.2012.04.011

Eskiocak, U., Kim, S. B., Roig, A. I., Kitten, E., Batten, K., Cornelius, C., . . . Shay, J. W. (2010). CDDO-Me protects against space radiation-induced transformation of human colon epithelial cells. *Radiat Res*, *174*(1), 27-36. doi:10.1667/RR2155.1

- Ettinger, D. S., Akerley, W., Borghaei, H., Chang, A. C., Cheney, R. T., Chirieac, L. R., . . . National comprehensive cancer, n. (2013). Non-small cell lung cancer, version 2.2013. *J Natl Compr Canc Netw*, 11(6), 645-653; quiz 653.
- Evans, M. J., Cox, R. A., Shami, S. G., Wilson, B., & Plopper, C. G. (1989). The role of basal cells in attachment of columnar cells to the basal lamina of the trachea. *Am J Respir Cell Mol Biol*, 1(6), 463-469. doi:10.1165/ajrcmb/1.6.463
- Fails, A. D., Magee, C., & Frandson, R. D. (2018). *Anatomy and physiology of farm animals*. In (pp. 1 online resource).
- Fearon, E. R. (1991). A genetic basis for the multi-step pathway of colorectal tumorigenesis. *Princess Takamatsu Symp*, 22, 37-48.
- Ganti, A. K., & Gerber, D. E. (2013). *Lung cancer*. Oxford ; New York: Oxford University Press.
- Gerelchuluun, A., Hong, Z., Sun, L., Suzuki, K., Terunuma, T., Yasuoka, K., . . . Tsuboi, K. (2011). Induction of in situ DNA double-strand breaks and apoptosis by 200 MeV protons and 10 MV X-rays in human tumour cell lines. *Int J Radiat Biol*, 87(1), 57-70. doi:10.3109/09553002.2010.518201
- Gibbons, D. L., Byers, L. A., & Kurie, J. M. (2014). Smoking, p53 mutation, and lung cancer. *Mol Cancer Res*, 12(1), 3-13. doi:10.1158/1541-7786.MCR-13-0539
- Goodarzi, A. A., Noon, A. T., & Jeggo, P. A. (2009). The impact of heterochromatin on DSB repair. *Biochem Soc Trans*, 37(Pt 3), 569-576. doi:10.1042/BST0370569

- Grant, E. J., Brenner, A., Sugiyama, H., Sakata, R., Sadakane, A., Utada, M., . . . Ozasa, K. (2017). Solid Cancer Incidence among the Life Span Study of Atomic Bomb Survivors: 1958-2009. *Radiat Res*, 187(5), 513-537. doi:10.1667/RR14492.1
- Granville, C. A., Memmott, R. M., Balogh, A., Mariotti, J., Kawabata, S., Han, W., . . . Dennis, P. A. (2009). A central role for Foxp3+ regulatory T cells in K-Ras-driven lung tumorigenesis. *PLoS One*, 4(3), e5061. doi:10.1371/journal.pone.0005061
- Greulich, H. (2010). The genomics of lung adenocarcinoma: opportunities for targeted therapies. *Genes Cancer*, 1(12), 1200-1210. doi:10.1177/1947601911407324
- Guerra, C., Schuhmacher, A. J., Canamero, M., Grippo, P. J., Verdaguer, L., Perez-Gallego, L., . . . Barbacid, M. (2007). Chronic pancreatitis is essential for induction of pancreatic ductal adenocarcinoma by K-Ras oncogenes in adult mice. *Cancer Cell*, 11(3), 291-302. doi:10.1016/j.ccr.2007.01.012
- Hada, M., Meador, J. A., Cucinotta, F. A., Gonda, S. R., & Wu, H. (2007). Chromosome aberrations induced by dual exposure of protons and iron ions. *Radiat Environ Biophys*, 46(2), 125-129. doi:10.1007/s00411-006-0083-y
- Hall, E. J., & Giaccia, A. J. (2006). *Radiobiology for the radiologist* (6th ed.). Philadelphia: Lippincott Williams & Wilkins.
- Hall, E. J., & Giaccia, A. J. (2019). *Radiobiology for the radiologist* (Eighth edition. ed.). Philadelphia: Wolters Kluwer.

- Hanahan, D., & Coussens, L. M. (2012). Accessories to the crime: functions of cells recruited to the tumor microenvironment. *Cancer Cell*, 21(3), 309-322. doi:10.1016/j.ccr.2012.02.022
- Hanahan, D., & Weinberg, R. A. (2011a). Hallmarks of cancer: the next generation. *Cell*, 144(5), 646-674. doi:10.1016/j.cell.2011.02.013
- Hanahan, D., & Weinberg, R. A. (2011b). Hallmarks of Cancer: The Next Generation. *Cell*, 144(5), 646-674. doi:10.1016/j.cell.2011.02.013
- Heintz, N. H., Janssen-Heininger, Y. M., & Mossman, B. T. (2010). Asbestos, lung cancers, and mesotheliomas: from molecular approaches to targeting tumor survival pathways. *Am J Respir Cell Mol Biol*, 42(2), 133-139. doi:10.1165/rcmb.2009-0206TR
- Heist, R. S., Mino-Kenudson, M., Sequist, L. V., Tammireddy, S., Morrissey, L., Christiani, D. C., . . . Iafrate, A. J. (2012). FGFR1 amplification in squamous cell carcinoma of the lung. *J Thorac Oncol*, 7(12), 1775-1780. doi:10.1097/JTO.0b013e31826aed28
- Hekim, N., Cetin, Z., Nikitaki, Z., Cort, A., & Saygili, E. I. (2015). Radiation triggering immune response and inflammation. *Cancer Lett*, 368(2), 156-163. doi:10.1016/j.canlet.2015.04.016
- Hendry, J. H. (2001). Genomic instability: potential contributions to tumour and normal tissue response, and second tumours, after radiotherapy. *Radiother Oncol*, 59(2), 117-126.

- Herriges, M., & Morrisey, E. E. (2014). Lung development: orchestrating the generation and regeneration of a complex organ. *Development*, 141(3), 502-513. doi:10.1242/dev.098186
- Hislop, A. A. (2002). Airway and blood vessel interaction during lung development. *J Anat*, 201(4), 325-334.
- Hori, S., Nomura, T., & Sakaguchi, S. (2003). Control of regulatory T cell development by the transcription factor Foxp3. *Science*, 299(5609), 1057-1061. doi:10.1126/science.1079490
- Inamura, K. (2017). Lung Cancer: Understanding Its Molecular Pathology and the 2015 WHO Classification. *Front Oncol*, 7, 193. doi:10.3389/fonc.2017.00193
- Jacob, P., Ruhm, W., Walsh, L., Blettner, M., Hammer, G., & Zeeb, H. (2009). Is cancer risk of radiation workers larger than expected? *Occup Environ Med*, 66(12), 789-796. doi:10.1136/oem.2008.043265
- Johnson, B. E., Brennan, J. F., Ihde, D. C., & Gazdar, A. F. (1992). myc family DNA amplification in tumors and tumor cell lines from patients with small-cell lung cancer. *J Natl Cancer Inst Monogr*(13), 39-43.
- Keedy, V. L., Temin, S., Somerfield, M. R., Beasley, M. B., Johnson, D. H., McShane, L. M., . . . Giaccone, G. (2011). American Society of Clinical Oncology provisional clinical opinion: epidermal growth factor receptor (EGFR) Mutation testing for patients with advanced non-small-cell lung cancer considering first-line EGFR tyrosine kinase inhibitor therapy. *J Clin Oncol*, 29(15), 2121-2127. doi:10.1200/JCO.2010.31.8923

- Kilic, A., Landreneau, R. J., Luketich, J. D., Pennathur, A., & Schuchert, M. J. (2011). Density of tumor-infiltrating lymphocytes correlates with disease recurrence and survival in patients with large non-small-cell lung cancer tumors. *J Surg Res*, *167*(2), 207-210. doi:10.1016/j.jss.2009.08.029
- Kim, S. B., Bozeman, R. G., Kaisani, A., Kim, W., Zhang, L., Richardson, J. A., . . . Shay, J. W. (2016). Radiation promotes colorectal cancer initiation and progression by inducing senescence-associated inflammatory responses. *Oncogene*, *35*(26), 3365-3375. doi:10.1038/onc.2015.395
- Kim, S. B., Pandita, R. K., Eskiocak, U., Ly, P., Kaisani, A., Kumar, R., . . . Shay, J. W. (2012). Targeting of Nrf2 induces DNA damage signaling and protects colonic epithelial cells from ionizing radiation. *Proc Natl Acad Sci U S A*, *109*(43), E2949-E2955. doi:DOI 10.1073/pnas.1207718109
- Kim, S. B., Zhang, L., Barron, S., & Shay, J. W. (2014). Inhibition of microRNA-31-5p protects human colonic epithelial cells against ionizing radiation. *Life Sci Space Res (Amst)*, *1*, 67-73. doi:10.1016/j.lssr.2014.02.001
- Kitajima, S., Thummalapalli, R., & Barbie, D. A. (2016). Inflammation as a driver and vulnerability of KRAS mediated oncogenesis. *Semin Cell Dev Biol*, *58*, 127-135. doi:10.1016/j.semcdb.2016.06.009
- Krewski, D., Lubin, J. H., Zielinski, J. M., Alavanja, M., Catalan, V. S., Field, R. W., . . . Wilcox, H. B. (2005). Residential radon and risk of lung cancer: a combined analysis of 7 North American case-control studies. *Epidemiology*, *16*(2), 137-145.

- Kris, M. G., Johnson, B. E., Kwiatkowski, D. J., Iafrate, A. J., Wistuba, I. I., Aronson, S. L., . . . Bunn, P. A. (2011). Identification of driver mutations in tumor specimens from 1,000 patients with lung adenocarcinoma: The NCI's Lung Cancer Mutation Consortium (LCMC). *Journal of Clinical Oncology*, *29*(18).
- Lantz, P. M., Mendez, D., & Philbert, M. A. (2013). Radon, smoking, and lung cancer: the need to refocus radon control policy. *Am J Public Health*, *103*(3), 443-447. doi:10.2105/AJPH.2012.300926
- Laskin, D. L., Sunil, V. R., Gardner, C. R., & Laskin, J. D. (2011). Macrophages and tissue injury: agents of defense or destruction? *Annu Rev Pharmacol Toxicol*, *51*, 267-288. doi:10.1146/annurev.pharmtox.010909.105812
- Latimer, K. M., & Mott, T. F. (2015). Lung cancer: diagnosis, treatment principles, and screening. *Am Fam Physician*, *91*(4), 250-256.
- Leisa Johnson¹, Kim Mercer^{1,3}, Doron Greenbaum^{1,4}, Roderick T. Bronson⁵, Denise Crowley^{1,3}, David A. Tuveson^{1,3,6} & Tyler Jacks^{1,3}. (2001). Somatic activation of the K-ras oncogene causes early onset lung cancer in mice.
- Li, M., Gonon, G., Buonanno, M., Autsavapromporn, N., de Toledo, S. M., Pain, D., & Azzam, E. I. (2014). Health risks of space exploration: targeted and nontargeted oxidative injury by high-charge and high-energy particles. *Antioxid Redox Signal*, *20*(9), 1501-1523. doi:10.1089/ars.2013.5649
- Li, Z., Hudson, F. Z., Wang, H., Wang, Y., Bian, Z., Murnane, J. P., & Dynan, W. S. (2013). Increased mutagenic joining of enzymatically-induced DNA double-

- strand breaks in high-charge and energy particle irradiated human cells. *Radiat Res*, 180(1), 17-24. doi:10.1667/RR3332.1
- Li, Z., Wang, H., Wang, Y., Murnane, J. P., & Dynan, W. S. (2014). Effect of radiation quality on mutagenic joining of enzymatically-induced DNA double-strand breaks in previously irradiated human cells. *Radiat Res*, 182(5), 573-579. doi:10.1667/RR13723.1
- Liby, K., Risingsong, R., Royce, D. B., Williams, C. R., Ma, T., Yore, M. M., & Sporn, M. B. (2009). Triterpenoids CDDO-methyl ester or CDDO-ethyl amide and rexinoids LG100268 or NRX194204 for prevention and treatment of lung cancer in mice. *Cancer Prev Res (Phila)*, 2(12), 1050-1058. doi:10.1158/1940-6207.CAPR-09-0085
- Liby, K., Royce, D. B., Williams, C. R., Risingsong, R., Yore, M. M., Honda, T., . . . Sporn, M. B. (2007). The synthetic triterpenoids CDDO-methyl ester and CDDO-ethyl amide prevent lung cancer induced by vinyl carbamate in A/J mice. *Cancer Res*, 67(6), 2414-2419. doi:10.1158/0008-5472.CAN-06-4534
- Lorenz, J., Friedberg, T., Paulus, R., Oesch, F., & Ferlinz, R. (1994). Oncogene overexpression in non-small-cell lung cancer tissue: prevalence and clinicopathological significance. *Clin Invest*, 72(2), 156-163.
- Lubin, J. H., & Boice, J. D., Jr. (1997). Lung cancer risk from residential radon: meta-analysis of eight epidemiologic studies. *J Natl Cancer Inst*, 89(1), 49-57.

Lubin, J. H., Boice, J. D., Jr., Edling, C., Hornung, R. W., Howe, G. R., Kunz, E., . . . et al. (1995). Lung cancer in radon-exposed miners and estimation of risk from indoor exposure. *J Natl Cancer Inst*, 87(11), 817-827.

Luitel, K., Bozeman, R., Kaisani, A., Kim, S. B., Barron, S., Richardson, J. A., & Shay, J. W. (2018). Proton radiation-induced cancer progression. *Life Sci Space Res (Amst)*, 19, 31-42. doi:10.1016/j.lssr.2018.08.002

Luo, S. Y., & Lam, D. C. (2013). Oncogenic driver mutations in lung cancer. *Transl Respir Med*, 1(1), 6. doi:10.1186/2213-0802-1-6

Manem, V. S., Kohandel, M., Hodgson, D. C., Sharpe, M. B., & Sivaloganathan, S. (2015). The effect of radiation quality on the risks of second malignancies. *Int J Radiat Biol*, 91(3), 209-217. doi:10.3109/09553002.2014.980466

Mariotti, L. G., Pirovano, G., Savage, K. I., Ghita, M., Ottolenghi, A., Prise, K. M., & Schettino, G. (2013). Use of the gamma-H2AX assay to investigate DNA repair dynamics following multiple radiation exposures. *PLoS One*, 8(11), e79541. doi:10.1371/journal.pone.0079541

McPhee, J. C., Charles, J. B., & United States. National Aeronautics and Space Administration. (2009). *Human health and performance risks of space exploration missions : evidence reviewed by the NASA Human Research Program*. Houston, Texas

Washington, DC: National Aeronautics and Space Administration

For sale by the Supt. of Docs.

- Mentzer, S. J., Tsuda, A., & Loring, S. H. (2018). Pleural mechanics and the pathophysiology of air leaks. *J Thorac Cardiovasc Surg*, 155(5), 2182-2189. doi:10.1016/j.jtcvs.2017.12.062
- Metting, N. F., Rossi, H. H., Braby, L. A., Kliauga, P. J., Howard, J., Zaider, M., . . . Rapkin, M. (1988). Microdosimetry near the trajectory of high-energy heavy ions. *Radiat Res*, 116(2), 183-195.
- Mewaldt, R. A. (1994). Galactic cosmic ray composition and energy spectra. *Adv Space Res*, 14(10), 737-747.
- Mitchel, R. E., Burchart, P., & Wyatt, H. (2008). A lower dose threshold for the in vivo protective adaptive response to radiation. Tumorigenesis in chronically exposed normal and Trp53 heterozygous C57BL/6 mice. *Radiat Res*, 170(6), 765-775. doi:10.1667/RR1414.1
- Mossman, B. T., Bignon, J., Corn, M., Seaton, A., & Gee, J. B. (1990). Asbestos: scientific developments and implications for public policy. *Science*, 247(4940), 294-301.
- Multhoff, G., & Radons, J. (2012). Radiation, inflammation, and immune responses in cancer. *Front Oncol*, 2, 58. doi:10.3389/fonc.2012.00058
- National Research Council (U.S.). Task Group on the Biological Effects of Space Radiation., & National Research Council (U.S.). Commission on Physical Sciences Mathematics and Applications. (1996). *Radiation hazards to crews of interplanetary missions : biological issues and research strategies*. Washington, D.C.: National Academy Press.

- Ng, J., & Shuryak, I. (2015). Minimizing second cancer risk following radiotherapy: current perspectives. *Cancer Manag Res*, 7, 1-11. doi:10.2147/CMAR.S47220
- Norbury, J. W., Schimmerling, W., Slaba, T. C., Azzam, E. I., Badavi, F. F., Baiocco, G., . . . Zeitlin, C. J. (2016). Galactic cosmic ray simulation at the NASA Space Radiation Laboratory. *Life Sci Space Res (Amst)*, 8, 38-51. doi:10.1016/j.lssr.2016.02.001
- Okayasu, R. (2012). Repair of DNA damage induced by accelerated heavy ions--a mini review. *Int J Cancer*, 130(5), 991-1000. doi:10.1002/ijc.26445
- Olcina, M. M., & Giaccia, A. J. (2016). Reducing radiation-induced gastrointestinal toxicity - the role of the PHD/HIF axis. *J Clin Invest*, 126(10), 3708-3715. doi:10.1172/JCI84432
- Otterson, G. A., Kratzke, R. A., Coxon, A., Kim, Y. W., & Kaye, F. J. (1994). Absence of p16INK4 protein is restricted to the subset of lung cancer lines that retains wildtype RB. *Oncogene*, 9(11), 3375-3378.
- Ovesna, Z., Vachalkova, A., Horvathova, K., & Tothova, D. (2004). Pentacyclic triterpenoic acids: new chemoprotective compounds. Minireview. *Neoplasma*, 51(5), 327-333.
- Ozasa, K., Shimizu, Y., Suyama, A., Kasagi, F., Soda, M., Grant, E. J., . . . Kodama, K. (2012). Studies of the mortality of atomic bomb survivors, Report 14, 1950-2003: an overview of cancer and noncancer diseases. *Radiat Res*, 177(3), 229-243.

- Pershagen, G., Akerblom, G., Axelson, O., Clavensjo, B., Damber, L., Desai, G., . . . et al. (1994). Residential radon exposure and lung cancer in Sweden. *N Engl J Med*, 330(3), 159-164. doi:10.1056/NEJM199401203300302
- Preston, D. L., Ron, E., Tokuoka, S., Funamoto, S., Nishi, N., Soda, M., . . . Kodama, K. (2007). Solid cancer incidence in atomic bomb survivors: 1958-1998. *Radiat Res*, 168(1), 1-64. doi:10.1667/RR0763.1
- Preston, D. L., Shimizu, Y., Pierce, D. A., Suyama, A., & Mabuchi, K. (2012). Studies of mortality of atomic bomb survivors. Report 13: solid cancer and noncancer disease mortality: 1950-1997. 2003. *Radiat Res*, 178(2), AV146-172.
- Rawlins, E. L. (2011). The building blocks of mammalian lung development. *Dev Dyn*, 240(3), 463-476. doi:10.1002/dvdy.22482
- Rawlins, E. L., Ostrowski, L. E., Randell, S. H., & Hogan, B. L. (2007). Lung development and repair: contribution of the ciliated lineage. *Proc Natl Acad Sci U S A*, 104(2), 410-417. doi:10.1073/pnas.0610770104
- Rekhtman, N., Ang, D. C., Riely, G. J., Ladanyi, M., & Moreira, A. L. (2013). KRAS mutations are associated with solid growth pattern and tumor-infiltrating leukocytes in lung adenocarcinoma. *Mod Pathol*, 26(10), 1307-1319. doi:10.1038/modpathol.2013.74
- Robinson, B. W., & Lake, R. A. (2005). Advances in malignant mesothelioma. *N Engl J Med*, 353(15), 1591-1603. doi:10.1056/NEJMra050152
- Robles, A. I., Linke, S. P., & Harris, C. C. (2002). The p53 network in lung carcinogenesis. *Oncogene*, 21(45), 6898-6907. doi:10.1038/sj.onc.1205563

- Rodel, F., Frey, B., Multhoff, G., & Gaipf, U. (2015). Contribution of the immune system to bystander and non-targeted effects of ionizing radiation. *Cancer Lett*, 356(1), 105-113. doi:10.1016/j.canlet.2013.09.015
- Rodman, C., Almeida-Porada, G., George, S. K., Moon, J., Soker, S., Pardee, T., . . . Porada, C. D. (2017). In vitro and in vivo assessment of direct effects of simulated solar and galactic cosmic radiation on human hematopoietic stem/progenitor cells. *Leukemia*, 31(6), 1398-1407. doi:10.1038/leu.2016.344
- Saenko, V. A., Thomas, G. A., & Yamashita, S. (2017). Meeting report: the 5th International expert symposium in Fukushima on radiation and health. *Environ Health*, 16(1), 3. doi:10.1186/s12940-017-0211-y
- Saint-Criq, V., & Gray, M. A. (2017). Role of CFTR in epithelial physiology. *Cell Mol Life Sci*, 74(1), 93-115. doi:10.1007/s00018-016-2391-y
- Sandor, N., Schilling-Toth, B., Kis, E., Fodor, L., Mucsanyi, F., Safrany, G., & Hegyesi, H. (2015). TP53inp1 Gene Is Implicated in Early Radiation Response in Human Fibroblast Cells. *Int J Mol Sci*, 16(10), 25450-25465. doi:10.3390/ijms161025450
- Sasaki, H., Shitara, M., Yokota, K., Okuda, K., Hikosaka, Y., Moriyama, S., . . . Fujii, Y. (2012). Braf and erbB2 mutations correlate with smoking status in lung cancer patients. *Exp Ther Med*, 3(5), 771-775. doi:10.3892/etm.2012.500
- Sato, M., Larsen, J. E., Lee, W., Sun, H., Shames, D. S., Dalvi, M. P., . . . Minna, J. D. (2013). Human lung epithelial cells progressed to malignancy through

- specific oncogenic manipulations. *Mol Cancer Res*, 11(6), 638-650.
doi:10.1158/1541-7786.MCR-12-0634-T
- Scaltriti, M., & Baselga, J. (2006). The epidermal growth factor receptor pathway: a model for targeted therapy. *Clin Cancer Res*, 12(18), 5268-5272.
doi:10.1158/1078-0432.CCR-05-1554
- Schmid, K., Oehl, N., Wrba, F., Pirker, R., Pirker, C., & Filipits, M. (2009). EGFR/KRAS/BRAF mutations in primary lung adenocarcinomas and corresponding locoregional lymph node metastases. *Clin Cancer Res*, 15(14), 4554-4560. doi:10.1158/1078-0432.CCR-09-0089
- Schneider, C. A., Rasband, W. S., & Eliceiri, K. W. (2012). NIH Image to ImageJ: 25 years of image analysis. *Nat Methods*, 9(7), 671-675.
- Scott, B. R. (2011). Residential radon appears to prevent lung cancer. *Dose Response*, 9(4), 444-464. doi:10.2203/dose-response.11-027.Scott
- Shaw, A. T., Kim, D. W., Nakagawa, K., Seto, T., Crino, L., Ahn, M. J., . . . Janne, P. A. (2013). Crizotinib versus chemotherapy in advanced ALK-positive lung cancer. *N Engl J Med*, 368(25), 2385-2394. doi:10.1056/NEJMoa1214886
- Shaw, A. T., Yeap, B. Y., Solomon, B. J., Riely, G. J., Gainor, J., Engelman, J. A., . . . Camidge, D. R. (2011). Effect of crizotinib on overall survival in patients with advanced non-small-cell lung cancer harbouring ALK gene rearrangement: a retrospective analysis. *Lancet Oncol*, 12(11), 1004-1012.
doi:10.1016/S1470-2045(11)70232-7

- Sher, T., Dy, G. K., & Adjei, A. A. (2008). Small cell lung cancer. *Mayo Clin Proc*, 83(3), 355-367. doi:10.4065/83.3.355
- Siegel, R. L., Miller, K. D., & Jemal, A. (2019a). Cancer statistics, 2019. *CA Cancer J Clin*, 69(1), 7-34. doi:10.3322/caac.21551
- Siegel, R. L., Miller, K. D., & Jemal, A. (2019b). Cancer statistics, 2019. *CA Cancer J Clin*. doi:10.3322/caac.21551
- Simonsen, L. C., Wilson, J. W., Kim, M. H., & Cucinotta, F. A. (2000). Radiation exposure for human Mars exploration. *Health Phys*, 79(5), 515-525.
- Sos, M. L., Dietlein, F., Peifer, M., Schottle, J., Balke-Want, H., Muller, C., . . . Thomas, R. K. (2012). A framework for identification of actionable cancer genome dependencies in small cell lung cancer. *Proc Natl Acad Sci U S A*, 109(42), 17034-17039. doi:10.1073/pnas.1207310109
- Sridharan, D. M., Asaithamby, A., Bailey, S. M., Costes, S. V., Doetsch, P. W., Dynan, W. S., . . . Pluth, J. M. (2015). Understanding cancer development processes after HZE-particle exposure: roles of ROS, DNA damage repair and inflammation. *Radiat Res*, 183(1), 1-26. doi:10.1667/RR13804.1
- Suh, N., Wang, Y., Honda, T., Gribble, G. W., Dmitrovsky, E., Hickey, W. F., . . . Sporn, M. B. (1999). A novel synthetic oleanane triterpenoid, 2-cyano-3,12-dioxolean-1,9-dien-28-oic acid, with potent differentiating, antiproliferative, and anti-inflammatory activity. *Cancer Res*, 59(2), 336-341.
- Sun, S., Schiller, J. H., & Gazdar, A. F. (2007). Lung cancer in never smokers--a different disease. *Nat Rev Cancer*, 7(10), 778-790. doi:10.1038/nrc2190

- Sutherland, B. M., Cuomo, N. C., & Bennett, P. V. (2005). Induction of anchorage-independent growth in primary human cells exposed to protons or HZE ions separately or in dual exposures. *Radiat Res*, 164(4 Pt 2), 493-496.
- Suttie, A. E., Leininger, J. R., & Bradley, A. E. (2018). *Boorman's pathology of the rat : reference and atlas* (Second edition. ed.). London ; San Diego, CA: Academic Press, an imprint of Elsevier.
- Suzuki, Y., Orita, M., Shiraishi, M., Hayashi, K., & Sekiya, T. (1990). Detection of ras gene mutations in human lung cancers by single-strand conformation polymorphism analysis of polymerase chain reaction products. *Oncogene*, 5(7), 1037-1043.
- Tanoue, L. T., & Matthay, R. A. (2011). Lung Cancer Preface. *Clin Chest Med*, 32(4), Xiii-Xiv. doi:10.1016/j.ccm.2011.08.016
- Trachootham, D., Zhou, Y., Zhang, H., Demizu, Y., Chen, Z., Pelicano, H., . . . Huang, P. (2006). Selective killing of oncogenically transformed cells through a ROS-mediated mechanism by beta-phenylethyl isothiocyanate. *Cancer Cell*, 10(3), 241-252. doi:10.1016/j.ccr.2006.08.009
- Trani, D., Nelson, S. A., Moon, B. H., Swedlow, J. J., Williams, E. M., Strawn, S. J., . . . Fornace, A. J., Jr. (2014). High-energy particle-induced tumorigenesis throughout the gastrointestinal tract. *Radiat Res*, 181(2), 162-171. doi:10.1667/RR13502.1

- Treuting, P. M., Dintzis, S. M., Frevert, C. W., Liggitt, H. D., & Montine, K. S. (2012). *Comparative anatomy and histology : a mouse and human atlas* (1st ed.). Amsterdam ; Boston: Elsevier/Academic Press.
- Vogelstein, B., & Kinzler, K. W. (1993). The multistep nature of cancer. *Trends Genet*, 9(4), 138-141.
- Wallig, M. A., Haschek, W. M., Rousseaux, C. G., Bolon, B., & Mahler, B. W. (2018). *Fundamentals of toxicologic pathology* (Third edition. ed.). London, United Kingdom: Elsevier/Academic Press.
- Wang, J., Zhang, X., Wang, P., Wang, X., Farris, A. B., 3rd, & Wang, Y. (2016). Lessons learned using different mouse models during space radiation-induced lung tumorigenesis experiments. *Life Sci Space Res (Amst)*, 9, 48-55. doi:10.1016/j.lssr.2016.04.002
- Wang, X., Farris Iii, A. B., Wang, P., Zhang, X., Wang, H., & Wang, Y. (2015). Relative effectiveness at 1 gy after acute and fractionated exposures of heavy ions with different linear energy transfer for lung tumorigenesis. *Radiat Res*, 183(2), 233-239. doi:10.1667/RR13884.1
- Wang, X., Spandidos, A., Wang, H., & Seed, B. (2012). PrimerBank: a PCR primer database for quantitative gene expression analysis, 2012 update. *Nucleic Acids Res*, 40(Database issue), D1144-1149. doi:10.1093/nar/gkr1013
- Weil, M. M., Bedford, J. S., Bielefeldt-Ohmann, H., Ray, F. A., Genik, P. C., Ehrhart, E. J., . . . Ullrich, R. L. (2009). Incidence of acute myeloid leukemia and

- hepatocellular carcinoma in mice irradiated with 1 GeV/nucleon (56)Fe ions. *Radiat Res*, 172(2), 213-219. doi:10.1667/RR1648.1
- Weinberg, F., Hamanaka, R., Wheaton, W. W., Weinberg, S., Joseph, J., Lopez, M., . . . Chandel, N. S. (2010). Mitochondrial metabolism and ROS generation are essential for Kras-mediated tumorigenicity. *Proc Natl Acad Sci U S A*, 107(19), 8788-8793. doi:10.1073/pnas.1003428107
- Weinberger, S. E., Cockrill, B. A., & Mandel, J. (2019). *Principles of pulmonary medicine* (Seventh edition. ed.). Philadelphia, PA: Elsevier.
- Wheater, P. R., & Burkitt, H. G. (1987). *Functional histology : a text and colour atlas* (2nd ed.). Edinburgh ; New York: Churchill Livingstone.
- Xu, Y., & Price, B. D. (2011). Chromatin dynamics and the repair of DNA double strand breaks. *Cell Cycle*, 10(2), 261-267. doi:10.4161/cc.10.2.14543
- Young, B., O'Dowd, G., & Woodford, P. (2014). *Wheater's functional histology : a text and colour atlas* (Sixth edition / ed.). Philadelphia, PA: Churchill Livingston/Elsevier.
- Zdanov, S., Mandapathil, M., Abu Eid, R., Adamson-Fadeyi, S., Wilson, W., Qian, J., . . . Khleif, S. N. (2016). Mutant KRAS Conversion of Conventional T Cells into Regulatory T Cells. *Cancer Immunol Res*, 4(4), 354-365. doi:10.1158/2326-6066.CIR-15-0241
- Zhang, X., Lin, S. H., Fang, B., Gillin, M., Mohan, R., & Chang, J. Y. (2013). Therapy-resistant cancer stem cells have differing sensitivity to photon versus proton

beam radiation. *J Thorac Oncol*, 8(12), 1484-1491.
doi:10.1097/JTO.0b013e3182a5fdcb

Zhao, W., & Robbins, M. E. (2009). Inflammation and chronic oxidative stress in radiation-induced late normal tissue injury: therapeutic implications. *Curr Med Chem*, 16(2), 130-143.

Zhou, G., Bennett, P. V., Cutter, N. C., & Sutherland, B. M. (2006). Proton-HZE-particle sequential dual-beam exposures increase anchorage-independent growth frequencies in primary human fibroblasts. *Radiat Res*, 166(3), 488-494. doi:10.1667/RR0596.1